Using an Astrophysical Model to Characterize Nuclear Dust

THESIS

Anita N. Dunsmore, 2nd Lt, USAF

AFIT-ENP-MS-18-M-079

DEPARTMENT OF THE AIR FORCE
AIR UNIVERSITY

AIR FORCE INSTITUTE OF TECHNOLOGY

Wright-Patterson Air Force Base, Ohio

AFIT-ENP-MS-18-M-079

USING AN ASTROPHYSICAL MODEL TO CHARACTERIZE NUCLEAR DUST

THESIS

Presented to the Faculty

Department of Engineering Physics

Graduate School of Engineering and Management

Air Force Institute of Technology

Air University

Air Education and Training Command

in Partial Fulfillment of the Requirements for the

Degree of Master of Science in Nuclear Engineering

Anita N. Dunsmore, BS

2nd Lt, USAF

22 March 2017

AFIT-ENP-MS-18-M-079

USING AN ASTROPHYSICAL MODEL TO CHARACTERIZE NUCLEAR DUST

THESIS

Anita N. Dunsmore, BS
2nd Lt, USAF

Committee Membership:

Dr. John W. McClory
Chair

Lt Col Brian J. Fry, PhD
Member

Lt Col James R. Fee, PhD
Member

AFIT-ENP-MS-18-M-079

Abstract

Dust clouds resulting from nuclear explosions are physically and chemically complex phenomena, and knowledge on the specifics of how they form is lacking. Noting the similarities between a supernova explosion and a nuclear explosion led to the concept of modeling the nuclear dust cloud using a supernova simulation. MOCASSIN uses a Monte Carlo approach to model photons traveling through dust and gas clouds, allowing the characteristics of these clouds to be discovered by comparing an observed spectrum to one calculated by the code, and then changing the appropriate parameters to make the spectra match. Data files describing two nuclear fireballs of varying yields were created and analyzed using MOCASSIN, but yielded spectra of zero energy. After varying the parameters of the tests, analyzing the spectra that resulted, and comparing them to data from the 1.2 MT nuclear test Operation Dominic Harlem, it was found that the differences between the nuclear explosion and supernova were too significant for MOCASSIN to accurately model both. Insufficient input data for compounds relevant to nuclear explosions, low ionization levels in the fireball, and high densities in the fireball were all major issues that could not be overcome. Ultimately, it was concluded that MOCASSIN is not a viable method for analyzing nuclear explosions.

Table of Contents

List of Figures

List of Tables

USING AN ASTROPHYSICAL MODEL TO CHARACTERIZE NUCLEAR DUST

I. Introduction

1.1   Motivation

When planning for the effects of a nuclear explosion, there are many factors that must be considered. Some are obvious, like the blast wave and fallout, and have been thoroughly studied. Other factors, like the dust cloud itself, have not been examined fully, but could cause devastating consequences if not properly understood and if the effects of the dust cloud are not anticipated.

In 1980, the eruption of Mount St. Helens created thick dust clouds in Washington State, causing several jet engines in nearby aircraft to shut down. This brought the dust problem to the attention of military planners, who realized that the knowledge they had regarding dust clouds from nuclear explosions was not adequate to facilitate proper planning [10]. Having a full picture of a nuclear dust cloud involves knowing, at the least, the cloud's shape, size, and rate of growth, tracking its location and velocity, monitoring the particle types and sizes, and knowing the radiative properties of these particles. These physical properties are the result of complex chemical processes, and modeling them accurately has proven to be a difficult task.

It is a vital task, however, for the planning and consequence management related to any nuclear event. As the observers of the Mount St. Helens eruption can attest, any aircraft flying into the vicinity of a dust cloud, whether civilian or military, must know the cloud's properties before they can fly through safely. Military aircraft conducting surveillance, nuclear forensics, or those performing various wartime tasks

might need to fly very close to a nuclear cloud, and would need to know zones to avoid. Communications could also be affected, as radar and other signals are potentially negatively affected by the dust. In addition, any nearby facilities or cities could experience issues related to the dust density.

If an adversary knows of these possible effects and the US remains blinded, they could be used against the military in a conflict. On the other hand, if the US knows more than its enemies, their lack of knowledge can be used against them. Just like with any weapon, the US military needs to gain a full understanding of the effects of a nuclear blast so that it can plan accordingly. This paper will explore one option for gaining such insight.

1.2 Research Goals

The overarching goal of this research is to determine whether the use of an astrophysical supernova modeling code to model a nuclear dust cloud is a viable and reliable option. The following are the specific goals:

1. Determine whether there is an astrophysical code with the potential to produce information about the cloud based on parameters in the source code.

2. Adapt the code to the nuclear detonation problem in any way possible. If not possible, determine why.

3. Determine the accuracy and reliability of the method by comparing data from observations to results from the code.

1.3 Historical Background

A majority of the work that has been performed regarding dust particles and the growth of nuclear dust clouds after a nuclear blast has concentrated on fallout, since

the distribution of activity is of great importance after an explosion. Much of this work has been in the form of fallout codes, such as DELFIC, HPAC, and HYSPLIT. These codes generally concentrate on dispersion of fallout particles after a nuclear event, showing both the transport of the particles through the air and deposition of the particles on the ground. Some of the codes were meant to be used by responders to nuclear events, allowing them to determine the areas of highest activity and the directions in which the fallout was spreading. The codes do often include information about particle size, but they are normally related to the subsequent spread of different sized particles on the surface, rather than early distributions in the cloud [11].

Other methods of looking at fallout often included analysis of particles collected after nuclear tests, either on the ground or from an airborne platform. Researchers have analyzed properties such as the particle size distribution and composition of particles [12]. However, work in this area does not give a complete picture of particles in the dust cloud. Regarding the measurements taken on the ground, "fallout itself cannot provide adequate information about the distribution of smaller size ranges because they are not completely removed from the cloud during sampling" [13]. And samples taken using aircraft are often collected hours to days after the detonation, since "earlier cloud penetrations by aircraft were not possible because of the high radiation field" [13].

In many cases where dust particles were used in research, they were not important enough in the calculations to merit much thought or effort. The authors would simply assume a simple approximation and move on. For example, one paper that specifically analyzed properties of these particles concluded that, for a high altitude air burst, the size of particles was "seldom greater than 20 microns diameter," but that overall the distribution was "unknown," though it did "var[y] inversely with yield" [14]. For a low altitude air burst there was even less information - the authors concluded that the

3

particles "range from a few microns to several hundred or a few thousand microns," depending on "nature and amount of interacting soil, etc." [14].

This could hardly be used in any situation where an actual distribution was required. In another paper that was used to analyze the types of particle collection filters needed on an aircraft based on the particles it would encounter after a nuclear detonation, the assumption was made that the dust cloud was homogeneous in both particle types and densities (which is obviously far from accurate), and assumed that there was 1 MT of dust per 1 MT of yield 10 minutes after a surface burst [15]. Besides the approximate nature of this value, it is also not applicable to instances other than a 1 MT surface burst, and there was no discussion of linear or other scalability to different yields.

Even in instances where the researchers were specifically looking at the particle properties, the results are insufficient. One paper called "The Particle Size Distribution of Nuclear Cloud Samples," definitely did more than others in determining the actual distribution, but even those results are not at all complete. The final conclusion was that small particles have a log-normal distribution while the distribution of larger particles is based on a "power law" [13]. The actual power was not determined however, since there wasn't enough data available to make broader conclusions. "Chemistry and Spectroscopy of a Fireball" is another paper that addresses this issue; it used chemical analysis to calculate how air particles surrounding the fireball would be affected by the radiation [16]. Specifically, the authors chose certain molecules (such as NO_2, O_3, and HNO_2), calculated how the amount of each would change after an explosion, and then examined how that would affect an x-ray spectrum collected from the fireball. The main problem with the work is that it was done in 1982, and thus the computational capabilities were extremely limited. This meant that many shortcuts were taken in the calculations, which effected the accu-

racy of the subsequent results. Also, the results only show the composition of the air milliseconds after the explosion, and do not include the composition at later times, seconds to hours after the detonation.

A method is needed to model a nuclear fireball's dust cloud, with minimal background to build on. The next section covers a proposed plan.

II. Theory

2.1 Proposed Solution

Modeling a physical situation as complex as the fireball and dust cloud after a nuclear explosion is not an easy task. Taking into account all of the different physical processes occurring, which are rapidly changing in time and space, is a substantial undertaking. It would be much easier to use an existing model from a physical situation similar to a nuclear blast. Adapting such a code, if possible, would take much less time and effort than creating something new.

One possibility of a similar physical situation is a supernova explosion. Astrophysical methods for modeling supernovae are not uncommon, and some have been modified and improved many times over. One such code, called MOCASSIN, was chosen, and will be adapted to attempt to model an atmospheric nuclear detonation.

2.2 Nuclear Fireball vs. Supernova

Though a nuclear fireball and supernova may appear to be irredeemably different, there are some significant similarities. The overall physical situation that occurs is quite similar: material compresses to a hot, dense plasma, and then explodes. This results in many of the same physical effects for both cases, such as shock waves, radiation fields, and dust clouds. All of these physical occurrences end up affecting particle nucleation in the cloud, which implies that code which mimics them could model the particles in both clouds [16].

However, there are differences that need to be considered. Most importantly, the scope of a supernova is different than a nuclear explosion in basically every way. The amount of time that a supernova takes to form a dust cloud after the explosion is on the order of years, while this same process occurs for a nuclear explosion on the order

of seconds [3]. A supernova is orders of magnitude larger than a nuclear explosion, in terms of both volume and mass. And, the density of the cloud at just a few seconds after a nuclear explosion is orders of magnitude higher than that of the supernova after a few years [17].

All of these differences in parameters such as time, density, volume, etc., might seem like values that would just be part of the input files for the code, and it is possible some of them will be. However, it is also possible that parts of the code might depend on the input parameters being within certain limits, and going beyond these limits might either cause the code to fail or not converge. Either way, experimenting with the limits of the code will help determine which, if any, of the differences between the supernova and fireball scenarios might cause future problems.

2.3   Overview of Astrophysical Options

Since part of this project was exploring various astrophysical methods for researching dust, and choosing which option would best suit the nuclear dust cloud problem, a brief overview of the options that were *not* chosen and the reasoning behind the choice is provided here.

Many of the other approaches found were based on similar methodologies. The papers listed the rules and equations that they used regarding nucleation and evolution of the dust, and applied them to different cases. The complexity varied widely: one paper had only about 1 page of equations [18], while another included 12 pages of stoichiometric equations [8]. Each followed the growth of varying numbers of selected compounds, and included different processes. For example, the Sluder paper accounted for processes like "accretion," "coagulation," "radioactive decay," "grain electric charge," "surface-tension-corrected evaporation rate," "van der Waals forces," and "weathering" [8].

In order to make full use of the equations that were applied in the astrophysical supernova models, it would be necessary for the nuclear model to use the same equations, putting in the corresponding general properties (temperature, size, etc.). The issue with that is that each paper had a relatively small number of compounds that they tracked (14 in the Sluder article), so these would be the only compounds the nuclear model could assess. And the elements that are abundant and influential in astrophysics are not the same as those that are important in an atmospheric nuclear detonation. Elements in the Sluder equations included He, Ne, Mg, S, Ar, and Ni, none of which are in an atmospheric detonation in significant quantities, and do not include Pu or U, which are present.

It would certainly be possible to use the astrophysicist's methods without using their actual equations, and create new equations. However, this would negate the purpose of using an astrophysical method, and would not save any time. The equations that could be created in the given time frame would be rudimentary, and could not take any complex processes into account.

The method chosen, MOCASSIN, is different than these other methods in a few important ways. Any elements or compounds can be entered into it, and the entire physical description of the situation is entered by the user. In using MOCASSIN, the work done by the astrophysics community is being fully utilized, with the option to modify the parameters to the new problem. A full description of how the code works is given in the next section.

2.4 MOCASSIN

MOCASSIN, which stands for MOnte CArlo SimulationS of Ionized Nebulae, is a code used to model various astrophysical phenomena including supernovae. It has been improved and updated several times since its initial release in 2002, with the

most recent version released in August 2017. Other codes using the same Monte Carlo approach have been in development since the 1980s, but MOCASSIN comes with a number of changes and improvements. The most notable of these improvements is that it is one of the first codes of its kind to be 3-dimensional; most predecessors assumed some level of symmetry and only did calculations in one or two dimensions [19]. This means that asymmetrical circumstances can be accounted for in the model.

In astrophysics, this code has been applied to various phenomena, such as modeling the formation of stars and planetary nebulae (which are always asymmetrical) [20]. Most relevant to research in this paper is version 2 of the code, the dusty MOCASSIN, which includes radiative transfer of both gas and dust [21]. This version has been used to model the dust formed by a supernova explosion [3]. This research will attempt to use this method to model the dust cloud formed by a nuclear explosion, in order to determine the characteristics of the dust cloud that can be discerned from the solution.

Overall Properties

As can be determined from the name, MOCASSIN uses the Monte Carlo method to model radiative transport through a field. This method is widely used in circumstances that include radiative processes, and involves repeated random sampling to obtain statistically significant results. By sampling a large number of times, the law of large numbers states that the results will converge to the correct solution. This method is often more computationally efficient than attempting to solve a large number of equations directly.

In this case, the equations that the code solves are thermal balance and ionization equilibrium equations imposed in cells on a grid. Each model consists of a 3D Cartesian grid that covers the area of interest, with the source placed anywhere on

the grid. The code runs through all of the cells repeatedly, and during each iteration the sets of equations are solved. The iterations continue until they converge on a solution. Several convergence criteria are possible, all of which depend on the difference between the solutions from subsequent iterations being small.

Initial Setup

Before the code can be run, a model must be created describing the specific situation in question. The source must be placed on the grid (the location usually depends on any symmetries that exist - i.e. if the model is spherically symmetric, the source can be placed in the corner of the grid, and the solution of that corner will be the same for the other 7 identical corners), and given a certain radius, temperature, and luminosity. This temperature will be used to determine the flux of photons leaving the source, and the luminosity will be used to determine the total energy output of the source.

Distributions must then be determined for the area surrounding the source. The chemical makeup of the stellar (or otherwise) atmosphere is required; it should be noted that this does not have to be homogeneous. The density of gas in the area in question must also be provided (which also does not have to be homogeneous) [19]. Regarding the grains of dust in the cloud, a distribution must be given for both the grain size and the grain species, as well as location of the dust. The grain species is defined by the species' optical constants, n and k (since these will determine how photons are affected by a grain). The code contains optical constants for common astrophysical dust species, but other species can easily be added if desired [21].

The Algorithm

The core of MOCASSIN tracks photons from the source through the gas and dust field. But, rather than tracking individual photons, MOCASSIN tracks energy packets, each of which have a specified number of photons of a specified frequency. This simplification greatly increases the computational efficiency of the program. At the beginning of the run, the code uses a probability density function based on the flux and radius of the source to determine the frequencies of the energy packets. These packets are then emitted isotropically from the source, with each packet given a random direction of travel. [19]

The packets are tracked by the code as they move through the grid. When a packet reaches a cell in the grid, the code determines what occurs in the cell based on a Monte Carlo probability. There are two possibilities in a dusty environment: scattering and absorption [21]. If the packet scatters off of a dust particle, the frequency of the packet stays the same, but it is re-emitted in a new direction. If the packet is absorbed, however, both the frequency and the direction change. The new frequency is sampled from the spectral distribution of the total local emissivity, and the direction is chosen randomly [19]. The total energy of the packet, however, remains the same in both cases. What changes after a frequency change is the number of photons in the packet, since the energy of a packet is proportional to the product of the number of photons at a certain frequency. This ultimately allows the packet method to naturally preserve energy conservation at every point in the grid [19]. This process continues until the packets reach the edge of the grid. At this point, the frequency and direction of the packet is recorded, and the tracking stops [21].

After all of the packets have reached the edge, the code calculates a value: the mean intensity of the radiation field. This is used to relate the quantities we observe during our Monte Carlo experiment to the physical quantities we want to determine

11

[19]. Other values are then calculated based on this mean intensity, allowing the ionization balance and thermal equilibrium equations to be solved at each grid point.

After this is done, the convergence criterion is checked to see if the solution converged. There are several different values that can be checked, such as the hydrogen ionization structure, helium ionization structure, and electron temperature. Each of these is checked between successive iterations, and the convergence criterion is met if the change is small.

End Result

The output of the code is thus the compilation of the frequencies and direction of all of the energy packets leaving the grid area. These values can be used to create a spectral energy distribution, or SED, that describes the radiative output of the dust cloud. The frequencies can of course be converted into wavelengths, while the directions are only important in an asymmetrical circumstance, where the outputs are different in unique directions.

The usable output of the code is thus the SED. MOCASSIN produces these distributions in different wavelength ranges, including the infrared range. This is important when analyzing dust clouds because dust formation may be detected by the development of an infrared excess due to optical photons being absorbed and re-emitted at longer wavelengths [3]. The second version of MOCASSIN was specifically designed to look at these wavelengths so that dust could be detected.

Comparison With Observed Data

After obtaining the SED, it can be compared to observed data of the supernova or other astrophysical entity. If the two do not match, then the input parameters should be changed, and another SED plot produced. This process should continue

12

until a plot is found that closely matches the observed data. This is useful because, in astrophysics, the only measurements that can really be recorded are of the radiation coming from astrophysical entities. Because of this, it is important to be able to work backwards and discover the physical parameters that match a given observation.

Figure 1 on the next page shows an example of observed data vs. MOCASSIN output. The colored lines represent different trials in MOCASSIN, where a single parameter was changed at a time to work at determining the true values. In the top figure, the total mass of dust was changed, and in the bottom figure the grain composition ratio was changed (carbon:silicates) [3].

This is a relatively approximate method for determining input values, but current knowledge of early fireball dust clouds is so lacking that it still might yield results. However, since the best method is to only change one value at a time, good estimates for all of the input values will be required. The next chapter will discuss how all of these estimates were obtained.

2.5 Problem Space

All of the MOCASSIN inputs and outputs represent the supernova at a specific instant in time; the iterations are used to find a convergent solution at a point in time, not to develop the situation as time passes. So, in order to apply this to a nuclear explosion, it was necessary to choose an appropriate time at which to calculate the input values.

Dust does not start forming until between 2000-3000 K [18], so this was the initial fireball temperature chosen. It was then possible to calculate the time it would take for the fireball to cool to this temperature. This time was vital to knowing the phase of growth of the fireball, and thus the general physical situation of the fireball. It should be noted that, in order to minimize the differences between the supernova and
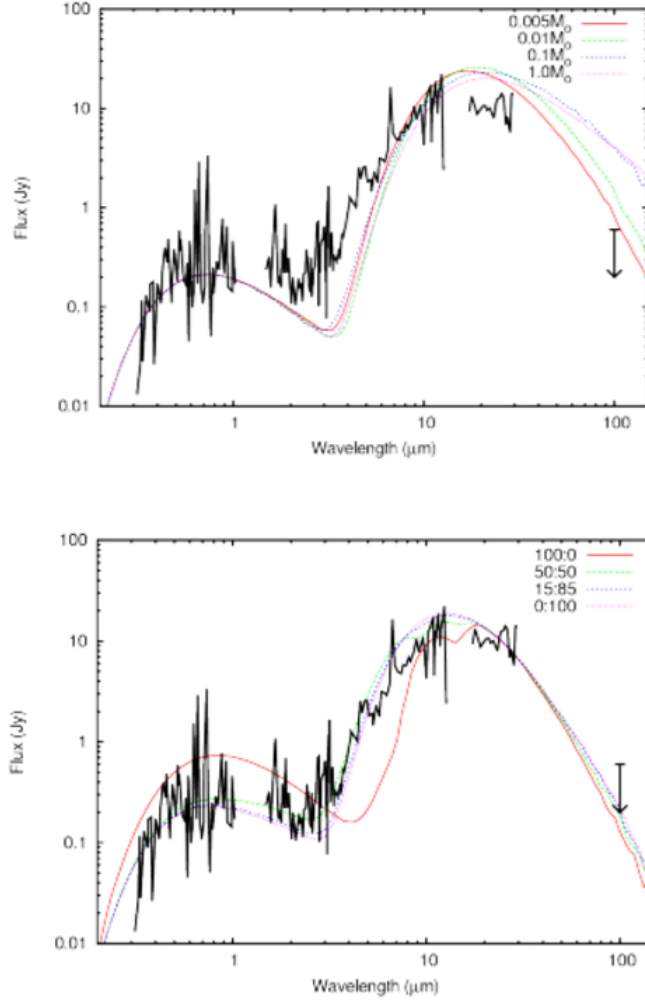
Figure 1. Spectral energy distribution for SN1987A (a supernova observed in 1987). Colored lines are MOCASSIN output, black line is observed data. The top shows the results of changing the overall mass of dust in terms of solar masses, M_0, and the bottom shows the results of changing the carbon:silicate ratio in the dust composition. Reproduced with permission from [3], figures 2 and 4 .

nuclear explosion, an air burst is assumed (and thus it is not necessary to factor in dust from the ground).

In this section the phases of growth of the fireball will be reviewed, concentrating on the physical properties of the fireball in the chosen problem space.

Fireball Growth

There are three main phases of fireball growth. The fireball used in this research will be in the third phase, so the first two will only be briefly covered.

The first phase of growth is burn out. Immediately following detonation, x-rays travel outward from the bomb and are absorbed by the surrounding case material. Assuming the bomb is large enough, the case will be completely ionized. The cross section for absorption of x-ray photons is very small for completely ionized materials, and thus the x-rays are able to pass through the bomb case out to the surrounding air. The x-rays then ionize the air surrounding the bomb. This phase of growth ends when all of the primary x-rays have been consumed, leaving a completely ionized sphere of air and weapon debris behind, at a temperature on the order of 10^6 K. The radius of this sphere is the "burn out radius." [4]

The next phase of growth is diffusive growth. In this phase, photons travel outward from the bomb by diffusion, continuing to heat the surrounding air. As this volume of air grows, and the surface area that the photons must heat increases, the speed of growth of the fireball slows. However, the speed of the shock wave accompanying the fireball does not slow. When the speed of this shock wave (the local acoustic velocity) becomes larger than the rate of growth of the fireball, the shock wave separates from the fireball. This is called "hydrodynamic separation," and it marks the end of the diffusive growth phase. At this point, the fireball's temperature is still on the order of 10^5 K; not yet low enough for dust to form. [4]

In the last phase of growth, the hydrodynamic phase, there are actually two different growth rates to keep track of - the inner, thermal fireball, and the shock front. Since the shock front has a very high temperature and pressure, it heats the air that it encounters so much that it emits radiation at visible wavelengths. This "fireball" keeps the inner fireball from being visible (though it is still inside, continuing to grow diffusively). Eventually, however, the temperature and pressure of the shock front decrease, and the air cools enough that it is transparent to visible light again. This occurrence is called "breakaway." After breakaway, the inner fireball can be seen again. [4]
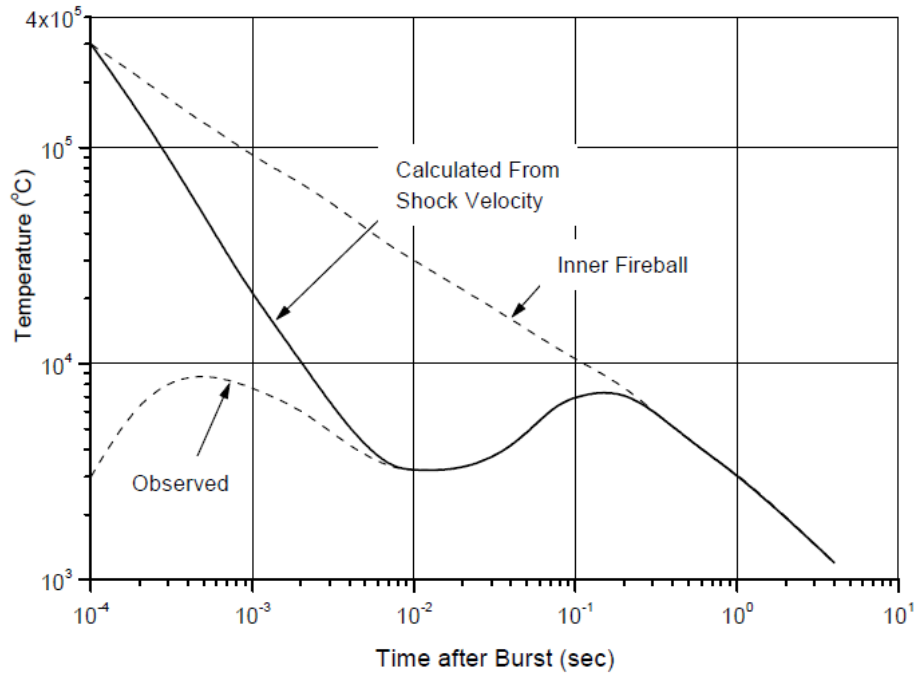
Figure 2. Fireball temperature as a function of time for a 20 kT air burst. Reproduced with permission from [4].

Figure 2 shows the temperature of the fireball from a 20 kT air burst, starting at hydrodynamic separation. The upper dotted line is the temperature of the inner fireball, while the solid line is the temperature of the shock front. The lower dotted line is the observed temperature of the shock front for a detonation in the lower

16

atmosphere (radiation emitted early in the detonation produces gases such as ozone and nitrogen dioxide ahead of the shock front, and these gases absorb a substantial amount of the radiation from the shock front, making the temperature calculated from photographic/spectroscopic measurements lower than the actual temperature) [22]. Breakaway occurs in the time between the first minimum and the second observed maximum, ending with the shock heated air becoming fully transparent, unveiling an inner fireball that continues to emit in the visible spectrum. A temperature of 2500 K is achieved after this second maximum, and only the spectral output of the inner fireball must be considered, not that of the shock wave.

Type of Bomb

At first glance, it seems that it would desirable to model a fusion-fission, aka thermonuclear, bomb rather than a fission bomb using a supernova approach, since fusion is the main source of energy in a star and a supernova explosion, and thus the physical processes in a supernova and thermonuclear bomb are similar. However, MOCASSIN is potentially equally valid for both bomb types. For both fission and thermonuclear weapons, there will be a source emitting photons that will travel through gas and dust and emit a certain spectrum; all differences that exist can be included in the model.

When differences are discussed here between the two bomb types, it should be noted that only differences that depend *entirely* on the type of bomb are being discussed. For example, the general bomb components of a thermonuclear vs fission weapon are fundamentally different. On the other hand, something like the weapon yield, though dependent on the bomb type (with thermonuclear weapons generally having larger yields), can also vary greatly within a bomb type. Differences like these are easy to account for, since they affect the input parameters regardless of the bomb

type.

Fortunately, all of the known differences can be accounted for in the input files. The main difference is the bomb material components, which affect the compounds present in the early-stage fireball. This just means that the dust and gas components will be different between the two bomb types.

Summary

Incorporating all of the above information, the nuclear problem space being used has the following characteristics:

- The fireball is in the hydrodynamic growth phase, after breakaway. The shock wave is no longer visible, and the temperature of the fireball will only decrease from this time.

- The fireball is at 2500 K. The time this occurs will depend on the yield of the weapon.

- The materials in the fireball are from any ionized air, and the weapon components.

- A fission or thermonuclear bomb can be used; the input files should be created accordingly.

Obviously these characteristics do not fully define the fireball and surrounding air; they are simply a starting point for building MOCASSIN files. The next chapter will describe this process - estimating relevant values and creating input files from them.

III. Methodology

This chapter will describe how the MOCASSIN input decks were built. Since only the viability of this method needed to be determined, input values that were representative of nuclear explosions were all that was required. These files would then allow a determination of whether there were any issues in MOCASSIN with running values on the scale of nuclear explosions.

There were several different input file types that needed to be created. The main input file defines the source, and some general information. The density and dust density files show the hydrogen density distribution throughout the volume of interest, and provide information on the dust and gas composition at each location in space. The abundance files give the relative abundances of the dust compounds and gaseous elements in certain regions. The dust optical files give optical data about the dust in each area.

In this chapter, some values describing the explosion are calculated first, most of which will go into the main input file (size of source, luminosity, etc.). The elements, for both gas and dust, that would be present in different areas after the explosion are found next. After that the compounds that would be formed by these elements is determined, and whether, at the target temperature, the materials will remain in gaseous form or condense to dust.

3.1   Explosion Parameters

In order to model an explosion, the parameters of the burst needed to be defined first, including the yield, height of burst, and the components and design of the bomb itself. Ideally, the models would have all been based on actual explosions, so that the MOCASSIN results could be compared to recorded spectra of the test. However,

data of the kind needed proved difficult to find, or only available in classified sources, and thus only one of the model situations was chosen for this reason.

The first situation chosen was a 20 kT air burst based on Fat Man. The advantage of using this bomb was that the bomb design is published in the open literature (which is not common), and thus it was not necessary to make any estimates or guesses regarding materials and their arrangement in the bomb. The specifics of the components will be discussed later in the chapter, when they will be used to determine the elemental composition of the fireball. Fat Man's height of burst was approximately 550 m [7]. No spectra were recorded of the burst.

The second situation chosen was a 1.2 MT test called Operation Dominic Harlem. Though the bomb design was unpublished, this test had spectra collected of the fireball over the wavelengths and times of interest, which could be compared to MO-CASSIN spectra. The height of burst of the Harlem test was approximately 4160 m [6]. The assumptions made regarding the bomb design will be discussed later in this chapter. Note that a yield of 1 MT will be used for the calculations, while Dominic Harlem's yield was estimated as being between 1.1 MT and 1.2 MT. Most of the values that will be found are so approximate that the difference between 1.0, 1.1, or 1.2 MT is minimal.

3.2   General Input Values

This section will describe how the values for each nuclear explosion (20 kT and 1 MT) that went into the MOCASSIN input files were approximated. All of these values were based on the need for the fireball to be at or below 2500 K. This temperature was chosen for a few reasons. First, the code assumes that a significant amount of the gas around the source is ionized. This becomes less true as time passes, and thus earlier times are more relevant. Also, mixing between the fireball and the outside air

20

occurs as time passes, making it more difficult to model the gas and dust compositions and distributions. At the early times that were examined, minimal mixing will have occurred, allowing for simpler models. This temperature is assumed to be constant throughout the fireball, based on Figure 3. This figure clearly shows a temperature plateau for small radii, which is the inner fireball. It becomes less flat as time passes, but was still assumed to be constant.
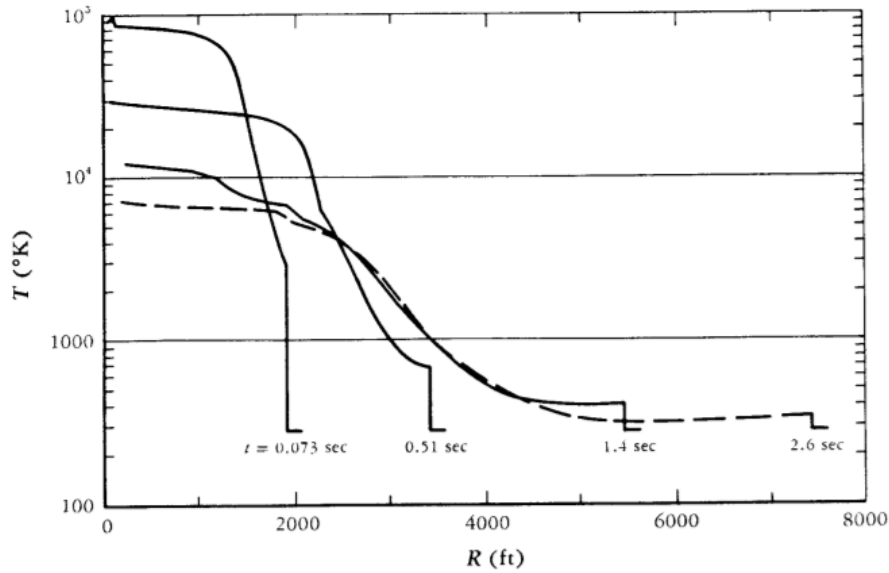
Figure 3. Fireball radius as a function of temperature for a 1 MT surface burst. Reproduced with permission from [5].

Time

The first value calculated based on the fireball temperature was the time after the explosion at which this temperature will be reached. For the 20 kT weapon, no calculations were necessary; Figure 2 from Chapter 2 shows a 20 KT burst's fireball temperature as a function of time. A temperature of 2500 K, or around 2226 C, was needed. The figure shows that this occurs at around 1 second after the burst (note: this is a very approximate method for finding the time, but for building the input files it is close enough).

For the 1 MT burst a new method for determining the time was needed. It is known that the shape of the temperature vs. time plot is similar to the 20 kT plot, but scaled up by some factor. It is also known that breakaway always occurs at approximately the same temperature for any fireball, since it is based on the temperature at which air becomes transparent to visible light [4]. So, the ratio between the time of breakaway and the time at which the fireball is at 2500 K must be the same for both yields.

The time of the 2nd maximum is $t_{max} = 0.0417Y^{0.44}$ [4]. The equation is therefore:

$$\frac{t_{max,20kT}}{t_{2500,20kT}} = \frac{t_{max,1MT}}{t_{2500,1MT}}. \tag{1}$$

where $t_{2500,y}$ is the time at which the fireball from the explosion of yield 'y' reaches 2500 K.

Entering known values yields:

$$\frac{0.0417 * 20^{0.44}}{1} = \frac{0.0417 * 1000^{0.44}}{t_{2500,1MT}}.$$

Solving this for $t_{2500,1MT}$ yields $t_{2500,1MT} = 5.6s$.

This was checked (very approximately) using Figure 3. Though this plot only goes up to 2.6 seconds, it shows that the inner fireball temperature on the far left would continue decreasing, and would end up at 2500 K sometime around 4-6 seconds. This is in agreement with the calculated value.

Power

The power output of the fireballs was computed next (called source luminosity in MOCASSIN). The following set of equations [4] were used:

$$P_{max} = 1.33 \times 10^{13} Y^{0.56} \tag{2}$$

$$\frac{P}{P_{max}} = \frac{2\tau^2}{1 + \tau^4} \tag{3}$$

where $\tau = \frac{t}{t_{max}}$, and P in $\frac{J}{s}$. The results are shown in Table 1.

Table 1. Table of Power Values

Yield kT	t s	t_max s	τ	P_max J/s	P J/s
20	1	0.16	6.4	7.1×10^{13}	3.5×10^{12}
1000	5.6	0.87	6.4	6.4×10^{14}	3.1×10^{13}

This value was checked for the 1 MT explosion against the data on Operation Dominick Harlem [6]. This data includes a chart of the power and energy of the fireball for the first 20 seconds after the explosion. This data shows that, at 5 seconds, the power is 7.20×10^{12} cal/s, and at 8 seconds is 3.5×10^{12} cal/s. Converting the equation to cal/s, the power computed from the equation at 5.6 seconds is around 7.4×10^{12} cal/s, which is very close to the data.

Fireball Radius at Time of Interest

In this section the fireball radius for each bomb at the time of interest will be computed, which will be used as the source radius in MOCASSIN.

For the 20 kT weapon, the radius was found using a plot of time vs radius in Glasstone and Dolan (Figure 2.121) [22]. It is apparent from this plot that the fireball's radius at $t = 1$ second is approximately 750 feet, or 230 meters.

The corresponding radius was found for the 1 MT weapon by using proportionality again. The equation for the radius of a fireball at breakaway for any air burst is the following [22]:

$$R = 110Y^{0.4}. \tag{4}$$

It was assumed that the ratio of the fireball's radius at breakaway to the radius at the time of interest is the same for both yields, so that

$$\frac{r_{breakaway,20kT}}{r_{TOI,20kT}} = \frac{r_{breakaway,1MT}}{r_{TOI,1MT}}. \tag{5}$$

Substituting in known values yields

$$\frac{110 * 20^{0.4}}{230} = \frac{110 * 1000^{0.4}}{r_{TOI,1MT}}.$$

This led to a value of 1095 meters.

This was checked with data from the 1 MT weapon, shown in Figure 4. The figure shows that the fireball's diameter at 5.6 seconds is approximately 2.2 km, and thus the radius is around 1100 meters, almost exactly the same as the estimated value.

Shock Wave Radius at Time of Interest

The next value that was found was the shock wave radius at the time of interest. This radius will help determine the air density distribution in the volume inside the shock wave (to be accomplished later in this chapter).

For both weapons, Figures 3.77a and 3.77b from Glasstone and Dolan were used [22]. Since the plots are both on the 1 kT scale, the 1/3 yield scaling law was necessary to scale the results. These scaling laws are all of the form:

$$\frac{x}{x_1} = Y^{1/3}, \tag{6}$$
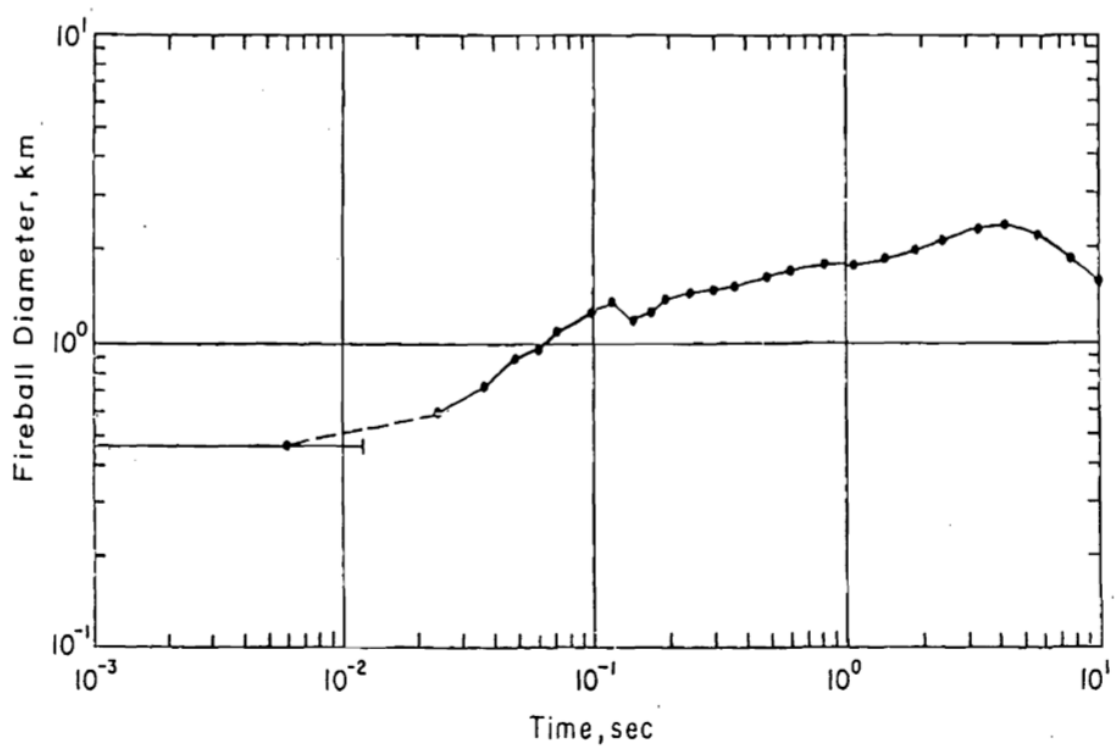
Figure 4. Fireball diameter as a function of time for Operation Dominic Harlem. Reproduced with permission from [6].

where x is the value, and x_1 is the value scaled to a yield of 1 kT [22].

The 20 kT weapon, with a height of burst of $h \approx 1800 ft$ [7], had to be scaled down to the 1 kT case, which yielded

$$h_1 = \frac{h}{Y^{1/3}} = \frac{1800}{20^{1/3}} \approx 663 \ ft.$$

The time of $t = 1$ second also needed be scaled to the 1 kT case, which resulted in

$$t_1 = \frac{t}{Y^{1/3}} = \frac{1}{20^{1/3}} = 0.37 \ s.$$

The next step was to use a figure from Glasstone and Dolan that relates the shock wave radius to time (Figure 3.77a) [22]. The spot on the graph where an HOB of 663 feet meets the approximate area where the 0.37 second curve would be (in between the 0.3 and 0.4 curves) gave the corresponding distance from ground zero. This distance was approximately 650 feet. This distance then had to be scaled back up to the 20 kT case:

$$d = d_1 Y^{1/3} = 650 * 20^{1/3} \approx 1750 \ ft.$$

However, this number had to be further adjusted, because the value of interest was not the radius at which the shock wave would reach certain spots on the ground, it was the total radius of the shock wave. It was therefore necessary to find the hypotenuse of the triangle formed by the burst location, ground zero, and the spot on the ground where the shock wave would have reached at the time of interest.

$$r_{shock} = \sqrt{d^2 + h^2} = \sqrt{1750^2 + 1800^2} = 2510 \ ft \approx 765 \ m.$$

Technically, this is not quite right, since the shock wave does not travel the same speed over the ground as it does through the open air. However, in examining the

figure, it can be seen that the curves representing time are approximately quarter-circles that intersect similar values on the x and y axes. This indicates that the two speeds are fairly similar, and thus the approximation is close.

The same process was repeated for the 1 MT weapon, with an HOB of $h = 13645$ ft [6] and a time of $t = 5.6$ seconds. The scaled values were then:

$$h_1 = \frac{h}{Y^{1/3}} = \frac{13645}{1000^{1/3}} = 1364.5 \ ft$$

$$t_1 = \frac{t}{Y^{1/3}} = \frac{5.6}{1000^{1/3}} = 0.56 \ s.$$

For this later time Glasstone and Dolan Figure 3.77b was used [22]. It appears that the shock wave has not quite reached the ground; however, all that matters is that the intersection of the relevant time is at around 1200 ft (this can be found either by assuming HOB $= 0$ and looking at the ground distance, or by assuming the ground distance is 0 and looking at the HOB). Since only the shock radius matters, this is the value that was scaled back up.

$$r_{shock} = d_1 Y^{1/3} = 1200 * 1000^{1/3} = 12000 \ ft \approx 3660 \ m.$$

Note that since the shock wave has not reached the ground, the one side of the previous "triangle" is all that was needed to find the radius.

Fireball Radius at Hydrodynamic Separation

This section describes how the fireball radius at hydrodynamic separation was found. This value will be used to help determine the elements present in the fireball at the time of interest later in this chapter.

Recall from Chapter 2 that hydrodynamic separation is the point at which the shock wave begins to grow faster than the fireball, and separates from it. The radius

at which this process occurs needed to be found. The following equation gives this approximate radius in terms of the yield:

$$R_{HS} = 47(Y_{MT})^{0.324} \left(\frac{\rho_{alt}}{\rho_{sl}} \right)^{-1/2} \tag{7}$$

where R_{HS} is the radius of hydrodynamic separation in meters, Y_{MT} is the yield in MT, and ρ_{alt} and ρ_{sl} are the air densities at the altitude of burst and sea level, respectively. This radius was computed for the 20 kT burst, which has an air density of $\rho_{alt} \approx 1.2 kg/m^3$ at 1800 ft [23], with the sea level density being is $\rho_{sl} = 1.225 kg/m^3$. Thus the radius of hydrodynamic separation was found:

$$R_{HS} = 47 \left(\frac{20}{1000} \right)^{0.324} \left(\frac{1.2}{1.225} \right)^{-1/2} \approx 13.4 \ m.$$

For the 1 MT burst, the air density is $\rho_{alt} \approx 0.8$ at 13645 ft [23], so:

$$R_{HS} = 47 \left(\frac{1000}{1000} \right)^{0.324} \left(\frac{0.8}{1.225} \right)^{-1/2} \approx 58.2 \ m.$$

Summary

Table 2 shows the results of all of the above calculations.

<center>Table 2. Table of Input Values</center>

	20 kT	1 MT
Height of Burst (m)	550	4160
Time (s)	1	5.6
Power (J/s)	3.5×10^{12}	3.1×10^{13}
Fireball Radius at TOI (m)	230	1100
Shock Radius at TOI (m)	730	3660
Air Density (kg/m^3)	1.2	0.8
Fireball Radius at HS (m)	13.4	58.2

3.3 Chemical Makeup of Dust and Gas by Zone

This section shows how the elemental composition of the gas and dust in three different areas was determined: in the fireball, outside the fireball but inside the shock wave, and outside the shock wave. No distinction will be made yet between what will be gas and what will be dust; that is the next step in the process and will occur later in this chapter. A few vital assumptions were necessary before starting. As stated earlier, the time of interest was made as early as possible to minimize the mixing between the components inside and outside the fireball. With this value thus minimized, there was assumed to be no mixing. A clear distinction could thus be made between the composition inside vs. outside the fireball, and each could come from different sources.

The materials inside the fireball came from two different sources: the weapon debris and air that was ionized during the initial fireball growth. The exact specifications of the weapon debris obviously depend on the weapon design, and due to the classified nature of most weapons it will be necessary to make some estimates. Outside the fireball and inside the shock wave is just air (since no mixing, and thus no escaped weapon debris is assumed). However, the density of the air must be determined, with a distribution caused by the shock wave. Finally, outside the shock wave it is assumed that there is just air, of normal atmospheric density based on the altitude.

Due to the way the input files are organized, all of the values need to be found relative to the local hydrogen density. So, for each zone the distribution of hydrogen in the zone is needed, along with the distribution and amount of the other elements relative to hydrogen.

Weapon Debris

This section shows how an approximate model of a nuclear weapon was used to determine the number of moles of the most prominent elements in the fireball. Since Fat Man's design is well known, this was used for the 20 kT weapon.
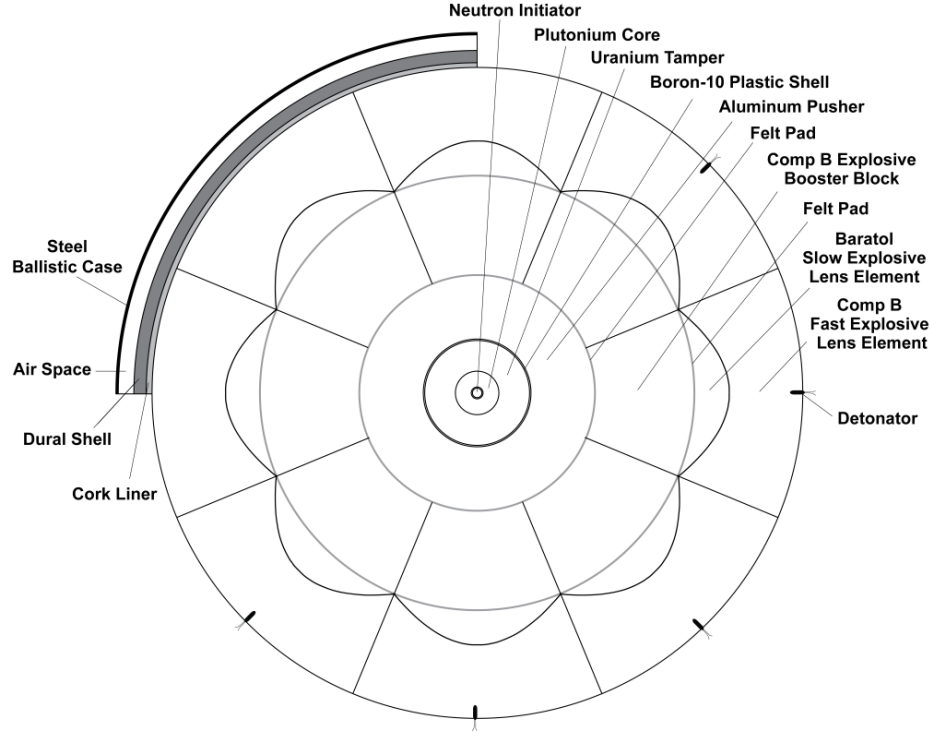
Figure 5. Cross-section of the device inside Fat Man. Reproduced with permission from [7].

Figure 5 is a cross-section of Fat Man. All of the dimensions of the different sections are known, which will be used to compute the number of moles of each element in the bomb. Not every piece mentioned in the figure will be used, since some of them occur in relatively insignificant amounts and can thus be omitted. The pieces that were omitted are the initiator, the boron-plastic shell, the felt pads, and the cork liner. It will be further assumed that the duraluminum, which is 90% aluminum, is 100% aluminum [24], that the steel shell, which is around 98% iron, is 100% iron [25], and that the natural uranium, which is usually around 99.3% U-238,

is entirely U-238 [26].

In order to compute the number of moles of each element included in the debris, it was necessary to know a few things: the elemental composition of each material in the weapon, the mass of that material, and the molecular weight of each element. Table 3 below shows the first two of these. Most of the masses were provided in a description of the weapon, but for some only the dimensions were provided and the mass needed to be computed based on the density and volume (these are the starred mass values) [7]. The mass of the steel casing was calculated based on the assumption that all of the mass not accounted for in the weapon components was part of the "steel armor egg" that surrounded the weapon [7].

Using the results from Table 3, the masses all of the different molecules were added to get the total masses in Table 4. The molecular weights, in g/mol, were then used to find the number of moles of each molecule, by dividing the mass by the molecular weight.

The results of this are shown in Table 4. After finding this value, the number of moles of each molecule, it was possible to find the number of moles of each element. This was done for every element in the debris, adding the contributions from the different molecules together. This process resulted in Table 5.

The 1 MT weapon design was based on the device that was used for Operation Dominic Harlem. The device that was tested was a W-47Y2 Polaris warhead, which was designed to be put in a nuclear submarine missile [30]. For this test, however, it was put into a Mk-36 bomb casing and dropped from a plane [31]. The Mk-36 bomb casing was meant for a 9-10 MT bomb, and together with its intended device resulted in a mass of almost 8000 kg [32]. The Harlem device, meant for a submarine based missile, only had a mass of 350 kg [31]. Together with the the Mk-36 bomb casing it was 4272 kg [33], giving the Mk-36 casing a mass of 3922 kg (all of which were

Table 3. Table of Weapon Debris, 20 kT. (*based on density/volume calculations, **made final mass correct) [7]

Section	Description	Composition	Mass (kg)
Plutonium Core	Highly Enriched Pu	Pu-239	6.2
Uranium Tamper	Natural U	U-238	108
Aluminum Pusher	Aluminum	Al	130
Inner Explosive	Comp B (64% RDX, 36% TNT) [27]	RDX: $C_3H_6N_6O_6$, TNT: $C_7H_5N_3O_6$ [27]	590
Explosive Lens	25% Baratol, 75% Comp B [7]	Baratol: 33% TNT [28], 67% $Ba(NO_3)_2$ [27]	1800
Duraluminum Case	Aluminum	Al	456* [29]
Inner Steel Case	Steel	Fe	543* [29]
Outer Steel "Egg"	Steel	Fe	1036.8** [29]
Total Mass			**4670**

Table 4. Table of Moles of Molecules in Weapon Debris, 20 kT

Molecule	Mass (kg)	Molecular Weight (g/mol)	Number of Moles (mol)
Pu-239	6.2	239.05	25.9
U-238	108	238.03	454
Al	586	26.98	2.17×10^4
Fe	1580	55.85	2.83×10^4
RDX ($C_3H_6N_6O_6$)	1164	222.12	5240
TNT ($C_7H_5N_3O_6$)	924.5	227.13	4070
Barium Nitrate ($Ba(NO_3)_2$)	301.5	347.45	868

Table 5. Table of Moles of Elements in Weapon Debris, 20 kT

Element	Moles
Pu-239	25.9
U-238	454
Al	2.17×10^4
Fe	2.83×10^4
C	4.42×10^4
H	5.18×10^4
N	4.54×10^4
O	6.11×10^4
Ba	868

assumed to be steel, and thus iron).

Unfortunately, that is where the publicly available information ends. Since the W-47Y2 device was a two-stage thermonuclear device [31], it was necessary to account for the materials in both the primary and secondary. By mass, this would be largely depleted uranium from the secondary, so a mass of 300 kg for U-238 was assumed. The rest of the secondary would be mostly lighter elements, so they were disregarded.

All of this left 50 kg for the primary. It was assumed to have similar components to Fat Man (in terms of weight ratios), but it was necessary to scale it down considerably to end up with the correct mass. This was done by multiplying each relevant mass from Fat Man by the ratio of the masses of each device. The results of this are shown in Table 6 below.

Table 6. Table of Scaled Masses, 1 MT

Section	Mass in 20 kT	Mass in 1 MT
Plutonium	6.2	0.1
Uranium Tamper	108	1.7
Aluminum Pusher	130	2.1
Inner Explosive	590	9.6
Explosive Lens	1800	29.1
Duraluminum Case	456	7.4
Total Mass	**3090.2**	**50**

Since the plutonium value is so small, it was assumed to be 0. It should be noted that, though this method may seem too approximate to be useful, the vast majority of the mass is known to be iron from the Mk-36 case, and thus these smaller values will not make much of a difference. They will still be included, but the most influential part will be the iron. Since it was therefore known how much of each element was in the debris, it was possible to perform the same calculations that were done for Fat Man, producing the same Tables (Table 7, 8, and 9), ending with the total number of moles of each element.

In the future, the barium will be omitted from the calculations. This is because

Table 7. Table of Weapon Debris, 1 MT

Section	Description	Composition	Mass (kg)
Uranium Tamper	Natural U	U-238	1.7
Aluminum Pusher	Aluminum	Al	2.1
Inner Explosive	Comp B (64% RDX, 36% TNT) [27]	RDX: $C_3H_6N_6O_6$, TNT: $C_7H_5N_3O_6$ [27]	9.5
Explosive Lens	25% Baratol, 75% Comp B [7]	Baratol: 67% $Ba(NO_3)_2$ [27], 33% TNT [28]	29.1
Duraluminum Case	Aluminum	Al	7.4
Uranium of Secondary	Depleted Uranium	U_{238}	300
Steel Case	Steel	Fe	8647
Total Mass			**9420**

Table 8. Table of Moles of Molecules in Weapon Debris, 1 MT

Molecule	Mass (kg)	Molecular Weight (g/mol)	Number of Moles (mol)
U-238	301.7	238.03	1270
Al	9.5	26.98	351
Fe	3922	55.85	7.02×10^4
RDX $(C_3H_6N_6O_6)$	18.8	222.1	84.8
TNT $(C_7H_5N_3O_6)$	15.0	227.1	65.9
Barium Nitrate $(Ba(NO_3)_2)$	4.9	347.45	14.0

Table 9. Table of Moles of Elements in Weapon Debris, 1 MT

Element	Moles
U-238	1270
Al	351
Fe	7.02×10^4
C	1100
H	1310
N	737
O	861
Ba	14.0

there is a relatively insignificant amount of it, so it will not make a difference. It is noted that although the amounts of plutonium and uranium may be similarly small, they are elements that will be present in almost every nuclear explosion, and thus it is important to make sure the code is able to deal with them. No such concerns exist regarding barium.

Air

This section will show how the distribution of the air in the first two zones was determined: inside the fireball, and outside the fireball but inside the shock wave (the third zone, outside the shock wave, has air or normal atmospheric composition and density).

The methods used for both zones depended on knowing the densities of different elements in regular air, so these values needed to be found first. Though the amount of water in air depends on the humidity, a value of 1% (0.01 moles of H_2O per mole of air) was assumed, with the rest of the air being 78% N_2 and 21% O_2 [34]. These values, along with the molecular weights of the compounds, are shown in Table 10 below.

Table 10. Table of Molecules in Air

Molecule	Mole Fraction	Molecular Weight
	mol/mol air	*g/mol*
N_2	0.78	27
O_2	0.21	32
H_2O	0.01	17

The values that were needed were the amounts of each element when the molecules split into their component elements (which they are at the temperatures of the fireball). The values were needed in terms of the hydrogen density.

The equation below was used to find the total number of moles of atoms per mole

of molecules:

$$n_{atoms} = 2n_{N_2} + 2n_{O_2} + 3n_{H_2O}$$
$$= 2.01 \tag{8}$$

where each n_x value describes the number of moles of x.

The moles of each element per mole of air molecules were then found. The results of this are shown in Table 11. Column 2 was found, for each element, by multiplying the number of atoms of that element in each molecule by the mole fraction of that molecule in air, and adding the products together. An example calculation for oxygen is below:

$$mol_O = 0.78n_{N_2,O} + 0.21n_{O_2,O} + 0.01n_{H_2O,O}$$
$$= 0.78 * 0 + 0.21 * 2 + 0.01 * 1 \tag{9}$$
$$= 0.43$$

where $n_{N_2,O}$ is the number of atoms of oxygen per molecule of N_2 (the other molecule variables are defined similarly).

Column 3 was found by dividing all of the column 2 values by the total number of moles of atoms per mole of air molecules, 2.01. Finally, column 4 was found by dividing column 3 by the elemental mole fraction of hydrogen.

Table 11. Table of Elements in Air

Element	Moles/Mole of Air Particles	Mole Fraction	Moles/Mole H
H	0.0201	0.00995	1.00
N	1.56	0.776	78.0
O	0.430	0.214	21.5

At this point, the only number that was still needed in order to fully define the number of constituent particles in the fireball due to ionized air was the hydrogen

density of regular air (since the fractions of the other particles in terms of hydrogen were known).

In order to compute this value, the total mass of 1 mole of air was needed. This was found by multiplying the molecular weights of each molecule by their mole fraction (all from Table 10), and adding the products together. It was determined that 1 mole of air has a mass of around 28.74 g.

The hydrogen density was computed using the equation below:

$$n_{H,normal} = N_A f_H \rho_{air,alt} m_{mol\ air} \qquad (10)$$

where $n_{H,normal}$ is the hydrogen number density of normal air (at a given altitude) in num/cm^3, N_A is Avogadro's number, f_H is the number of moles of H atoms per mole of air, $\rho_{air,alt}$ is the mass density of normal air at a given altitude, and $m_{mol\ air}$ is the mass of a mole of air in g.

Table 12 below shows the results of this, given the air densities at each altitude [23].

Table 12. Table of Hydrogen Density at Different Altitudes

Bomb	Altitude	Air Density	H Density
	cm	g/cm^3	num/cm^3
Fat Man	5.50×10^4	1.2×10^{-3}	5.03×10^{17}
Harlem	4.16×10^5	8×10^{-4}	3.35×10^{17}

These hydrogen density values are necessary for all three zones of the problem, and they will now be used to find the hydrogen distributions in each zone.

The hydrogen distribution in the fireball volume was computed first. The air inside the fireball at the time of interest was all air that was enveloped by the growing fireball before hydrodynamic separation. This is because, after hydrodynamic separation, the shock wave pushed any air that it encountered outward, keeping it from being engulfed

by the fireball. However, before hydrodynamic separation the fireball was growing with the shock wave, and thus most of the air stayed inside. This was a bit of an overestimate, since some air must have been used to build up the shock wave and thus would not remain in the fireball, but it was a sufficient estimate. It was assumed that the air from the time of hydrodynamic separation was homogeneously distributed throughout the fireball at the time of interest.

Given the hydrogen density values from Table 12, the total amount of hydrogen in the fireball was found, which was then combined with the total number of moles of each element from the weapon debris. The total number of moles of hydrogen were found by multiplying the density of hydrogen in regular air by the volume of the fireball at hydrodynamic separation (for the reasons stated above, using the radius at hydrodynamic separation that that was found earlier in the chapter). It was then possible to find the total amount of nitrogen and oxygen by multiplying the amount of hydrogen by the respective mole fractions that were previously found. Tables 13 and 14 show the results of these calculations.

Table 13. Table of Hydrogen in Fireball from Air

Bomb	H Density	Vol at HS	Total Moles of H
	num/cm^3	cm^3	mol
20 kT	5.03×10^{17}	1.00×10^{10}	8.36×10^3
1 MT	3.35×10^{17}	8.24×10^{11}	4.59×10^5

Table 14. Table of Elements in Fireball from Air

Element	Moles/Mole H	Total Moles (20 kT)	Total Moles (1 MT)
N	78.0	6.52×10^5	3.58×10^7
O	21.5	1.80×10^5	9.86×10^6

The next zone that was examined is the volume between the fireball and the shock wave. The only component that needed to be considered was the air, and all that occurred to affect the air was that it was pushed outward by the shock wave, changing

the density (but not the composition). In order to find the new density distribution, the Sedov-Taylor solution for blast waves was used. This solution provided the density distribution between the explosion point and the shock wave.

In an article by D.L. Book [35], explicit equations are given for finding the Sedov-Taylor solution. These equations were programmed by Lieutenant Colonel Brian J. Fry (see Appendix B). This solution is useful because it provides the density, pressure, and velocity of the gas inside the shock wave in terms of what the values are in ambient air.

There were only three input values needed for the code. The first was ω, which describes the original density distribution ($\omega = 0$ in this case, since the atmosphere has an approximately uniform density) [35]. The second was ν, which is the number of dimensions that were desired to perform the calculation in ($\nu = 3$). The last was γ, the adiabatic index. This value is $\gamma = 7/5$ for a diatomic gas, which is approximately valid for air [36]. When all of these values were put into the code, the plot in Figure 6 was produced.

The x-axis shows the ratio of the radius to the shock wave radius (so that the value of 1 is at the shock front). The y-axis gives the percentage of each of the three quantities in terms of their value outside the shock wave (ambient air). Since hydrogen density for ambient air at the given altitude was already found, the distribution of hydrogen between the fireball and shock wave has thus been fully determined.

Combining Air and Debris

At this point, all of the contributing components of dust and gas have been found, both in the fireball and outside of it. Tables 15 and 16 show the total number of moles of each element in the fireball, from weapon debris and air, for the different yields.

Note that only the number of moles of each were needed because it was still nec-
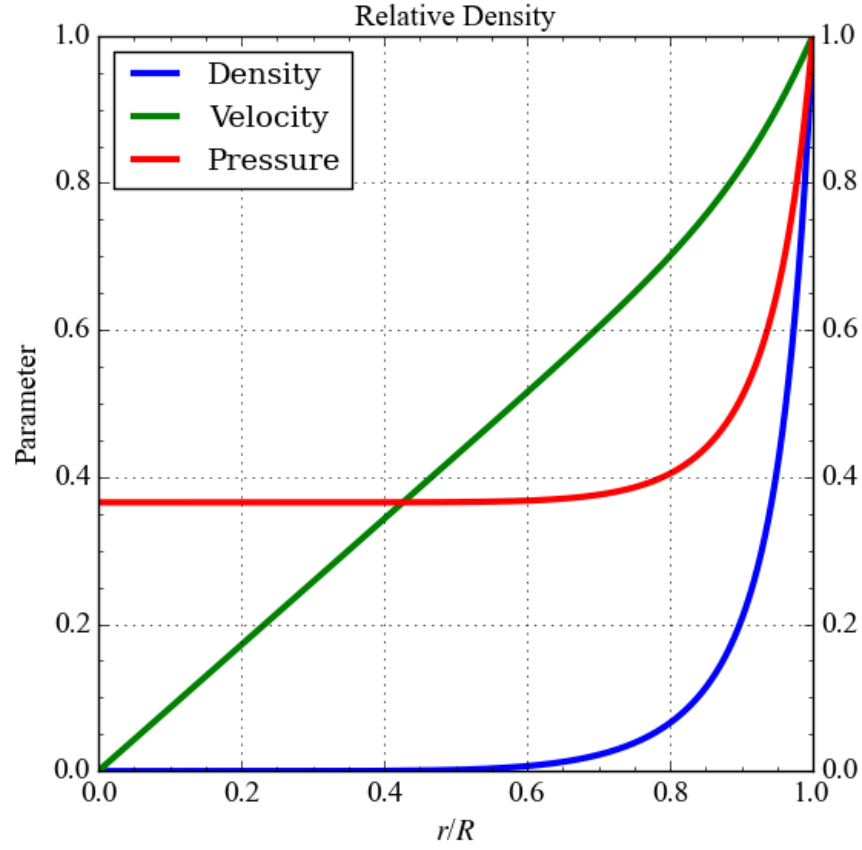
Figure 6. Graphical output of Sedov-Taylor calculations, from code produced by Lieutenant Colonel Brian Fry.

Table 15. Table of Total Moles of Elements in Fireball, 20 kT

Element	Moles From Weapon	Moles From Air	Total Moles
Pu-239	25.9	0	25.9
U-238	454	0	454
Al	2.17×10^4	0	2.17×10^4
Fe	2.83×10^4	0	2.83×10^4
C	4.42×10^4	0	4.42×10^4
H	5.18×10^4	8.36×10^3	6.02×10^4
N	4.54×10^4	6.52×10^5	6.97×10^5
O	6.11×10^4	1.80×10^5	2.41×10^5

Table 16. Table of Total Moles of Elements in Fireball, 1 MT

Element	Moles From Weapon	Moles From Air	Total Moles
U-238	1270	0	1270
Al	351	0	351
Fe	7.02×10^4	0	7.02×10^4
C	715	0	715
H	838	4.59×10^5	4.60×10^5
N	734	3.58×10^7	3.58×10^7
O	988	9.86×10^6	9.86×10^6

essary to determine what compounds would form, and how much of each. Eventually it will be necessary to find the total hydrogen density, and dust and gas ratios based on this hydrogen density. For the area outside the fireball, the assumption is that no dust forms, and thus the ratios and hydrogen density distribution found thus far were the only components needed.

3.4 Differentiating Between Dust and Gas

At this point all of the elements that contributed to dust and gas in the fireball have been found, and some way to determine what would form was needed. It is noted that the method was used is very approximate and probably not very accurate; this is because, though it is easy to tell what compounds are present in a dust cloud after the explosion, knowing what molecules have formed at very early times and the amounts of each is much more complicated. However, as with previous approximations, this is part of what would eventually be determined using MOCASSIN. Thus, the decision was made to spend a minimal amount of time on this issue since it would not ultimately affect whether the code worked or not.

Ultimately, it was necessary to end up with two things for the dust and gas input files:

- A list and the amount of the dust compounds that will have condensed at the

specified temperatures.

- A list and the amount of the remaining elements, which will be those in gaseous form.

Note that it was not required to know which, if any, gaseous compounds would form, since the code only accepts gas in elemental form. However, if there were any gases that would form compounds at the specified temperatures and use up elements that might otherwise go into dust compounds, it was necessary to know so that the elements could be allocated properly.

So, the first requirement was to figure out which particles would form. Several different sources were used to determine this, from both conventional explosions and supernovae. From the astrophysics side, it was noted that one of the first major compounds that is noticeable in supernovae dust clouds is CO [37]. Though CO is a gas, it will form at temperatures around 2500 K, as "the temperature in the CO region was $\gtrsim$ 2000 K..., perhaps as high as 3000-4000 K." It was known from Tables 15 and 16 that the nuclear fireball would have significantly more oxygen than carbon. So the assumption was made that all of the carbon would be used to form CO.

It was also known that "nuclear debris formed at high temperatures in explosions" would consist "primarily of oxides of uranium, plutonium, and structural metals" [14]. So, all of the metals the fireballs would have - plutonium, uranium, iron, and aluminum - would form oxides. It was unknown which oxides, especially since some metals form "suboxides" during explosions which later change into other oxide forms. For example, after aluminum in a conventional explosion melts and then becomes gaseous, it oxidizes to form suboxides like AlO and AlO_2, which then condense to Al_2O_3 after cooling down [38]. Based on Al_2O_3's condensation temperature of around 3250 K [39], condensation would be occurring at 2500 K - however, based on the very short time scales in a nuclear explosion, it would be likely that many of the suboxides

would not have condensed yet, and would still exist in gaseous form. So, an estimation was made of the percentage of aluminum in each form (with the suboxides in gaseous form, and the oxide as a dust).

A similar problem exists for the iron oxides - many exist, and it was not known which would form. Unfortunately, they are not as well studied in explosives as aluminum, so astrophysics was referenced again. Figure 7 shows how the total masses of different materials changed over time after a supernova explosion; though these specific times are obviously not relevant to the situation at hand, it was still possible to pull relevant information from the figure.
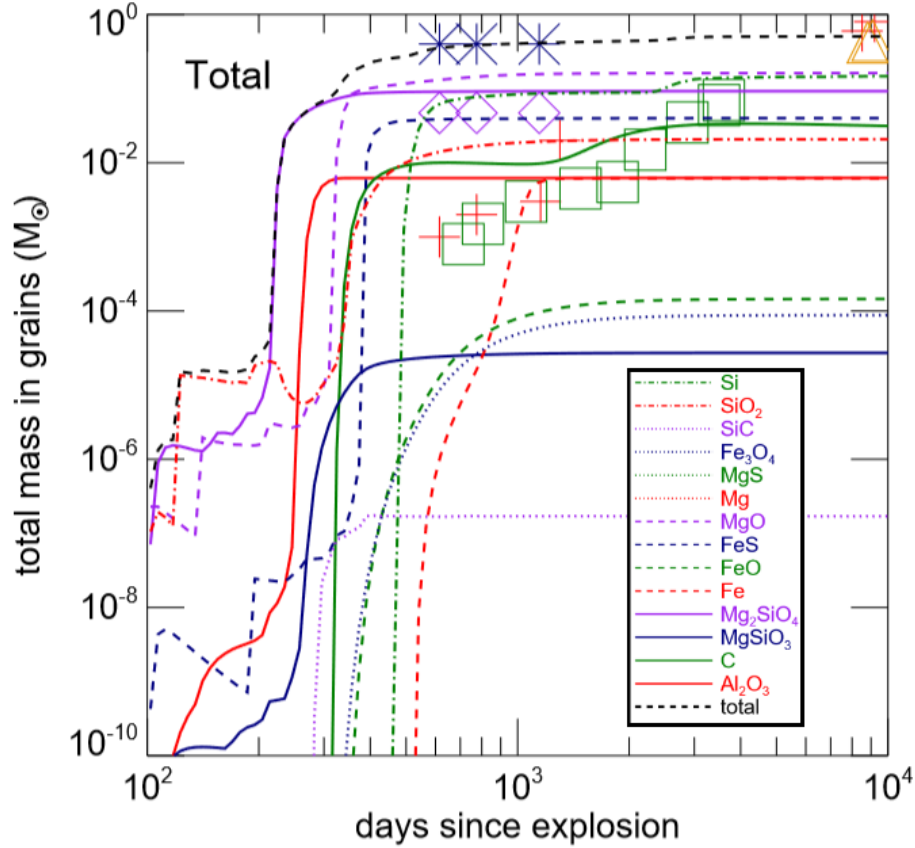
Figure 7. Time evolution of mass of different materials in the dust cloud of SN1987A. Reproduced with permission from [8].

Because there was such abundance of oxygen, the order in which any of the metal oxides formed was not important - there was enough oxygen for all, and a lot left

43

over. The main piece of information gained from Figure 7 was that FeO and Fe_3O_4 were the iron oxides present, and they would be in approximately equal amounts by mass. Though iron was also shown forming by itself, there was so much oxygen it seems likely that this would not be common. It was then checked that both of these iron oxides would be in solid form using their condensation temperatures, which are 2785 K and 2896 K, respectively [40]. Figure 7 was also used to verify that the main solid form of aluminum oxide would be Al_2O_3.

The last two metals - plutonium and uranium - would also form oxides; however, unlike aluminum and iron, it was not necessary to know the exact form. This was a result of how dust particles are defined in MOCASSIN - a table of the particle's optical constants n and k as a function of wavelength, along with a few constants, is the entire description of the particle (this will be discussed more later). Unfortunately, the optical constants of plutonium and uranium oxides have not been well researched, and the only source found was for uranium or plutonium metal with "an oxide thickness of a few nm" [9]. Thus, MOCASSIN will not differentiate between the oxides, so it doesn't matter which are formed.

It is technically still necessary to know how much of each of the oxides the fireball contained so that the amount of oxygen that was used up could be accounted for; however, there was so little plutonium and uranium, and so much oxygen, that it didn't make much of a difference. PuO_2 and UO_2 were chosen as the oxides to form. To make sure these would be solids at 2500 K, the condensation temperature of each metal oxide was checked, finding that plutonium oxide's is 3073 K [41], and uranium oxide's is over 3100 K [42].

To summarize, the following rules were used to form compounds (recognizing that there would be so much oxygen that the order wouldn't matter):

1. Use all available carbon to form CO.

44

2. Form PuO_2 and UO_2.

3. Form AlO, AlO_2, and Al_2O_3, splitting the aluminum equally between them (note - this means that there will be fewer moles of the *molecule* Al_2O_3, since each molecule requires 2 aluminum atoms). The first two are in gaseous form, while the third is a dust particle.

4. Form FeO and Fe_3O_4, splitting the iron equally between them.

5. The remaining elements - hydrogen, nitrogen, oxygen - remain in gaseous form.

It was then possible to calculate the number of moles of each of the compounds. Note that the entire mass of each of the metals was used to form oxides, while keeping track of the amount of oxygen used so that it would be known how much was left in gaseous form. Following the rules leads to Tables 17 and 18.

Table 17. Table of Oxygen Used in Dust, 20 kT

Element	Moles	Compound	Moles in Compound	Moles O	Type
C	4.42×10^4	CO	4.42×10^4	4.42×10^4	Gas
Al	2.17×10^4	AlO	7.24×10^3	7.24×10^3	Gas
		AlO_2	7.24×10^3	1.45×10^4	Gas
		Al_2O_3	7.24×10^3	1.09×10^4	Dust
Fe	2.83×10^4	FeO	1.41×10^4	1.41×10^4	Dust
		Fe_3O_4	1.41×10^4	1.89×10^4	Dust
Pu	25.9	PuO_2	25.9	25.9	Dust
U	454	UO_2	454	908	Dust
Total Oxygen Used in Dust				$\mathbf{4.48 \times 10^4}$	

At this point it was known how much of each element was used for dust vs. gas, making it possible to do some necessary calculations for each. The calculations follow in the next two sections.

45

Table 18. Table of Oxygen Used in Dust, 1 MT

Element	Moles	Compound	Moles in Compound	Moles O	Type
C	715	CO	715	715	Gas
Al	351	AlO	117	117	Gas
		AlO_2	117	234	Gas
		Al_2O_3	117	176	Dust
Fe	7.02×10^4	FeO	3.51×10^4	3.51×10^4	Dust
		Fe_3O_4	3.51×10^4	4.68×10^4	Dust
U	1270	UO_2	1270	2350	Dust
Total Oxygen Used in Dust				$\mathbf{8.46 \times 10^4}$	

Dust Summary

Note that in Tables 17 and 18 the "Moles in Compound" column recorded how many moles of an element were in the compound, rather than how many moles of the compound there were. Tables 19 and 20 show the number of moles of each compound, which were found by dividing the moles of the element by the number of atoms of that element in the compound. How these values were used is described in the 'Dust and Gas Abundance Files' section, and the files themselves can be seen in Appendix E.

Table 19. Table of Moles of Dust Molecules, 20 kT

Compound	Moles
Al_2O_3	3620
FeO	14100
Fe_3O_4	4710
PuO_2	25.9
UO_2	454

Table 20. Table of Moles of Dust Molecules, 1 MT

Compound	Moles
Al_2O_3	58.6
FeO	35100
Fe_3O_4	11700
UO_2	1270

Gas Summary

It was then necessary to find the total number of moles of each element in gaseous form. Since the moles of dust had already been found, and dust and gas were the only two options for a molecule, it was possible to just subtract the moles of each element in dust form from the total moles. See Tables 21 and 22 below for the results.

Table 21. Table of Moles of Elements in Gaseous Form, 20 kT

Element	Total Moles	Used in Dust	Left as Gas	Gas Mol/H
Pu	25.9	25.9	0	0
U	454	454	0	0
Al	2.17×10^4	1.45×10^4	7240	0.12
Fe	2.83×10^4	2.83×10^4	0	0
C	4.42×10^4	0	4.42×10^4	0.74
H	6.02×10^4	0	6.02×10^4	1
N	6.97×10^5	0	6.97×10^5	12
O	2.41×10^5	4.48×10^4	1.96×10^5	3.3

Table 22. Table of Moles of Elements in Gaseous Form, 1 MT

Element	Total Moles	Used in Dust	Left as Gas	Gas Mol/H
U	1270	1270	0	0
Al	351	243	117	0.00025
Fe	7.02×10^4	7.02×10^4	0	0
C	715	0	715	0.0016
H	4.60×10^5	0	4.60×10^5	1
N	3.58×10^7	0	3.58×10^7	77.9
O	9.86×10^6	8.46×10^4	9.78×10^6	21.3

Note that since each of the values were needed in terms of the molar ratio with hydrogen, this value was calculated as well.

3.5 Grain Radius Distribution

A list of the dust compounds that will be present in the fireball has thus been fully determined. However, to fully describe the dust grains at the time of interest,

it is necessary to know what sizes the grains will be. It is generally accepted that, in a dust cloud, the particle radii have a log-normal distribution, with a mean value of around 0.1 microns for an air burst (larger for a surface burst) [4]. However, this distribution describes the dust cloud at a much later time than the time of interest; at earlier times, particles would be smaller since they would not have had time to form. Unfortunately, there is no available information on particle sizes in the early fireball. The assumption was made that the distribution would still be log-normal, but with a mean of 0.01 microns (10 times smaller than the later time). This is another very approximate distribution that would be able to be refined with the MOCASSIN approach. Figure 8 shows the log-normal distribution of radii.
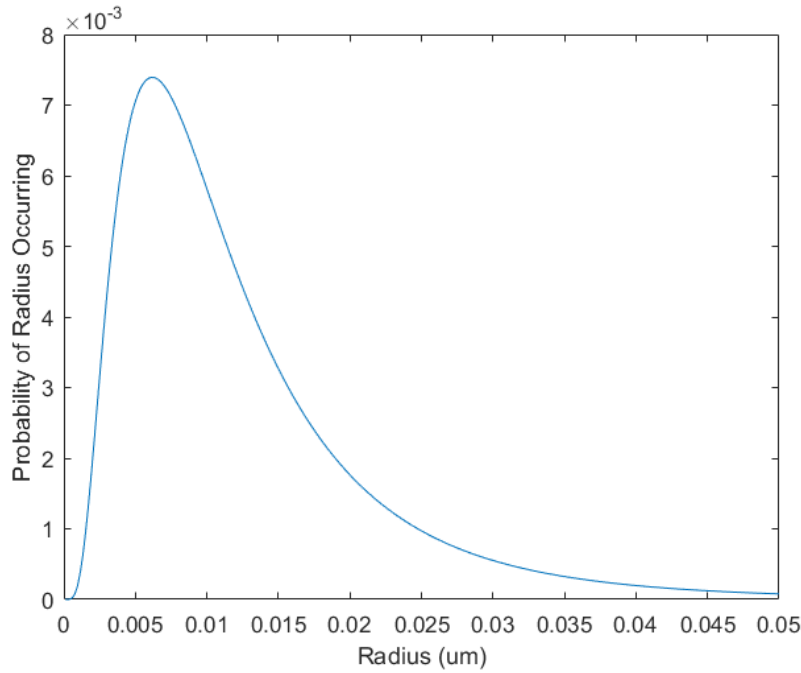
Figure 8. Probability function for grain radii (log-normal).

3.6   Creating Input Files

In this section the components that go into the actual input files for running MOCASSIN will be shown. There are five main file types that needed to be built

- the main input file, the density file, the dust abundance files, the gas abundance files, and the dust optical files. All of these together describe the fireball completely at the time of interest. There are other file types that are optional - such as a file describing the precise shape of the fireball's spectral output - but assumptions were made so that these would not be necessary. Example input files for all five file types can be found in the Appendices.

Main Input File

The most important purposes of the main input file were to describe the source (fireball temperature, power, radius), and to provide the names of the other files in use. A few assumptions went into the file: that the overall situation is spherically symmetric, and the source (fireball) emits blackbody radiation with a curve determined by the temperature. Either of these assumptions could be changed to more precisely describe the fireball; however, this was not in the scope of the project, and was not necessary to determine the viability of the process.

The input file also included information on the chosen convergence limit, number of grid points, number of photons used, and various other choices. An example input file can be found in Appendix A, with descriptions of all of the options.

Density File

The density file is the central file describing the 3D layout of the fireball, including the dust and gas. The file consists of six columns. The first three give a physical location in space (x, y, z coordinate), the fourth gives the hydrogen density at that location, the fifth gives the relevant gas file at that location, and the sixth gives the relevant dust file. There is an auxiliary density file called the "Ndust" file, which has the same three first columns as the density file, but then gives the number density of

the dust at each location.

The "mesh" of points could be split up in any way - the points do not have to be evenly spaced (this is important in a supernova, where only a relatively small area is full of anything other than empty space). The number of mesh points is restricted only by the memory of the computer being used.

It was decided to split the mesh points up evenly between the three zones - inside the fireball, between the fireball and shock wave, and outside the shock wave. This was because the fireball would be so much smaller than the other zones, and might be completely overlooked if the mesh points were spaced evenly throughout the volume.
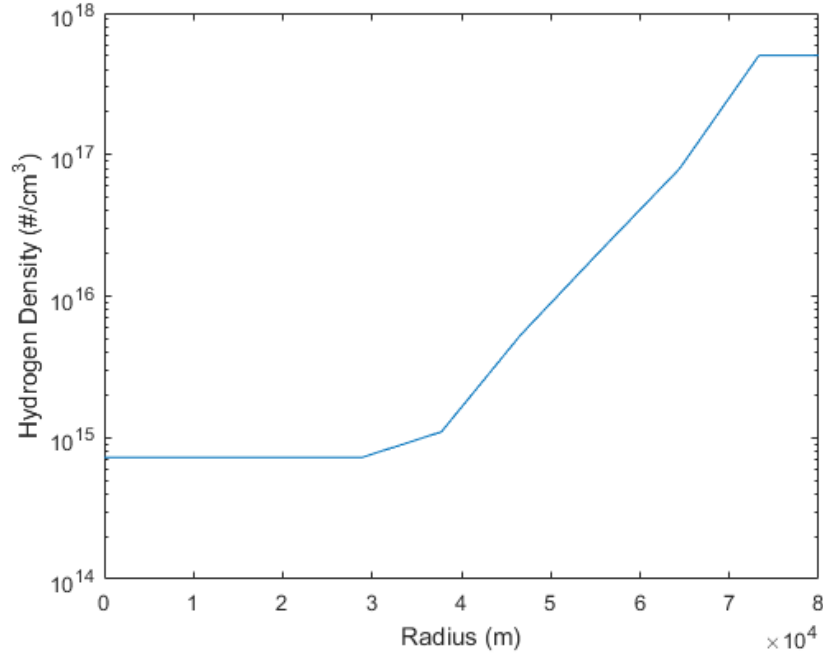
Figure 9. Hydrogen density as a function of radius from the explosion for 1 MT weapon.

Figure 9 shows the overall hydrogen density that was calculated for the 1 MT weapon (in one dimension, since it is the same in all three dimensions). In reality it would not have sharp edges like those in the figure; these are just a product of how the area was split into three zones with the density calculated differently in each. The 20 kT hydrogen density has a similar shape. Appendix C shows the code that was

50

used to create each density file, and two small example files.

Dust and Gas Abundance Files

The dust and gas abundance files are very similar. Both describe locations determined by the density file, and both give abundances of elements/compounds relative to the local hydrogen density.

Only one dust abundance file was needed, since there was only dust in the fireball. The abundance file gives the relative molar abundances of each type of dust (which should add up to one), defining each dust type by its optical file (which will be discussed in the next section).

Two gas abundance files were needed. The first describes the relative molar abundances of elements in the fireball, and the second gives the relative molar abundances of regular air. Note that the density of the air did not affect the gas abundance file itself, since the density could be changed by just changing the hydrogen density. The abundance file would stay the same, however, with hydrogen always having a value of 1. Example abundance files can be found in Appendix E.

Dust Optical Files

The dust optical files each describe one type of dust in the fireball - PuO_2, UO_2, FeO, Fe_3O_4, and Al_2O_3. They consist of a line of numbers (described below), and a list of wavelengths, with the optical constants - the refractive index n and extinction coefficient k - at each of the wavelengths. The optical constants are described first, followed by the initial numbers in the file.

Finding the optical constants was complex because the information that was needed simply did not exist in some cases. Optical constants, in general, cannot be calculated - they must be experimentally determined. And, they are not only

dependent on wavelength, they also vary based on the material's temperature. Unfortunately, the optical constants of metal oxides at 2500 K are generally not available in the literature.

A method was found for determining the temperature dependence of the optical constants [43], but it was simply too involved to be a viable option. One paper (written by the author of the book) partially used this method to find the temperature and frequency dependence of Al_2O_3, demonstrating that the method is possible [44], but it would not have been viable to do this for all of the compounds in the fireball in the given time frame. Therefore, room temperature optical constants were used for all of the compounds, with the understanding that this would increase the error of any results. (Recall as well that restrictions on the optical constants that exist was the reason it didn't matter which plutonium or uranium oxides were in the fireball, since there were only one set of optical constants for each, and they were for general plutonium or uranium oxides.)

The remainder of the optical files were then found. Several of the necessary values were more complicated than expected because of the expectations of the astrophysicists who built MOCASSIN. They did not think that anyone would use MOCASSIN for anything other than astrophysical purposes, and thus did not expect that users would need to create their own dust files (they had a large number of dust files with the types of particles that are most common in astrophysics). For that reason, the dust files all contain sections with numbers that were not explained or commented, and it was not clear what these numbers meant. By searching through all of the provided files, explanations were found for the meaning of all the numbers, but without any files or comments with more information it cannot be certain that these explanations are correct.

The first value was the sublimation temperature of the compound at the pressure

it would experience (the pressure in the fireball). In order to find this temperature, then, the pressure in the fireball was thus needed first. Fortunately, this issue had already been solved - Figure 6 shows that the pressure in the fireball would be fairly constant at around $0.37P_{atm}$, where $P_{atm} = 101\ kPa$. So, it was necessary to look for sublimation temperatures at around $37\ kPa$. Unfortunately, this was another value that proved hard to find, for the simple reason that at most pressures and temperatures of concern, metal oxides will not sublime. It was only possible to find one of the five sublimation temperatures - Al_2O_3 will sublime at that pressure at around 3000 K [29]. For the others, the sublimation temperature was replaced by the vapor pressure, which is the pressure at which a solid is in equilibrium with its vapor form at a certain temperature [29]. It was reasoned that this would be relatively close to the sublimation temperature if both the solid and gaseous forms exist at the same time. Another approximation had to be accepted, however, when it was not possible to find vapor pressure values for the metal oxides; it was necessary to accept the vapor pressures of the pure metals instead. The values are displayed in Table 23 below.

The next value in the list was less complicated - it was just the density of the material. The one after was also fairly simple - it most likely represented the mean mass of an atom in the compound, and thus the values were found by averaging over the masses of the compound's constituent atoms (the MOCASSIN authors called it the "mass of the surface atom of a grain").

The last column - dubbed by the writers of MOCASSIN as the "neutral grain potential" - was a little more difficult. Based on a paper cited within MOCASSIN's source code, it was most likely the "photoelectric yield per absorbed photon [of a] neutral surface" [45]. In this paper, they were calculating the amount of heat in an environment in space that would result from photoelectric emission of dust grains,

which makes sense for the nuclear fireball situation. The approximate equation they gave for finding this value was:

$$Y_n = 0.5(1 - V_n/h\nu) \tag{11}$$

where Y_n is the photoelectric yield, V_n is the work function of the material, and $h\nu = 13.6\ eV$. Thus, it was necessary to find the work functions for all of the compounds (they are shown in parenthesis next to the neutral grain potential values on the table). It should be noted that these values cannot be taken as exact, since work functions for metal oxides are very sensitive to the precise conditions of the compound. They are so sensitive, in fact, that one source said their "absolute value has little significance," and can depend heavily on "step or point defect densities [and] traces of adsorbed molecules" [46], among other small changes. However, all of these possibilities cannot be accounted for in MOCASSIN, and thus the values stated were used. Appendix F contains all five of the optical files that were created.

Table 23. Table of Optical File Values

Compound	$\mathbf{T_{Sublimation}}$ [29] K	Density g/cm^3	Avg. Mass [29] amu	$\mathbf{Y_n}$ [45] $N/A\ (eV)$
Al_2O_3	2750	3.97 [39]	20.4	0.445 (1.5) [47]
FeO	3000	5.7 [1]	35.9	0.358 (3.85) [48]
Fe_3O_4	3000	5.18 [49]	33.1	0.298 (5.5) [50]
UO_2	4000	10.97 [42]	90.0	0.383 (3.19) [51]
PuO_2	3100	11.5 [41]	92.0	0.272 (6.19) [52]

Radial Distribution File

The radial distribution file describes the distribution of radii for dust grains. The file has three columns - the first is the index (which just tells the line number), the second is a grains size in micrometers, and the third is the weight of that size (the weights should all add to 1). There could be as many sizes as desired to describe

the distribution. Since the distribution used was a log-normal one, a large number of sizes were desired so that the distribution would be smooth. The radial distribution file used can be found in Appendix D.

This concludes the work needed to build the input files for MOCASSIN. The next chapter will show the results of putting these files into the code.

IV. Results and Analysis

This section covers the different tests that were run using MOCASSIN, and the subsequent analysis of these tests.

To facilitate understanding of the results, a quick overview of the user experience when MOCASSIN is running is provided. Each test that runs in MOCASSIN goes through many iterations that attempt to increase the overall convergence of the cells. As the program is running, it shows the progress of the iterations - the convergence level, the run time, the current number of photons, the number of cells not hit in the grid (cells where no photon interactions occurred), and more. Each test can stop in one of three ways. Firstly, it could converge and stop on its own. Secondly, it could reach the maximum number of iterations defined in the main input file and stop. Or, under certain circumstances, it could be manually stopped by the user.

These three circumstances fit almost perfectly with three possible combinations of convergence level and "no-hit cells." When 100% convergence is reached, which always corresponds to very low percentages of no-hit cells, the program stops on its own, and produces an SED (spectral energy distribution) output. When the maximum number of iterations are reached without attaining convergence, this usually corresponds to 0% convergence levels with 100% no-hit cells, and a non-zero SED output (implying that all of the photons escaped the area of interest without interacting with any materials inside). When the program needs to be manually stopped, it is usually because it is stuck at a low convergence level, with a very high percentage of no-hit cells, and an SED of all zero values (implying that the photons were stopped at some point before reaching the outside).

It is also necessary to understand the expectations for the resulting MOCASSIN output files. The spectral output coming directly from the source is a blackbody curve, based on the source temperature (see Appendix A). The curve is affected by the dust

and gas, which will mostly create either absorption or emission lines. Therefore, it is expected that the output spectrum will be a curve that is generally shaped like a blackbody, but with some discrepancies. These discrepancies are the important part of the output - they are what will eventually be matched to an observed output, to get specific details about the dust. However, the discrepancies have to be independent of the stochastic nature of MOCASSIN, and only dependent on the input parameters.

4.1 Initial Tests

With all of the input files created, there were two initial tests to run - the 1 MT explosion, and the 20 kT explosion. Both of these tests ended up needing to be manually stopped, as they each ran for hundreds of computational hours, but did not reach 100% convergence. The 1 MT test reached 3% convergence with 95% no-hit cells in grid after the first iteration, and did not improve for the next 1300 computational hours, at which point the test was terminated. The 20 kT test achieved 0% convergence with 84% no-hit cells after the first iteration, and then stopped for the next 600 computational hours without completing any more iterations. Both ended with all spectral power values at zero.

Obviously, this was not the ideal outcome - however, it should be remembered that the fireballs were only modeled at a single point in time, with specific yields. The next step was to attempt a number of tests with slightly altered input values to see which, if any, would produce results, and how changing the code or input files could lead to more useful results. It was also decided that all of the tests would be run with just the gas in the input files, just the dust, and both, to see if one or the other was the main problem. In short, all of the subsequent tests would be attempts to isolate the variables in the code.

Since determining the viability of MOCASSIN was the main goal, and matching

data did not exist for the majority of the tests that were to be run, it should be noted that the overarching goal with running the tests was to figure out which results could and could not be obtained. The only analysis in the scope of the project will be examining the discrepancies between blackbody curves and the output files, as discussed before, testing the consistency of the output files, and comparing the 1 MT results to the Operation Dominic Harlem data.

4.2 Altering Values

In this section the test parameters will be varied, such as the gas and dust densities, the outer radii, and the temperature in the input files. Each of these will be accomplished for three files - one with just dust, one with just gas, and one with both.

Gas Only

When running tests and comparing the outputs, it was immediately apparent that the gas-only outputs would not be useful. There were two different possible outcomes after a gas-only run:

1. The test would finish the maximum number of iterations very quickly (in less than one minute, compared to hours for tests with dust), but would finish with 0% convergence, and 100% no-hit cells.

2. The test would freeze after one iteration with 0% convergence and 100% no-hit cells, and would not perform any further iterations.

The difference between these two cases was not known, nor was the reason that MOCASSIN was not even attempting to reach convergence. In an attempt to find out what had happened, the SED outputs were plotted to see what the results looked like. Figure 10 shows the outputs for three different changes that were made in the

1 MT explosion parameters, and Figure 11 shows the same for four different changes to the 20 kT explosion parameters.

(a) Initial Test

(b) Density Reduced by 10^2

(c) Outer Radius Reduced by 10^2
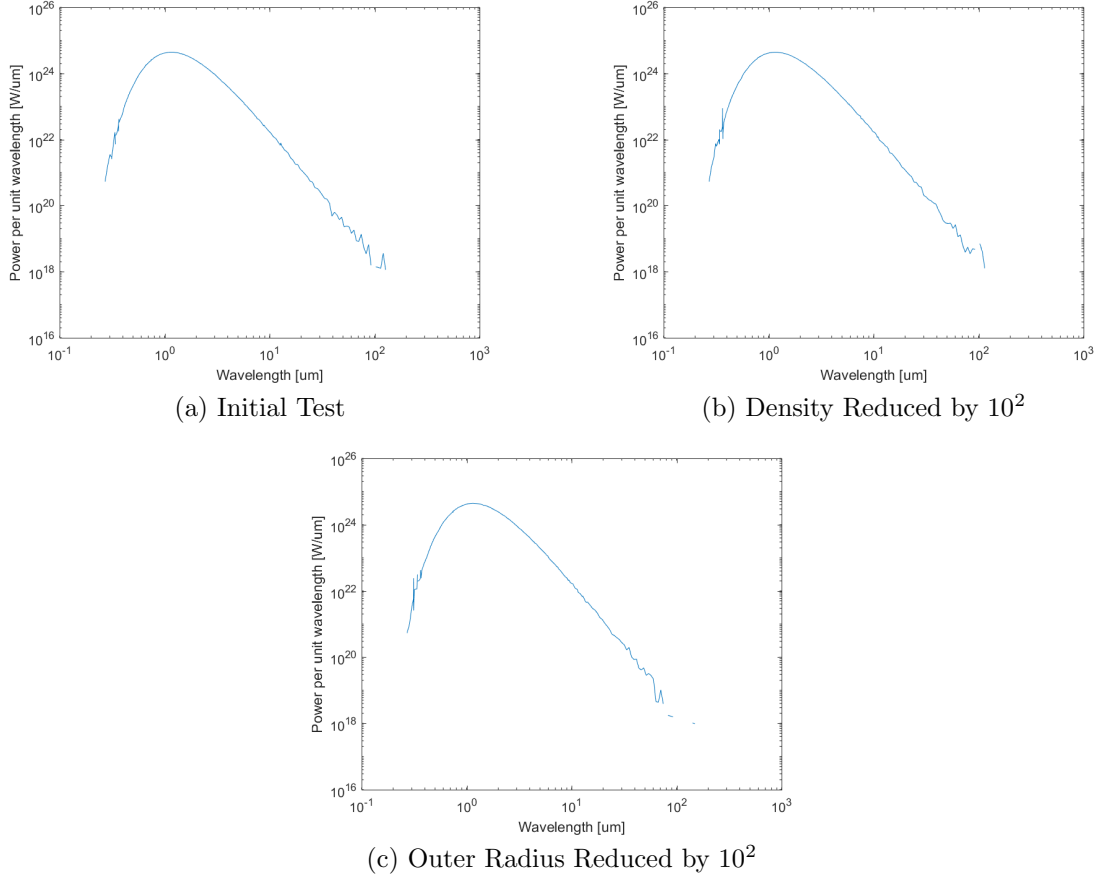
Figure 10. Spectral output trials for 1 MT with differing parameters, gas only.

These output files look about as expected - they are shaped approximately like blackbody curves, with some emission/absorption discrepancies. However, the fact that they had 100% no-hit cells (and that the tests all ran very quickly) probably means that there were no interactions between the photons and the gas. This, combined with the fact that the outputs all look basically the same, implies that the discrepancies are due to the stochastic nature of the Monte Carlo process, rather than being legitimate absorption or emission lines resulting from the code. In order to test this, the test from Figure 10 (a) was run four times, to see what stochastic
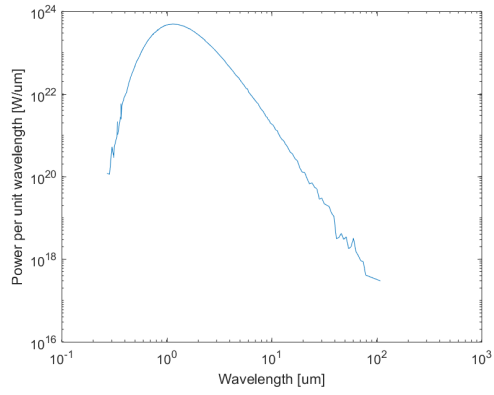
(a) Initial Test
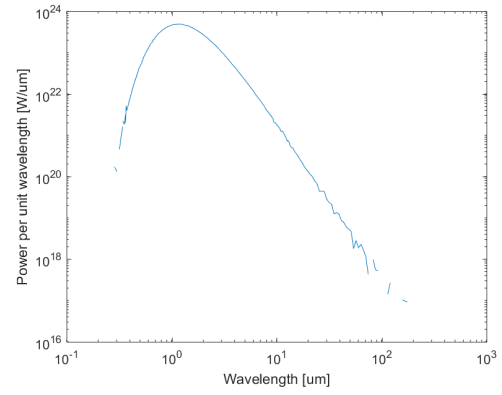
(b) Density Reduced by 10^2
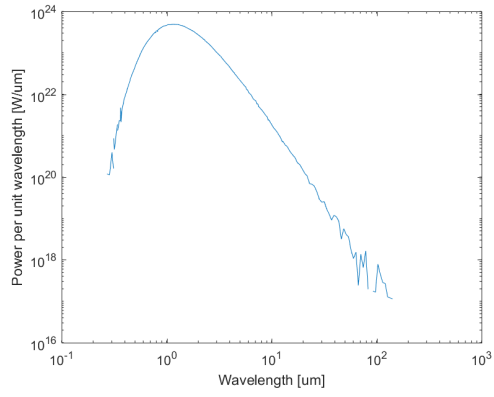
(c) Density Reduced by 10^4
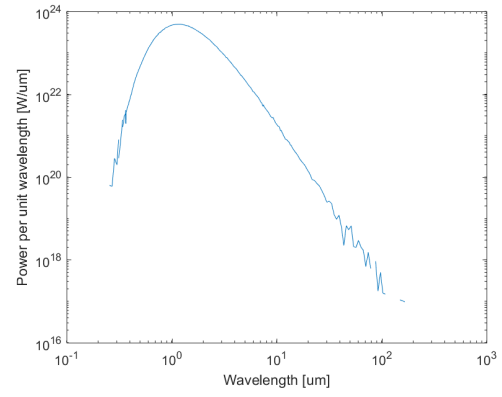
(d) Reduced Outer Radius by 10^2

Figure 11. Spectral output trials for 20 kT with differing parameters, gas only.

differences would look like. The results are shown in Figure 12.

(a) Trial 1   (b) Trial 2

(c) Trial 3   (d) Trial 4
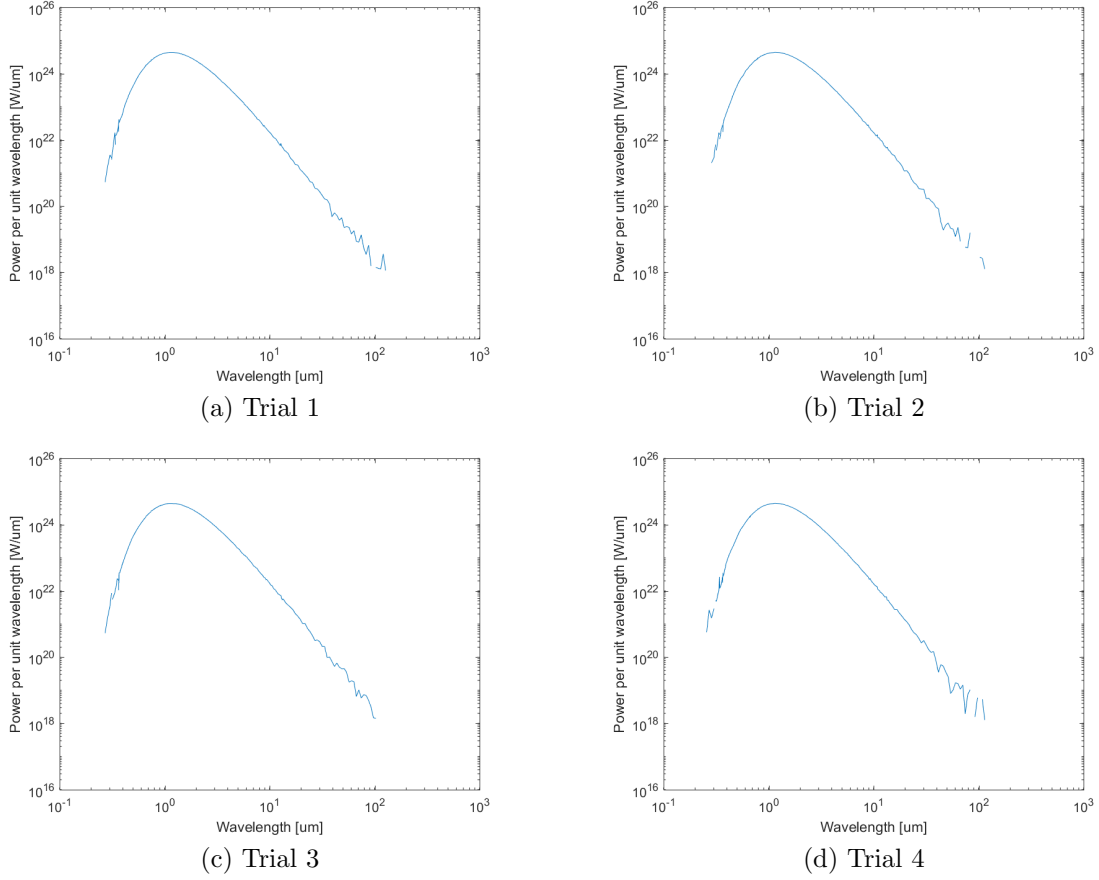
Figure 12. Spectral output trials for 1 MT, gas only.

These plots, which were all based on the same input values, look just as different as the plots from completely different input files did. This corroborates the hypothesis that the photons did not actually interact with the gas at all (as expected for 0% convergence, 100% no-hit cells), and means that gas-only runs cannot give any information about the accuracy of the input files. However, figuring out why this error is occurring could help produce actual results in a regular test.

One possible reason for the photons not interacting with the gas is that the ionization levels were not high enough in the gas. MOCASSIN's output includes a file called 'ionratio' which gives the percentage of each element in each ionization stage

(with stage 1 being a neutral element, stage 2 a singly ionized element, etc.). In all of the ratio files the stage one elements are dominant, with percentages almost always over 94%, and often at 100%. MOCASSIN's modeling of the gas depends largely on processes that occur for ions or elements, and not gaseous compounds (which are prevalent in the air, and largely in the fireball). So, if most of these elements did not fall in the right category, it is possible that MOCASSIN disregarded them, and the photons escaped from the gas and dust fields largely unaffected except by just a few interactions.

Two possible ways that the ionization levels could be increased were considered. First, the fireball could be modeled at an earlier time, when the source temperature, and thus the ionization, were higher. Or, the gas could be modeled in a different way, that would not require it to be ionized. The first option will be considered in the next section, and the second later in the chapter.

Increased Temperature

In an attempt to increase the ionization levels, the temperature of the source in the input files for both yield scenarios was raised from 2500 K to 15000 K.

The results were very similar to those at the lower temperature - the 1 MT plateaued at 4% convergence and 95% no-hit cells, and the 20 kT stopped after one iteration at 0% convergence and 94% no-hit cells.

Since the temperature was increased specifically to increase ionization levels, the ionization levels between the 1 MT test at 2500 K and the 1 MT test at 15000 K were compared. There was no significant change - for carbon, the percentage in the neutral stage went from 100% to 99.45%, nitrogen went from 100% to 99.0%, and oxygen went from 100% to 99.6%. For such a large increase in temperature, these values were smaller than expected. This was especially true after considering that, if

the fireball was being entirely modeled at a higher temperature (and thus an earlier time), the density of the dust and gas would have needed to be increased (since the fireball would not have been able to expand as much). And, modeling at earlier times did not seem useful - no dust could have formed, so even perfect spectra would not provide outputs to match the experimental spectra.

Dust Only

Since significant problems occurred with the gas-only outputs, it was possible that this was the cause of the problem with the initial tests that were run. It was decided that a dust-only test would be attempted without changing any other parameters. Unfortunately, the results were once again very similar to the initial tests. The 20 kT test had to be stopped after plateauing at 5% convergence and 94% no-hit cells, and the 1 MT test did the same, but with 3% and 96%, respectively. Unlike the gas-only tests, the SED outputs were like the initial outputs, with values of 0 for every wavelength. It had to be concluded that something else was causing the no-hit cell percentage to be high, since the SED would be a blackbody curve if the photons were all passing through the cells without interacting. The only other way that the cells could avoid interaction with every photon would be if the photons never made it to the cell - if there was some reason they were stopped before getting there. The most obvious cause of this would be a fireball density that was too high, preventing photons from escaping a small volume. In this case, only this volume would converge, leaving the rest of the mesh with no interactions. To test this, the densities of the dust and gas in the fireball were reduced, which is described in the next section.

Reduced Density

These tests were started by reducing the number densities of the gas and dust by two orders of magnitude, both inside and outside the fireball. The densities continued to be decreased by this amount until results were obtained, for tests containing just dust and both dust and gas.

Both 1 MT test - with gas and without - ran to 100% convergence and produced non-zero spectra. These spectra are shown in Figures 13 and 14.
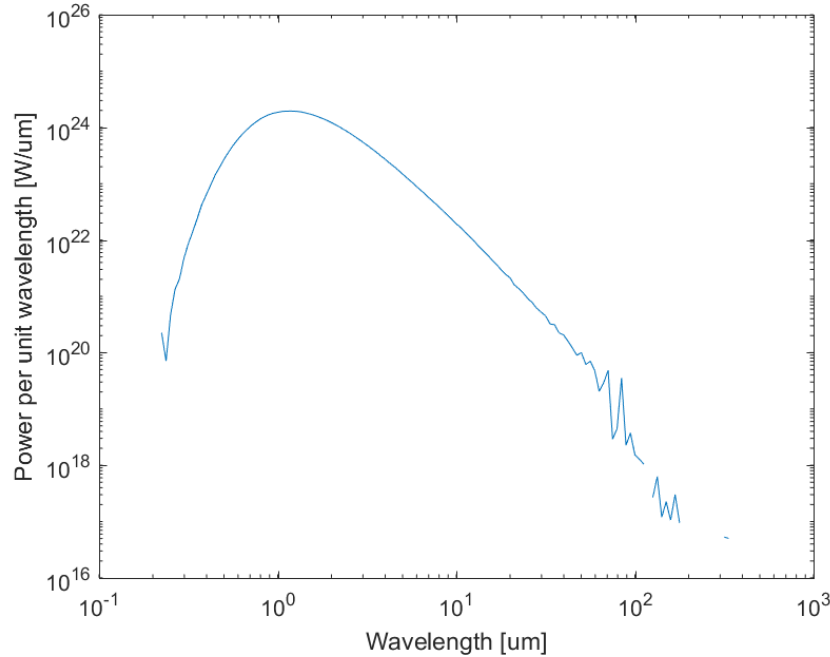
Figure 13. Spectral output for 1 MT, density reduced by 10^2, dust only.

Later Figure 14 and the observed 1 MT data from Operation Dominic Harlem will be compared; for now, it is merely noted that the overall shape of the curve is different than a normal blackbody curve, which had not previously been observed in any plots. The dust-only plot just looks like a blackbody curve; however, it ran to 100% convergence with 0% no-hit cells, so it was not yet fully discounted.

The densities were decreased in the same way for the 20 kT weapon, but the
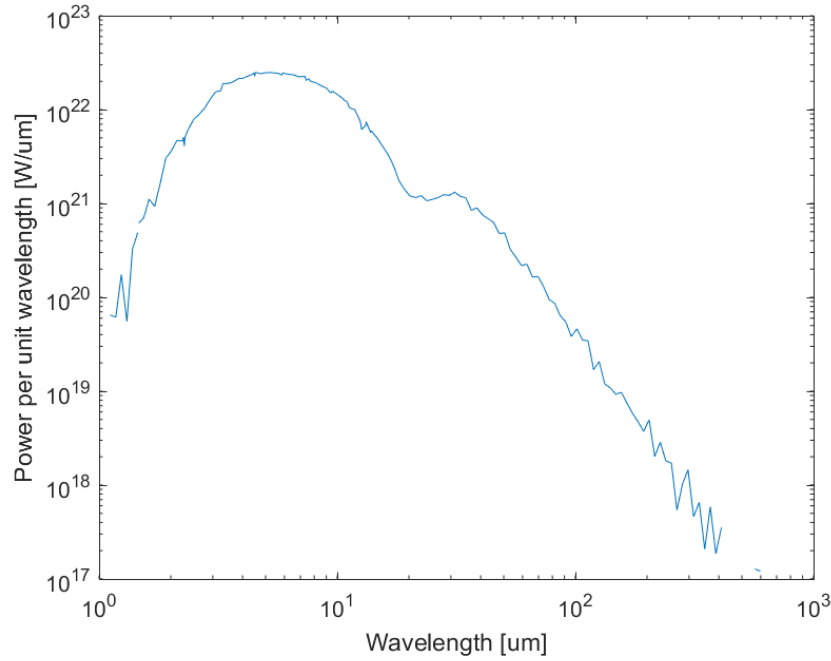
Figure 14. Spectral output for 1 MT, density reduced by 10^2, dust and gas.

results were all zero for both dust and dust and gas after decreasing the densities by two orders of magnitude. They were then decreased by two more orders of magnitude, which resulted in the spectra in Figures 15 and 16.

Figure 15 does not seem to vary much from the blackbody curve, but Figure 16 has some unique features that could be significant for characterization.

Repeated Trials

Based on previous experience with the gas results proving inconsistent after repetition, both of the 1 MT reduced density tests in Figures 13 and 14 were repeated several times to see if their features were statistically significant. Figures 17 and 18 are the results of these tests.

Though the smaller features are not consistent among each set of three plots, the general shapes and dip at the top of the curve in Figure 18 are very similar in each. The dust-only curves seem to suffer from an issue similar to the gas-only, where no
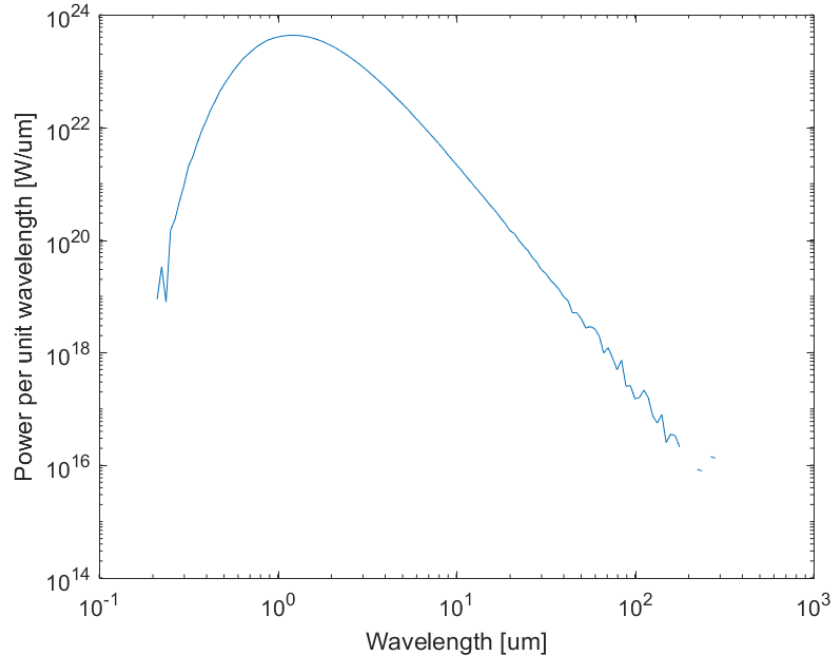
Figure 15. Spectral output for 20 kT, density reduced by 10^4, dust only.
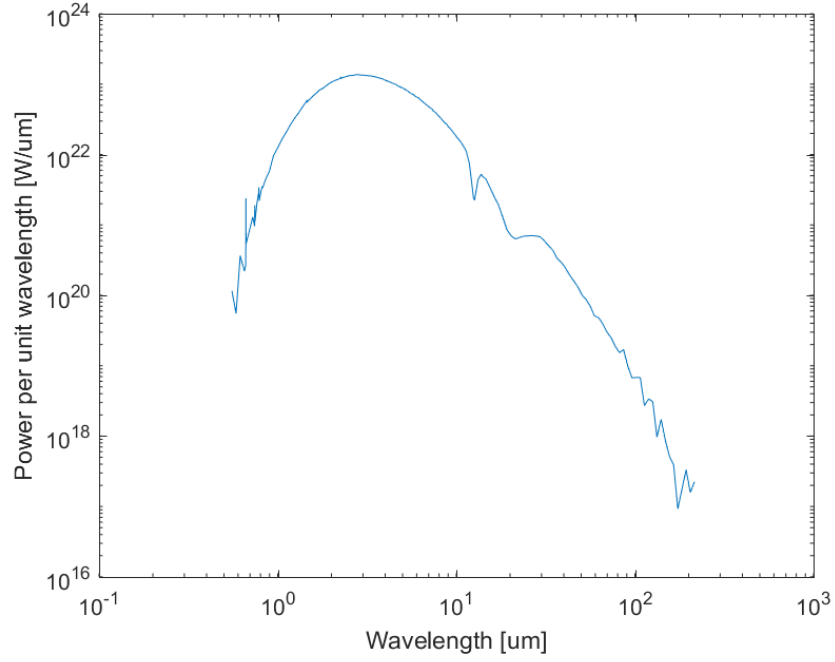
Figure 16. Spectral output for 20 kT, density reduced by 10^4, dust and gas.
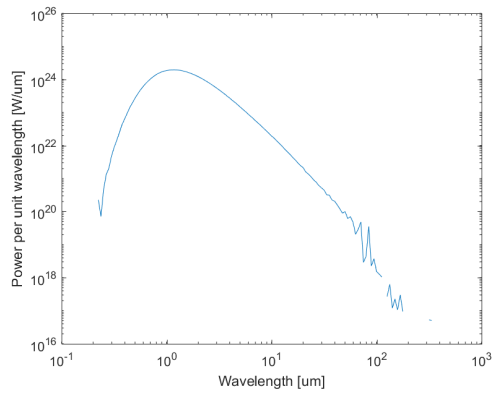
(a) Trial 1
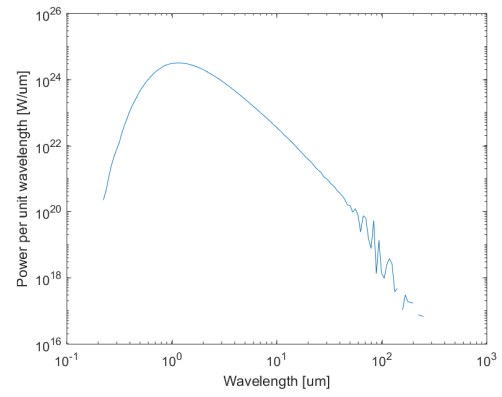
(b) Trial 2
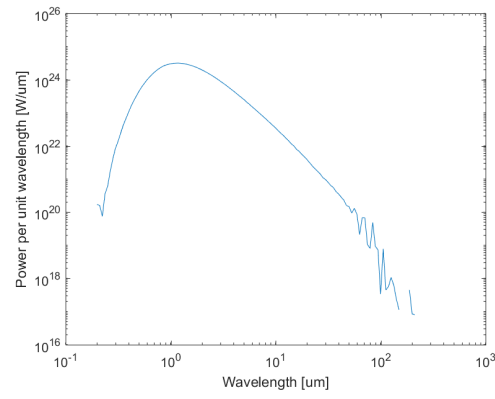
(c) Trial 3

Figure 17. Spectral output trials for 1 MT, density reduced by 10^2, dust only.
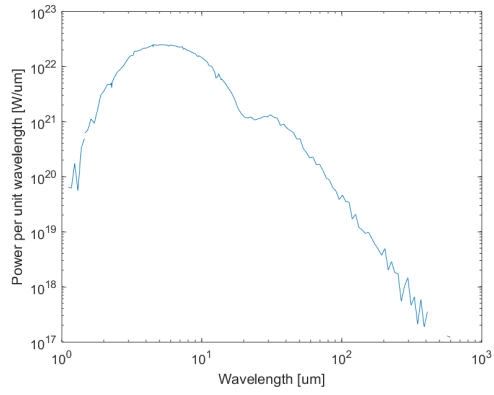
(a) Trial 1
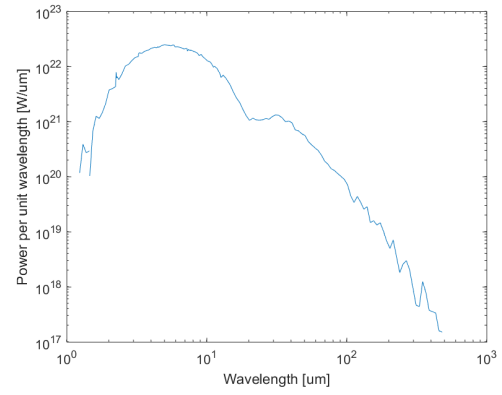
(b) Trial 2
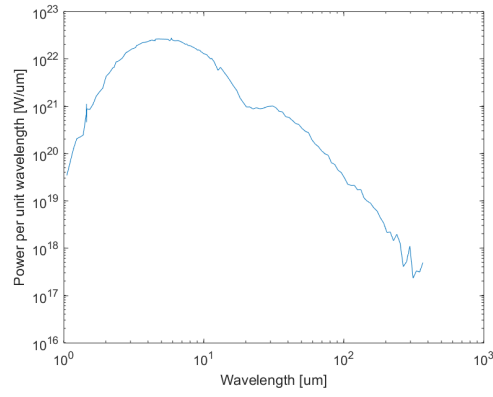
(c) Trial 3

Figure 18. Spectral output trials for 1 MT, density reduced by 10^2, dust and gas.

features appear, but the reason cannot be the same since interactions are occurring. However, since this issue did not occur for the plots with both dust and gas, which are ultimately what are important, it will not be examined further.

The next question, then, was how the reduced density could affect the sort of feature seen in Figure 18 - whether it would stay the same shape, with a smaller energy, or if the entire curve would change, leaving no recognizable features. Determining which of these is correct would indicate whether a plot with a reduced density could be potentially useful for selecting the correct input values, or if it would only be useful for testing concepts. This issue will be examined next.

Density Comparisons

In this section reduced density tests for the 1 MT weapon will be run, with densities reduced by 10^3 and 10^4 num/cm^3. The spectral outputs are shown in Figure 19.

As shown in the three figures, changing the density completely changes the spectral output. The ideal output would be three plots with the same features but different energies - unfortunately, this is not what the results showed, and thus the features of all of the plots obtained thus far are not useful. It looks like increasing the density reduces the strength of any features that might be evident - however, since these features would be the necessary factor for determining how accurate the output is, losing them is unacceptable. It is also noted that the entire curve shifts in wavelength with changing density values, meaning that it would be impossible to identify absorption or emission lines with a reduced density plot, as they would be at incorrect wavelengths.
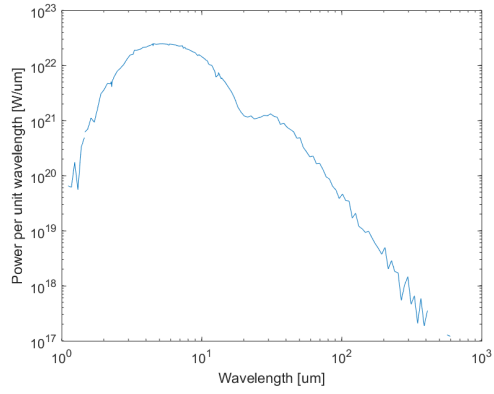
(a) Densities reduced by 10^2
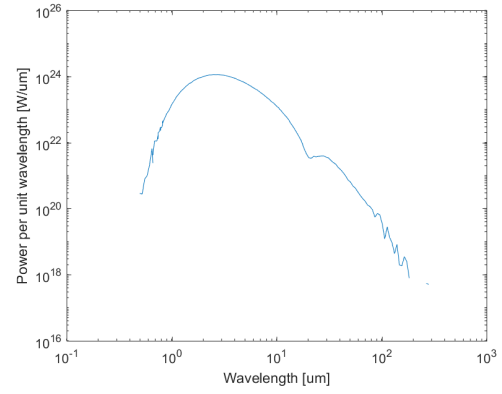
(b) Densities reduced by 10^3
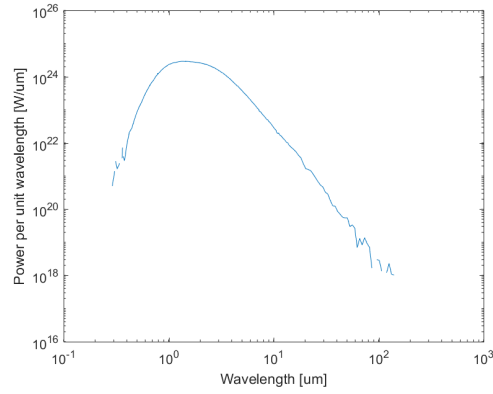
(c) Densities reduced by 10^4

Figure 19. Spectral output trials for 1 MT, densities reduced by varying amounts, dust and gas.

Reduced Outer Radius

The last change that was made was decreasing the outer radius where the SED was recorded (the outer limit of the Monte Carlo simulation). For the 1 MT tests, this radius was initially determined by the location of the aircraft that collected spectra, at a distance of around 10 times the fireball's radius. However, infrared radiation does not transport an appreciable distance in air, so it is possible that the large amount of air contributed to the empty spectra from the original tests [6]. Keeping the other variables constant, tests were run for both the 20 kT and 1 MT just outside the shock wave, just outside the fireball, and inside the fireball. All of the tests yielded SEDs of zero.

4.3   Alternate Modeling of Air

Thus far, it has been discovered that changing the density seems to be the only way to get spectra that are significant in the stochastic process, and that not much of a change is necessary to get these results. However, it is also apparent that the ionization percentages of the gases are very low, and are probably affecting the accuracy of the outputs. These problems seem impossible to resolve simultaneously - higher ionization percentages require a higher temperature, which only occurs at early times in the fireball. And at these times, the fireball density is much higher than at the values from the previous tests. The ideal situation would be to model the fireball at a later time, and have some way to model the gas without needing it to be ionized. Since the only other method of adding molecules to the MOCASSIN environment is as dust particles, it was decided to try and model the air outside the fireball using a dust optical file.

Unfortunately, issues were encountered with having two difference dust abundance files in one test. Every test that was run with two dust abundance files, regardless

71

of the rest of the parameters, ran into an allocation error. The source code was examined to find the cause. The error was within two loops: the outside loop ran once for each abundance file, and the inside loop ran once for each of the compounds within the abundance file. There was a portion of the inside loop that allocated memory for several different arrays, which were then used for all of the dust types. This section was only supposed to run one time (with the first dust compound), since an allocation error occurs if an array that is already allocated is coded to be allocated again. Unfortunately, the check to ensure it only ran one time was based on the index of the compound *in* the dust file, and not on the index *of* the dust file. This meant that when the second outside loop began, and restarted the inner loop on the new "compound #1", the code tried to re-allocate the arrays.

This issue sounds like an easy fix in the code. However, the complexity and massive size of the code (along with numerous warnings by the author), resulted in wariness of changing it at all. It is also hard to believe that a code that has been used so much (over 200 papers cited on the MOCASSIN website [20]) has such an egregious error, leading to the conclusion that something in the input files was wrong. One possibility is that something in the manual was incorrect - several other misspellings and errors were found, which seem like minor issues until they cause the code to break. It is also, of course, possible the the issue was a user error. Regardless, this attempted work-around of modeling dust as gas was not successful.

Another issue that arose with this idea was that it was only possible to have one radial distribution file, regardless of how many dust abundance files there were. This meant that the radial distribution of air molecules (which are on the order of angstroms) had to be the same as the dust particles in the fireball (which are significantly larger, especially if it had been tried at a later time in the evolution of the cloud). It is possible that there was a fix to this - there were two types of

dust optical files, the '.nk' file (which were used) and the '.q' file. However, the only description of these files is that they are "lambda dependent and radius dependent" [20], and the example showed different wavelengths having different radii. It is not clear if this would help, but it is clear that doing this change is outside the scope of the project.

4.4   Comparison With Observed Data

In this section the data from the Dominic Harlem test will be compared with the results shown thus far. Appendix G shows how the Dominic Harlem data set was used to create Figures 20 and 21 below, which show the data from two different perspectives.
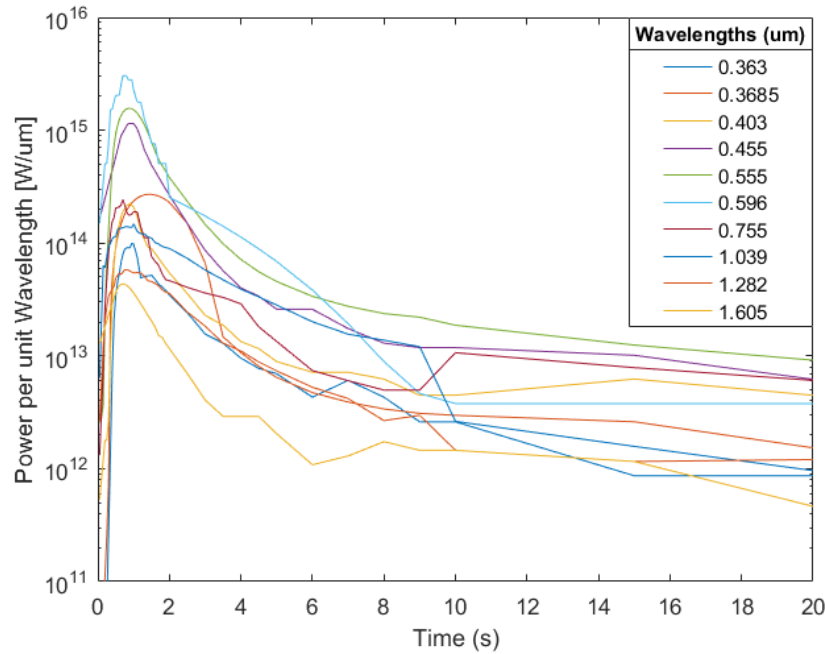
Figure 20. Spectral power as a function of time, produced from Dominic Harlem data [6].

Since the fireball plotted in MOCASSIN was at t = 5.6 s, the plot from t = 5 s (shown in Figure 22) will be used for comparison with the data.
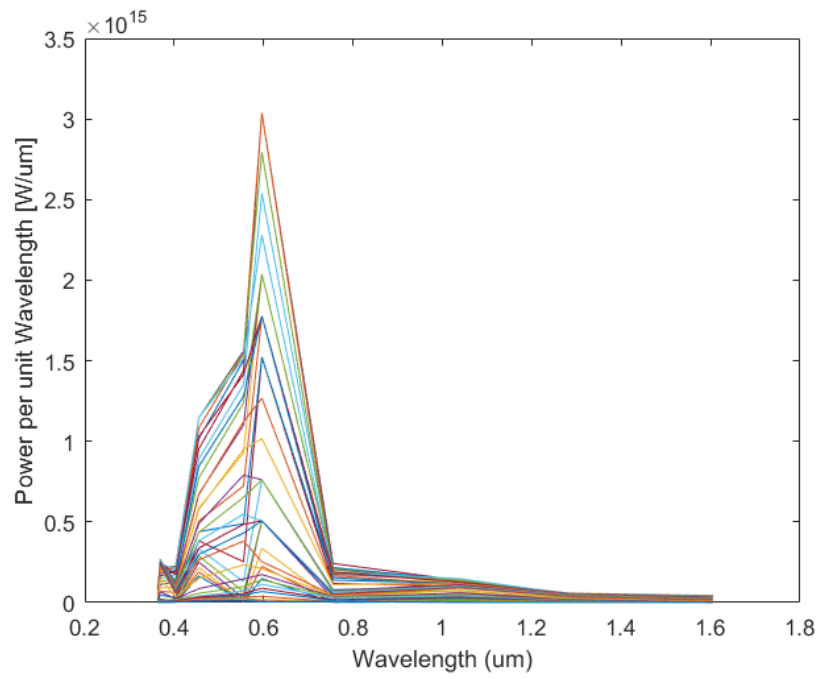
Figure 21. Spectral Power as a function of wavelength for times between 1-20 s, with different times represented by different colors, Dominic Harlem data [6].
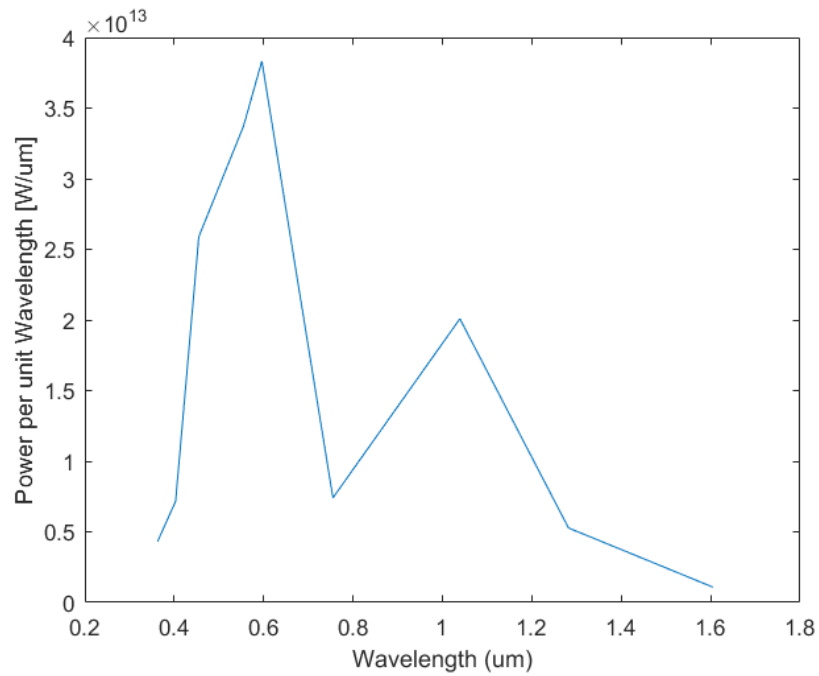
Figure 22. Spectral Power as a function of wavelength at t=5 s, Dominic Harlem data [6].

Because the data is over such a small wavelength range, it will only be possible to compare the overall energy values - any feature that size on one of the MOCASSIN results would probably not be a real feature of the spectrum (as was seen by running the same tests multiple times, it would change in another trial). However, it can be seen what the approximate energy is, which can be compared it to the energies calculated by MOCASSIN. Looking at Figure 14, which is the closest that was achieved to an actual plot for the 1 MT test, it is seen that the curve does not quite get to the 1 μm range. However, by extrapolating down a bit it can be seen that the power would be around 10^{18} or 10^{17} W/μm. Recall as well that plots with decreased density values had a wavelength shift, which would bring the power down at 1 μm even more. When the three plots in Figure 19 are examined, in can be seen that the spectral power generally decreases with rising density values. So the actual spectral power would be less than 10^{17} W/μm, probably by a few orders of magnitude.

The power values seen on the Dominic Harlem data are on the order of 10^{13} W/μm at five seconds, shown in Figure 22. These are relatively close to the extrapolated MOCASSIN spectral power.

V. Conclusions

Overall, a few issues were discovered with using MOCASSIN, both before and during the tests. The main problem before the tests was inaccuracies in the optical files. Optical constants at the correct temperatures were not found, and in some cases the constants could only be found for very small wavelength ranges. The way the sublimation temperatures and "neutral grain potential" values were calculated were also far too approximate to expect them to yield accurate results. The input values describing parts of the dust cloud - like the exact compounds and abundances - were expected to be approximate, since these would potentially be found using MOCASSIN. The optical files, however, needed to be accurate the first time to have any hope of yielding reliable results, and these files could not be generated within the scope of this work.

While running the test cases, two main problems emerged. The first was that the gas in the scenario was not at a sufficient ionization level to apply the MOCASSIN models - especially the air outside the fireball - and thus the methods used could not accurately model photons in the Monte Carlo process. The gas was always above 90% neutral atoms, and in reality would not have even been in atomic form (at least not for the outside air). The second problem was that the density values in the input files were too high, and caused the spectral outputs to go to zero. Attempting to solve these issues by increasing the temperature and decreasing the density, respectively, was unsuccessful. Increasing the temperature did not increase the ionization enough. Decreasing the density did lead to output SEDs, but it was later discovered that SED curves for different densities have different features, and are thus not effective for use in MOCASSIN. The attempted solution to these two problems was to try to model the air outside the fireball as a dust, which was unsuccessful for numerous reasons.

The overall conclusion is that MOCASSIN is not a viable option for analyzing a

nuclear dust cloud.

5.1   Future Work

Just because MOCASSIN cannot be used for nuclear dust cloud modeling does not mean that all astrophysical methods are off the table. MOCASSIN was chosen for this project because it was already complete and would *use* the source code rather than having to *build* new code. Applying MOCASSIN to the problem leveraged the work already done by the astrophysics community. The methods that were rejected early on would require the development of new source code. When dealing with a radiative transfer model, the most important differences between a nuclear explosion and supernova are the higher density values in the nuclear explosion, and the differences in ionization levels (largely due to the lower temperature). Any future model would need to be able to account for these differences. Hence, it seems a midpoint between these methods needs to be found - a modeling package where components of the code and the application of the underlying physics could be changed if necessary, since supernova and nuclear explosions are two very different phenomena, but where the inclusion of the characteristic features of nuclear explosion could be built on the previously developed features of the supernova problem.

A. Main Input File

There were two main tasks to accomplish when building the main input file - converting the values that had already been found to the correct units, and figuring out what certain options in MOCASSIN meant and how they should be used. This section will first go over the unit conversions, and then show an example input file, with explanations of the different options that were included.

Unit Conversions

There were a few numbers that were put directly into the main input file, rather than being defined in an auxiliary file. These included the inner and outer radii of the source, the "stellar temperature," or source temperature (the source in astrophysics is usually a star), the "luminosity," or power output of the source, and the minimum and maximum limits of the frequency (which determine the minimum and maximum wavelengths of the output). [53]

Building this file started with determining the inner and outer radii of the source. All length measurements in MOCASSIN are in cm, and these radii are no exception. Since the source here is the fireball, and a fireball is a full sphere, the inner radius was always 0 and the outer radius was the fireball radius.

The source temperature was also straightforward, with units of Kelvin. The source radius used in the nuclear case was usually 2500 K, except in the few trials where it was modified.

The power output of the fireball was found early in Chapter 3, but it was not in

the correct units. In MOCASSIN, the luminosity is in units of $\times 10^{36}$ erg/s. Since the fireball was much less luminous than a star, this number was always very low. The power values that were originally computed were in J/s. These were converted to erg/s using 1 J = 10^7 erg, and then divided by 10^{-36}.

The frequency limits used were numbers near those that were in all of the MO-CASSIN example files; however, it was necessary to verify that the desired spectra would fall in the range. The given values were about 1×10^{-10} and 15, with units of Rydberg energy. The conversion was done by multiplying the frequency by the Rydberg energy constant, where 1 Ryd = 2.180×10^{-18} J, and then dividing by Planck's constant $h = 6.626 \times 10^{-34}$ J*s. The resulting wavelength region was between 6.07×10^{-3} and 9.10×10^8 μm. According to Figure 6-8 in Bridgman, nearly all of the thermal energy emitted by the fireball (which is what will be seen) is within this range [4].

Example

An example input file will now be shown, with explanations of the various sections.

```
1    nPhotons 1000000
2    autoPackets 0.20 2. 10000000
3    symmetricXYZ
4    contShape  blackbody
5    maxIterateMC  20 100.
6    output
7    densityFile 'input/1density_file_test6.5_11.dat'
8    Ndust file 'input/1Ndust_test6.5_11.dat'
9    dustFile 'input/dust1MT.dat' 'input/radius_100.dat'
10   multiChemistry 2 'input/fireball_gas.in' 'input/air.in'
11   nx 16
12   ny 16
13   nz 16
14   nuMin 1.0e-10
15   nuMax 15.
16   TStellar 2500.
```

```
17   LStar 3.09E-16
18   Rin 0.
19   Rout 1.1E5
```

There are three main sections to the input file. Lines 1-6 are the first section, and they define the general parameters of the trial run (these values were held constant for all of the trials to preserve continuity in the SED outputs). Lines 7-13 give specific information regarding the auxiliary input files, and comprise the second section. The last section is lines 14-19, and this part lists the values that were described in the 'Unit Conversions' section previously. The meaning of each line is listed below in order:

1. The number of energy packets used in the Monte Carlo simulation

2. A condition on which to increase the number of photons if a convergence plateau is reached (e.g. if the amount that the convergence increases by is less than the first number, then the number of photons will increase by a factor of the second number, with a max value of the third number)

3. Enables a symmetric grid, which means that the source can be put in the corner of a grid rather than the center, and only one eighth of the volume will need to be computed

4. Defines the shape of the source's emission spectrum. A blackbody spectrum was used, since this is approximately correct for a fireball [6]

5. Defines when to stop the simulation; the first value gives the maximum number of Monte Carlo iterations that can be performed, and the second number defines the convergence level that must be reached to stop the simulation (the first number will overrule the second if the number of iterations is reached before convergence occurs)

80

6. This keyword is required for output files to be created

7. The name of the density file being used

8. The name of the Ndust file being used, with the keyword 'file' (if the keyword 'constant' is used then a constant dust number density can replace the file name)

9. The name of the dust abundance file, and the file describing the dust radius distribution

10. The number and names of the gas abundance files

Lines 11-13 are just the number of points in the density and Ndust files, and the rest of the lines were described previously. Lines 1-6 and 11-15 were the same in every input file that was run, and the others changed based on the weapon yield and the parameters of the trial.

B. Sedov-Taylor Calculations

The Sedov-Taylor code used to find the air density outside the fireball is shown here. The code was created by Lieutenant Colonel Brian J. Fry, and edited to give the density output as an array (discrete density values at certain distances from the explosion). This array was be used when creating the density files to find the hydrogen densities at mesh points outside the fireball.

Code

```python
1  # -*- coding: utf-8 -*-
2  """
3  Created on Mon Apr 14 19:22:49 2014
4
5  @author: Brian Fry
6  """
7
8  #import math
9  import numpy as np
10 import matplotlib as mpl
11 import matplotlib.pyplot as plt
12 from numpy import exp
13
14 N = 3 # number of dimensions, 'nu' in Book 1994
15 gamma = 7./5. # adiabatic index
16 omega = 0. # uniform density atmosphere
17
18 def Sedov(N, gamma, omega):
19     omega_1 = (3.*N-2.+gamma*(2.-N))/(gamma+1.)
20     omega_2 = (2.*(gamma-1.)+N)/gamma
21     omega_3 = N*(2.-gamma)
22
23     B_6 = 2./(N+2.-omega)
24     B_0 = 1./(N*gamma-N+2.)
25     B_2 = (gamma-1.)/(gamma*(omega_2-omega))
```

```python
26        B_1 = B_2+(gamma+1.)*B_0-B_6
27        B_3 = (N-omega)/(gamma*(omega_2-omega))
28        B_4 = B_1*(N-omega)*(N+2.-omega)/(omega_3-omega)
29        B_5 = (2.*N-omega*(gamma+1.))/(omega_3-omega)
30        B_7 = omega*B_6
31        B_8 = N*B_6
32
33        C_5 = 2./(gamma-1.)
34        C_6 = (gamma+1.)/2.
35        C_1 = gamma*C_5
36        C_2 = C_6/gamma
37        C_3 = (N*gamma-N+2.)/((omega_1-omega)*C_6)
38        C_4 = (N+2.-omega)*B_0*C_6
39
40        step = 10001
41
42        if format(omega, '.3f') < format(omega_3, '.3f'):
43            #print "omega < omega_3"
44            F = np.linspace(C_2, 1., step, endpoint=True)
45            xi = ((F)**(-B_6))*((C_1*(F-C_2))**(B_2))*((C_3*(C_4-F))**(-B_1)) # ...
                    xi = r/R_SN
46            D = ...
                    ((F)**(B_7))*((C_1*(F-C_2))**(B_3-omega*B_2))*((C_3*(C_4-F))**(B_4 ...
                    +omega*B_1))*((C_5*(C_6-F))**(-B_5))
47            V = xi*F
48            P = ((F)**(B_8))*((C_3*(C_4-F))**(B_4+(omega-2)*B_1))*((C_5*(C_6-F)) ...
                    **(1-B_5))
49        elif format(omega, '.3f') == format(omega_3, '.3f'):
50            #print "omega = omega_3"
51            F = np.linspace(C_2, 1., step, endpoint=True)
52            xi = ((F)**(-B_6))*((C_1*(F-C_2))**(B_2))*((C_5*(C_6-F))**(-B_1)) # ...
                    xi = r/R_SN
53            D = ...
                    ((F)**(B_7))*((C_1*(F-C_2))**(B_3-omega*B_2))*((C_5*(C_6-F))**(1.- ...
                    4.*B_0))*(exp(-N*gamma*(gamma+1.)*B_0*(1.-F)/(C_6-F)))
54            V = xi*F
55            P = ((F)**(B_8))*((C_5*(C_6-F))**(2*(N*gamma-N-gamma)*B_0))*(exp(-N* ...
                    gamma*(gamma+1.)*B_0*(1.-F)/(C_6-F)))
56        elif (format(omega, '.3f') > format(omega_3, '.3f')) & (format(omega, ...
                    '.3f') < format(omega_1, '.3f')):
```

83

```python
57          #print "omega_3 < omega < omega_1"
58          F = np.linspace(C_2, 1., step, endpoint=True)
59          xi = ((F)**(-B_6))*((C_1*(F-C_2))**(B_2))*((C_3*(C_4-F))**(-B_1)) # ...
                xi = r/R_SN
60          D = ...
                ((F)**(B_7))*((C_1*(F-C_2))**(B_3-omega*B_2))*((C_3*(C_4-F))**(B_4 ...
                +omega*B_1))*((C_5*(C_6-F))**(-B_5))
61          V = xi*F
62          P = ((F)**(B_8))*((C_3*(C_4-F))**(B_4+(omega-2)*B_1))*((C_5*(C_6-F)) ...
                **(1-B_5))
63      elif format(omega, '.3f') == format(omega_1, '.3f'):
64          #print "omega = omega_1"
65          xi = np.linspace(0., 1.0, 10000, endpoint=True)
66          D = xi**(N-2)
67          V = xi
68          P = xi**N
69      elif (format(omega, '.3f') > format(omega_1, '.3f')) & (format(omega, ...
            '.3f') < format(omega_2, '.3f')):
70          #print "omega_1 < omega < omega_2"
71          F = np.linspace(C_6, 1., step, endpoint=True)
72          xi = ((F)**(-B_6))*((C_1*(F-C_2))**(B_2))*((C_3*(C_4-F))**(-B_1)) # ...
                xi = r/R_SN
73          D = ...
                ((F)**(B_7))*((C_1*(F-C_2))**(B_3-omega*B_2))*((C_3*(C_4-F))**(B_4 ...
                +omega*B_1))*((C_5*(C_6-F))**(-B_5))
74          V = xi*F
75          P = ...
                ((F)**(B_8))*((C_3*(C_4-F))**(B_4+(omega-2)*B_1))*((C_5*(C_6-F))** ...
                (1-B_5))
76      elif format(omega, '.3f') == format(omega_2, '.3f'):
77          #print "omega = omega_2"
78          F = np.linspace(C_6, 1., step, endpoint=True)
79          xi = ((F)**(-B_6))*((C_1*(F-C_2))**((gamma-1.)*B_0))*(exp((gamma+1.) ...
                *B_0*(1.-F)/(F-C_2))) # xi = r/R_SN
80          D = ((F)**(B_7))*((C_1*(F-C_2))**(4.-N-2.*gamma))*((C_5*(C_6-F))** ...
                (-B_5))*(exp(-2.*(gamma+1.)*B_0*(1.-F)/(F-C_2)))
81          V = xi*F
82          P = ((F)**(B_8))*((C_1*(F-C_2))**(-N*gamma*B_0))*((C_5*(C_6-F))**(1- ...
                B_5))
83      else:
```

84

```python
84            #print "omega_2 < omega"
85            F = np.linspace(C_6, 1., step, endpoint=True)
86            xi = ((F)**(-B_6))*((C_1*(F-C_2))**(B_2))*((C_3*(C_4-F))**(-B_1)) # ...
                 xi = r/R_SN
87            D = ...
                 ((F)**(B_7))*((C_1*(F-C_2))**(B_3-omega*B_2))*((C_3*(C_4-F))**(B_4 ...
                 +omega*B_1))*((C_5*(C_6-F))**(-B_5))
88            V = xi*F
89            P = ...
                 ((F)**(B_8))*((C_3*(C_4-F))**(B_4+(omega-2)*B_1))*((C_5*(C_6-F))** ...
                 (1-B_5))
90
91        return xi, D, V, P
92
93   xi, D, V, P = Sedov(N, gamma, omega)
94
95   np.savetxt('I:\setup\Desktop\Thesis\MOCASSIN\Sedov.txt', np.c_[xi,D,V,P])
96
97   """
98   F_ini = C_2
99   F_fin = 1.
100
101  F = np.linspace(F_ini, F_fin, 10000, endpoint=True)
102
103  xi = ((F)**(-B_6))*((C_1*(F-C_2))**(B_2))*((C_3*(C_4-F))**(-B_1)) # xi = r/R_SN
104  D = ((F)**(B_7))*((C_1*(F-C_2))**(B_3-omega*B_2))*((C_3*(C_4-F))**(B_4+ ...
         omega*B_1))*((C_5*(C_6-F))**(-B_5))
105  V = xi*F
106  P = ((F)**(B_8))*((C_3*(C_4-F))**(B_4+(omega-2)*B_1))*((C_5*(C_6-F))**(1-B_5))
107  """
108
109  print "xi =", xi
110  print "D = ", D
111  print "V = ", V
112  print "P = ", P
113
114  params = {'legend.fontsize': 14,
115            'mathtext.fontset': 'stix',
116            'mathtext.default': 'regular',
117            'xtick.labelsize': 14,
```

```
118              'ytick.labelsize': 14} # changes font size in the plot legend

119

120  plt.rcParams.update(params)        # reset the plot parameters

121

122  mpl.rc('font',family='Times New Roman')

123

124  font = {'family' : 'Times New Roman',

125          'color'  : 'black',

126          'weight' : 'normal',

127          'size'   : 14}

128

129  legfont = {'family' : 'Times New Roman',

130             'weight' : 'normal',

131             'size'   : 14}

132

133

134  plt.figure(num = 1, figsize = [6, 6], dpi = 100, facecolor = 'w')

135  plt.title('Relative Density', fontdict = font)

136  plt.xlabel('${\it r}/{\it R}$', fontdict = font)

137  plt.ylabel('Parameter', fontdict = font)

138  plt.plot(xi, D, label = 'Density', lw = 3, c = 'b', ls = '-')

139  plt.plot(xi, V, label = 'Velocity', lw = 3, c = 'g', ls = '-')

140  plt.plot(xi, P, label = 'Pressure', lw = 3, c = 'r', ls = '-')

141  plt.minorticks_on()

142  plt.grid()

143  plt.tick_params(labelright=True)

144  plt.legend(prop = {'family' : 'serif'}, loc=2, framealpha=1.)

145  plt.show()
```

Output Array

Only the first 20 lines of the array are shown, as there are 1000. The left column is the distance from the center of the fireball, and the next three columns are the fractional density, velocity, and pressure at the given distance compared to ambient density.

```
0.000000000000000000e+00 0.000000000000000000e+00 0.000000000000000000e+00 3.654630784435998203e-01
3.765518947179079534e-01 2.046638602427038685e-04 3.227641462138456929e-01 3.654911309899206429e-01
```

86

```
4.050532162901342992e-01 3.537802773035603134e-04 3.472000440548662636e-01 3.655191868408932954e-01
4.227152218441294629e-01 4.872930667696568317e-04 3.623454493759042938e-01 3.655472459970704469e-01
4.357116908149248902e-01 6.115940875955968182e-04 3.734920613665536626e-01 3.655753084590038227e-01
4.460670530103167386e-01 7.294715974112796078e-04 3.823750502269151474e-01 3.656033742272457587e-01
4.547104081464184433e-01 8.424751561103190891e-04 3.897907535890569597e-01 3.656314433023485910e-01
4.621487746777984129e-01 9.515837988599938754e-04 3.961737360298664412e-01 3.656595156848652661e-01
4.686904470493780672e-01 1.057468320149461622e-03 4.017882335219868928e-01 3.656875913753481755e-01
4.745374128802328784e-01 1.160614917400440687e-03 4.068073658504271495e-01 3.657156703743502657e-01
4.798294687747932108e-01 1.261390911298032732e-03 4.113509488739334752e-01 3.657437526824240392e-01
4.846675262585897204e-01 1.360082804346124732e-03 4.155054702614889850e-01 3.657718383001231088e-01
4.891268978488176322e-01 1.456919791900645198e-03 4.193354770529035269e-01 3.657999272280002545e-01
4.932653350787627455e-01 1.552089040568736724e-03 4.228904650583112934e-01 3.658280194666088669e-01
4.971281297292499124e-01 1.645746030241408133e-03 4.262092511081601032e-01 3.658561150165021703e-01
5.007514812450429842e-01 1.738021794117524960e-03 4.293228592417322464e-01 3.658842138782337217e-01
5.041647941962951185e-01 1.829028132224885242e-03 4.322564898354978591e-01 3.659123160523573004e-01
5.073922903779469751e-01 1.918861456969043772e-03 4.350309013087606536e-01 3.659404215394260751e-01
5.104541676951002138e-01 2.007605689044107775e-03 4.376634033817789482e-01 3.659685303399944911e-01
5.133674509826976484e-01 2.095334477934740307e-03 4.401685862932933069e-01 3.659966424546164387e-01
...
```

C. Density Files

This section gives the code used to create the density files used in MOCASSIN. It creates one, or both, of two files (the density file and Ndust file), based on if the test used dust, gas, or both. The inputs that were regularly changed are toward the top of the file, and those that were the same for each test (within the same yield) are farther down. The file shown is for the 1MT tests; changing the values with ** in the comments can make it usable for the 20 kT test.

MATLAB Code

```matlab
1  dust = 1;                     % 1 if model includes dust, 0 if not
2  gas = 1;                      % 1 if model includes gas, 0 if not
3  test_num = 0;                 % numbered test for file labeling
4
5  % Values that will change based on the test
6  fireball_density = 4.96E13;   % ** #/cm^3 of hydrogen in fireball
7  dust_num_dens = 5.20E12;      % ** number density of all dust in the fireball
8  ambient_density = 3.35E17;    % ** #/cm^3 for hydrogen (will be adjusted based ...
       on Sedov percentages)
9  Size = 4.6E6;                 % ** cm, total radius of area of interest ...
       (symmetric, so source is in corner)
10
11 N = 6;                        % number of grid points in each direction
12 Nsplit = N/3;                 % number of grid points in each zone (if outside ...
       all 3 overall)
13
14 % Data about fireball
15 Rout = 1.1E5;                 % ** cm, radius of fireball
16 fireball_dust = 1;            % numbered file for dust composition in fireball
17 fireball_gas = 1;             % numbered file for gas composition in fireball
18
19 % Data about area between fireball and shock wave
20 Rshock = 3.66E5;              % ** cm, radius of shock wave
```

```matlab
21  dust_H_ratio2 = 0;              % no dust outside fireball
22  shock_dust = 1;                 % no dust assumed outside fireball, in shock ...
        wave (put in a random numbered file, since the dust/H ratio there will be ...
        0 anyway)
23  shock_gas = 2;                  % numbered file for gas composition in fireball
24
25  % Density between fireball and shock wave based on Sedov code values
26  Array=dlmread('I:\setup\Desktop\Thesis\MOCASSIN\Sedov.txt');    % array of ...
        Sedov code values
27  xX=Array(:,1);                  % radius/shock wave radius
28  dD=Array(:,2);                  % density/ambient density
29  Dist=Rshock*xX;                 % cm, actual radii up to Rshock
30  D=dD*ambient_density;           % #/cm^3 of H, actual density at different radii
31
32  % Data about area outside shock wave
33  outside_gas = shock_gas;        % same percentages as inside shock, but ...
        different H density
34  outside_dust = 1;               % no dust outside, dust
35
36  % Sets up a mesh with the same number of points inside the fireball,
37  % between the fireball and shock wave, and outside the shock wave
38  if Size > Rshock
39      X(1)=0;
40      Y(1)=0;
41      Z(1)=0;
42      for i=1:Nsplit
43          X(i+1)=Rout*i/Nsplit;
44          X(i+Nsplit+1)=Rout+(Rshock-Rout)/Nsplit*i;
45          X(i+2*Nsplit+1)=Rshock+(Size-Rshock)/Nsplit*i;
46          Y(i+1)=Rout*i/Nsplit;
47          Y(i+Nsplit+1)=Rout+(Rshock-Rout)/Nsplit*i;
48          Y(i+2*Nsplit+1)=Rshock+(Size-Rshock)/Nsplit*i;
49          Z(i+1)=Rout*i/Nsplit;
50          Z(i+Nsplit+1)=Rout+(Rshock-Rout)/Nsplit*i;
51          Z(i+2*Nsplit+1)=Rshock+(Size-Rshock)/Nsplit*i;
52      end
53  else
54      % If the outside point we are looking at is within the shock wave, the
55      % mesh is evenly distributed throughout
56      X=0:Size/N:Size;
```

89

```matlab
57        Y=0:Size/N:Size;
58        Z=0:Size/N:Size;
59   end
60
61   n=1;
62   for x=1:length(X)
63        for y=1:length(Y)
64            for z=1:length(Z)
65                point(n,1:3)=[X(x) Y(y) Z(z)];
66                Ndust(n,1:3)=[X(x) Y(y) Z(z)];
67                rad(n)=sqrt(sum(X(x)^2+Y(y)^2+Z(z)^2));
68                if rad(n)≤Rout
69                    point(n,4)=fireball_density;
70                    if gas==1, point(n,5)=fireball_gas; end
71                    if dust==1, point(n,6)=shock_dust; end
72                    Ndust(n,4) = dust_num_dens;
73                elseif rad(n)>Rout && rad(n)≤Rshock
74                    [m, i] = min(abs(Dist-rad(n)));          % use Sedov numbers, ...
                         find closest distance in array to rad
75                    point(n,4)=D(i);                         % use Sedov numbers, ...
                         use index of closest distance to get approx H density
76                    if gas==1, point(n,5)=shock_gas; end
77                    if dust==1, point(n,6)=shock_dust; end
78                    Ndust(n,4) = 0;                          % no dust outside ...
                         fireball
79                else
80                    point(n,4)=ambient_density;
81                    if gas==1, point(n,5)=outside_gas; end
82                    if dust==1, point(n,6)=shock_dust; end
83                    Ndust(n,4) = 0;                          % no dust outside ...
                         fireball
84                end
85                n=n+1;
86            end
87        end
88   end
89
90   % Saving the file(s) as '.out' file(s) that can be used by MOCASSIN
91   % Files saved depends on if using gas, dust, or both
92   a=num2str(dust); b=num2str(gas); c=num2str(test_num);
```

```
93
94   test=strcat(c,'_',a,b,'.dat');     % adding the correct file type to the file name
95   if gas==1
96       dlmwrite(strcat('C:\Users\ADunsmor\Documents\MOCASSIN\Input Files\1MT ...
                 files\1density_file_test',test),point,'delimiter','\t');
97   end
98   if dust==1
99       dlmwrite(strcat('C:\Users\ADunsmor\Documents\MOCASSIN\Input Files\1MT ...
                 files\1Ndust_test',test),Ndust,'delimiter',' ');
100  end
```

Example

The text files below show the two outputs of the density file (note: all of the meshes had more points; this file is just an example). The first file is the main density file, which defines the mesh using the first three columns (x, y, and z points), gives the hydrogen density at that mesh point in column 4, the gas abundance file number in column 5, and the dust abundance file number in column 6. Note that all distance values in these files are in cm, and density values are in num/cm^3. This file was made with only 4 mesh values in each direction; 15 were included for actual tests.

```
0         0         0         4.96e+13      1          1
0         0         1.1e+05       4.96e+13      1          1
0         0         3.66e+05      3.35e+17      2          1
0         0         4.6e+06       3.35e+17      2          1
0         1.1e+05       0         4.96e+13      1          1
0         1.1e+05       1.1e+05       1.6324e+14    2          1
0         1.1e+05       3.66e+05      3.35e+17      2          1
0         1.1e+05       4.6e+06       3.35e+17      2          1
0         3.66e+05      0         3.35e+17      2          1
0         3.66e+05      1.1e+05       3.35e+17      2          1
0         3.66e+05      3.66e+05      3.35e+17      2          1
0         3.66e+05      4.6e+06       3.35e+17      2          1
0         4.6e+06       0         3.35e+17      2          1
0         4.6e+06       1.1e+05       3.35e+17      2          1
```

91

0	4.6e+06	3.66e+05	3.35e+17	2	1
0	4.6e+06	4.6e+06	3.35e+17	2	1
1.1e+05	0	0	4.96e+13	1	1
1.1e+05	0	1.1e+05	1.6324e+14	2	1
1.1e+05	0	3.66e+05	3.35e+17	2	1
1.1e+05	0	4.6e+06	3.35e+17	2	1
1.1e+05	1.1e+05	0	1.6324e+14	2	1
1.1e+05	1.1e+05	1.1e+05	7.8827e+14	2	1
1.1e+05	1.1e+05	3.66e+05	3.35e+17	2	1
1.1e+05	1.1e+05	4.6e+06	3.35e+17	2	1
1.1e+05	3.66e+05	0	3.35e+17	2	1
1.1e+05	3.66e+05	1.1e+05	3.35e+17	2	1
1.1e+05	3.66e+05	3.66e+05	3.35e+17	2	1
1.1e+05	3.66e+05	4.6e+06	3.35e+17	2	1
1.1e+05	4.6e+06	0	3.35e+17	2	1
1.1e+05	4.6e+06	1.1e+05	3.35e+17	2	1
1.1e+05	4.6e+06	3.66e+05	3.35e+17	2	1
1.1e+05	4.6e+06	4.6e+06	3.35e+17	2	1
3.66e+05	0	0	3.35e+17	2	1
3.66e+05	0	1.1e+05	3.35e+17	2	1
3.66e+05	0	3.66e+05	3.35e+17	2	1
3.66e+05	0	4.6e+06	3.35e+17	2	1
3.66e+05	1.1e+05	0	3.35e+17	2	1
3.66e+05	1.1e+05	1.1e+05	3.35e+17	2	1
3.66e+05	1.1e+05	3.66e+05	3.35e+17	2	1
3.66e+05	1.1e+05	4.6e+06	3.35e+17	2	1
3.66e+05	3.66e+05	0	3.35e+17	2	1
3.66e+05	3.66e+05	1.1e+05	3.35e+17	2	1
3.66e+05	3.66e+05	3.66e+05	3.35e+17	2	1
3.66e+05	3.66e+05	4.6e+06	3.35e+17	2	1
3.66e+05	4.6e+06	0	3.35e+17	2	1
3.66e+05	4.6e+06	1.1e+05	3.35e+17	2	1
3.66e+05	4.6e+06	3.66e+05	3.35e+17	2	1
3.66e+05	4.6e+06	4.6e+06	3.35e+17	2	1
4.6e+06	0	0	3.35e+17	2	1
4.6e+06	0	1.1e+05	3.35e+17	2	1
4.6e+06	0	3.66e+05	3.35e+17	2	1
4.6e+06	0	4.6e+06	3.35e+17	2	1
4.6e+06	1.1e+05	0	3.35e+17	2	1
4.6e+06	1.1e+05	1.1e+05	3.35e+17	2	1

```
4.6e+06        1.1e+05        3.66e+05        3.35e+17        2        1
4.6e+06        1.1e+05        4.6e+06        3.35e+17        2        1
4.6e+06        3.66e+05        0        3.35e+17        2        1
4.6e+06        3.66e+05        1.1e+05        3.35e+17        2        1
4.6e+06        3.66e+05        3.66e+05        3.35e+17        2        1
4.6e+06        3.66e+05        4.6e+06        3.35e+17        2        1
4.6e+06        4.6e+06        0        3.35e+17        2        1
4.6e+06        4.6e+06        1.1e+05        3.35e+17        2        1
4.6e+06        4.6e+06        3.66e+05        3.35e+17        2        1
4.6e+06        4.6e+06        4.6e+06        3.35e+17        2        1
```

The next file is the 'Ndust' file, which defines the number density of the dust over the whole volume. This file can be used on its own, in a dust-only scenario, or in conjunction with a density file (the mesh values must be the same).

```
0 0 0 5.2e+12
0 0 1.1e+05 5.2e+12
0 0 3.66e+05 0
0 0 4.6e+06 0
0 1.1e+05 0 5.2e+12
0 1.1e+05 1.1e+05 0
0 1.1e+05 3.66e+05 0
0 1.1e+05 4.6e+06 0
0 3.66e+05 0 0
0 3.66e+05 1.1e+05 0
0 3.66e+05 3.66e+05 0
0 3.66e+05 4.6e+06 0
0 4.6e+06 0 0
0 4.6e+06 1.1e+05 0
0 4.6e+06 3.66e+05 0
0 4.6e+06 4.6e+06 0
1.1e+05 0 0 5.2e+12
1.1e+05 0 1.1e+05 0
1.1e+05 0 3.66e+05 0
1.1e+05 0 4.6e+06 0
1.1e+05 1.1e+05 0 0
1.1e+05 1.1e+05 1.1e+05 0
1.1e+05 1.1e+05 3.66e+05 0
1.1e+05 1.1e+05 4.6e+06 0
1.1e+05 3.66e+05 0 0
```

```
1.1e+05 3.66e+05 1.1e+05 0

1.1e+05 3.66e+05 3.66e+05 0

1.1e+05 3.66e+05 4.6e+06 0

1.1e+05 4.6e+06 0 0

1.1e+05 4.6e+06 1.1e+05 0

1.1e+05 4.6e+06 3.66e+05 0

1.1e+05 4.6e+06 4.6e+06 0

3.66e+05 0 0 0

3.66e+05 0 1.1e+05 0

3.66e+05 0 3.66e+05 0

3.66e+05 0 4.6e+06 0

3.66e+05 1.1e+05 0 0

3.66e+05 1.1e+05 1.1e+05 0

3.66e+05 1.1e+05 3.66e+05 0

3.66e+05 1.1e+05 4.6e+06 0

3.66e+05 3.66e+05 0 0

3.66e+05 3.66e+05 1.1e+05 0

3.66e+05 3.66e+05 3.66e+05 0

3.66e+05 3.66e+05 4.6e+06 0

3.66e+05 4.6e+06 0 0

3.66e+05 4.6e+06 1.1e+05 0

3.66e+05 4.6e+06 3.66e+05 0

3.66e+05 4.6e+06 4.6e+06 0

4.6e+06 0 0 0

4.6e+06 0 1.1e+05 0

4.6e+06 0 3.66e+05 0

4.6e+06 0 4.6e+06 0

4.6e+06 1.1e+05 0 0

4.6e+06 1.1e+05 1.1e+05 0

4.6e+06 1.1e+05 3.66e+05 0

4.6e+06 1.1e+05 4.6e+06 0

4.6e+06 3.66e+05 0 0

4.6e+06 3.66e+05 1.1e+05 0

4.6e+06 3.66e+05 3.66e+05 0

4.6e+06 3.66e+05 4.6e+06 0

4.6e+06 4.6e+06 0 0

4.6e+06 4.6e+06 1.1e+05 0

4.6e+06 4.6e+06 3.66e+05 0

4.6e+06 4.6e+06 4.6e+06 0
```

D. Radial Distribution File

Below is the code used to generate the grain radius distribution files for the dust. The code needed discrete radius values, so the distribution was split up with 100 different radii. The number of radii is limited only by the computer's memory and the desired run time (increasing the number of radii increases the run time). A plot of the radial distribution can be seen in the 'Grain Radius Distribution' section in Chapter 3 (Figure 8).

MATLAB Code

```matlab
1  % Inputs
2  r=0.0001:0.0001:0.05;     % um, possible radius values
3  mean=0.01;                % um, mean radius, Bridgman Table 12-1 - lessened by ...
       a factor of 10
4  B=log(2);                 % standard dev, Bridgman Table 12-1
5  a0=log(mean);
6
7  % Find likelihood of each radial value occurring
8  N=1./(sqrt(2*pi)*B*r).*exp(-1/2*((log(r)-a0)/B).^2);
9
10 % Normalize the N values so they are weights from 0:1
11 Ns=sum(N);
12 N2=N/Ns;
13
14 % Create an output array of the correct format
15 % Column 1 - index; column 2 - radius; column 3 - weight
16 a=1:length(r);
17 output=[a' r' N2'];
18
19 % Write the array to a file
20 loc='I:\setup\Desktop\Thesis\MOCASSIN\Radius Files\radius.txt';
21 fileID=fopen(loc,'w');
22 fprintf(fileID,'%d size\n', length(r));
```

```
23   fclose ( fileID );
24   dlmwrite ( loc , output , 'delimiter' , ' ' , '-append' );
```

Example

This is the radius file that was used in all the trials. The first line gives the number of sizes total, and the remaining lines have the index, radius in μm, and weight of the radius.

```
100 size
1 0.0001 7.559e-10
2 0.0006 0.00012822
3 0.0011 0.0016601
4 0.0016 0.005515
5 0.0021 0.010977
6 0.0026 0.01692
7 0.0031 0.022502
8 0.0036 0.027257
9 0.0041 0.031006
10 0.0046 0.033747
11 0.0051 0.035566
12 0.0056 0.036592
13 0.0061 0.036963
14 0.0066 0.036808
15 0.0071 0.036245
16 0.0076 0.035373
17 0.0081 0.034274
18 0.0086 0.033017
19 0.0091 0.031656
20 0.0096 0.030234
21 0.0101 0.028784
22 0.0106 0.027333
23 0.0111 0.025899
24 0.0116 0.024497
25 0.0121 0.023137
26 0.0126 0.021828
27 0.0131 0.020573
28 0.0136 0.019375
```

```
29 0.0141 0.018237
30 0.0146 0.017157
31 0.0151 0.016136
32 0.0156 0.015171
33 0.0161 0.014262
34 0.0166 0.013407
35 0.0171 0.012602
36 0.0176 0.011846
37 0.0181 0.011136
38 0.0186 0.01047
39 0.0191 0.0098454
40 0.0196 0.0092596
41 0.0201 0.0087105
42 0.0206 0.0081958
43 0.0211 0.0077135
44 0.0216 0.0072615
45 0.0221 0.0068378
46 0.0226 0.0064408
47 0.0231 0.0060686
48 0.0236 0.0057198
49 0.0241 0.0053926
50 0.0246 0.0050859
51 0.0251 0.0047981
52 0.0256 0.0045282
53 0.0261 0.0042748
54 0.0266 0.004037
55 0.0271 0.0038137
56 0.0276 0.0036039
57 0.0281 0.0034069
58 0.0286 0.0032217
59 0.0291 0.0030476
60 0.0296 0.0028839
61 0.0301 0.0027299
62 0.0306 0.002585
63 0.0311 0.0024486
64 0.0316 0.0023202
65 0.0321 0.0021992
66 0.0326 0.0020852
67 0.0331 0.0019778
68 0.0336 0.0018765
```

69 0.0341 0.0017809

70 0.0346 0.0016908

71 0.0351 0.0016057

72 0.0356 0.0015254

73 0.0361 0.0014495

74 0.0366 0.0013778

75 0.0371 0.0013101

76 0.0376 0.0012461

77 0.0381 0.0011856

78 0.0386 0.0011283

79 0.0391 0.0010741

80 0.0396 0.0010228

81 0.0401 0.00097422

82 0.0406 0.00092822

83 0.0411 0.00088464

84 0.0416 0.00084333

85 0.0421 0.00080417

86 0.0426 0.00076704

87 0.0431 0.00073182

88 0.0436 0.00069839

89 0.0441 0.00066667

90 0.0446 0.00063656

91 0.0451 0.00060796

92 0.0456 0.00058079

93 0.0461 0.00055497

94 0.0466 0.00053043

95 0.0471 0.0005071

96 0.0476 0.00048492

97 0.0481 0.00046381

98 0.0486 0.00044373

99 0.0491 0.00042462

100 0.0496 0.00040643

E. Abundance Files

Dust Files

Two different dust files were created - one for the compounds in the 1 MT fireball, and one for the compounds in the 20 kT fireball. Each file needed to show the molar fraction of each compound compared to all of the dust. Table 19 (for the 20 kT) and Table 20 (for the 1 MT) were used to find these values, by finding the total moles of dust and dividing the moles of each compound by this number. The two dust files are shown below.

20 kT dust file:

```
5
'dustData/Al2O3.nk'  0.157705
'dustData/FeO.nk'    0.616051
'dustData/Fe3O4.nk'  0.20535
'dustData/UO2.nk'    0.019763
'dustData/PuO2.nk'   0.00113
```

1 MT dust file:

```
4
'dustData/Al2O3.nk'  0.0012
'dustData/FeO.nk'    0.73
'dustData/Fe3O4.nk'  0.24
'dustData/UO2.nk'    0.026
```

Gas Files

Three different gas files were created - two for the gas in the two fireballs, and one for the air outside the fireball. Each file needed to show the abundances of the elements compared to hydrogen. Tables 21 and 22 show these values for the 20 kT and 1 MT fireballs, respectively. Table 11 shows the relative abundances in air. In the gas files, there is one line for every one of the first 30 elements (through zinc),

and zeros should be entered for elements not present (the element on each line is commented for ease of use). The three gas files are shown below.

20 kT fireball gas file:

```
1.      ! H
0.      ! He
0.      ! Li
0.      ! Be
0.      ! B
0.74    ! C
11.6    ! N
3.3     ! O
0.      ! F
0.      ! Ne
0.      ! Na
0.      ! Mg
0.12    ! Al
0.      ! Si
0.      ! P
0.      ! S
0.      ! Cl
0.      ! Ar
0.      ! K
0.      ! Ca
0.      ! Sc
0.      ! Ti
0.      ! V
0.      ! Cr
0.      ! Mn
0.      ! Fe
0.      ! Co
0.      ! Ni
0.      ! Cu
0.      ! Zn
```

1 MT fireball gas file:

```
1.      ! H
0.      ! He
0.      ! Li
```

```
0.      ! Be
0.      ! B
0.002   ! C
77.9    ! N
21.3    ! O
0.      ! F
0.      ! Ne
0.      ! Na
0.      ! Mg
0.0003  ! Al
0.      ! Si
0.      ! P
0.      ! S
0.      ! Cl
0.      ! Ar
0.      ! K
0.      ! Ca
0.      ! Sc
0.      ! Ti
0.      ! V
0.      ! Cr
0.      ! Mn
0.      ! Fe
0.      ! Co
0.      ! Ni
0.      ! Cu
0.      ! Zn
```

Air file:

```
1.      ! H
0.      ! He
0.      ! Li
0.      ! Be
0.      ! B
0.      ! C
78.     ! N
21.5    ! O
0.      ! F
0.      ! Ne
0.      ! Na
```

```
0.      ! Mg
0.      ! Al
0.      ! Si
0.      ! P
0.      ! S
0.      ! Cl
0.      ! Ar
0.      ! K
0.      ! Ca
0.      ! Sc
0.      ! Ti
0.      ! V
0.      ! Cr
0.      ! Mn
0.      ! Fe
0.      ! Co
0.      ! Ni
0.      ! Cu
0.      ! Zn
```

F. Dust Optical Files

These are the files that were used for the dust optical constants. The first line, 'nk,' is the type of file. The second line contains the file name and all of the constants that were found in Chapter 3. The remaining lines give a wavelength in μm, the refractive index n, and the extinction coefficient k. The wavelength ranges are not the same for the files; the ranges were determined by what could be found.

PuO_2

For both the plutonium oxide and uranium oxide optical files, data points hadd to be pulled off of plots. The plot for plutonium oxide is below, followed by the data points it yielded (DataThief was used to pull the data points [54]). It should be noted that these optical files are not specific to any plutonium or uranium oxide; they are simply their respective metals with "an oxide thickness of a few nm" [9].
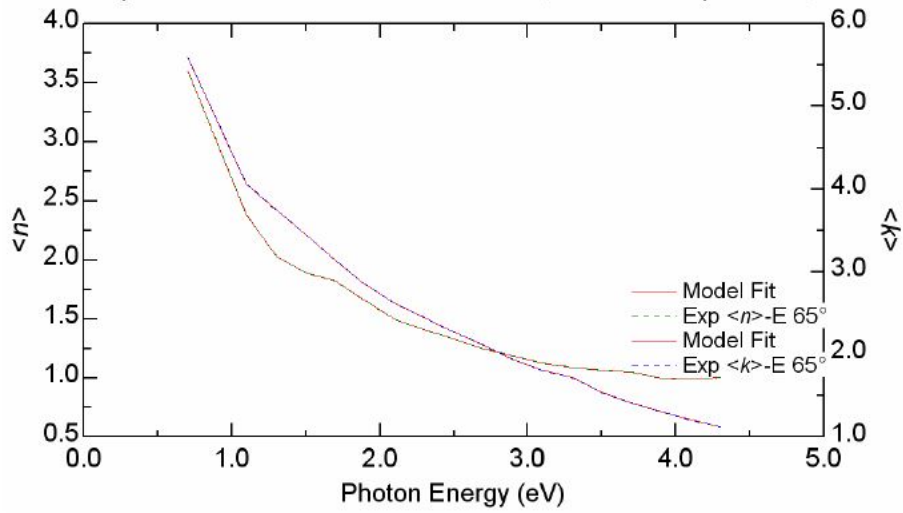
Figure 23. Optical constants for plutonium oxide as functions of photon energy. Reproduced with permission from [9].

```
nk
puox  3100. 11.5 0.272 92.0
```

103

```
0.288372    1.00    1.1
0.302439    1.00    1.2
0.326316    1.00    1.3
0.354286    1.05    1.5
0.400000    1.10    1.8
0.413333    1.15    1.9
0.442857    1.20    2.0
0.496000    1.30    2.3
0.539130    1.40    2.5
0.635897    1.60    2.8
0.729412    1.80    3.1
0.826667    1.90    3.5
0.953846    2.00    3.7
0.992000    2.10    3.8
1.127273    2.40    4.0
1.240000    2.70    4.5
1.458824    3.20    5.0
1.771429    3.70    5.5
```

UO_2
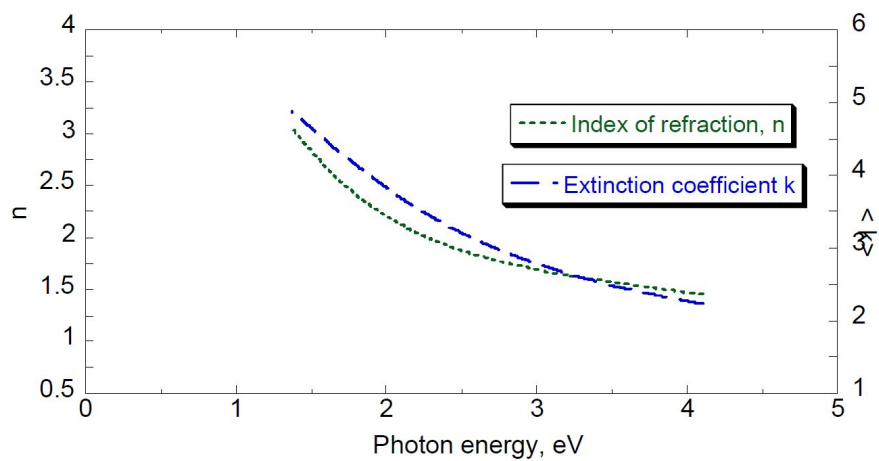
Figure 24. Optical constants for uranium oxide as functions of photon energy. Reproduced with permission from [9].

```
nk

urox   4000. 10.97 0.383 90.

    0.302439    1.46    2.246
```

0.306173	1.47	2.265
0.310000	1.48	2.28
0.313924	1.48	2.29
0.317949	1.50	2.311
0.322078	1.51	2.33
0.326316	1.52	2.347
0.330667	1.52	2.376
0.334232	1.53	2.395
0.338798	1.54	2.413
0.344444	1.55	2.441
0.349296	1.56	2.468
0.354286	1.56	2.488
0.358382	1.58	2.516
0.363636	1.58	2.543
0.370149	1.60	2.571
0.375758	1.60	2.599
0.380368	1.63	2.617
0.386293	1.64	2.655
0.393651	1.65	2.692
0.400000	1.66	2.729
0.406557	1.68	2.767
0.411960	1.69	2.795
0.418919	1.71	2.822
0.427586	1.73	2.859
0.435088	1.75	2.906
0.441281	1.76	2.934
0.449275	1.78	2.990
0.457565	1.80	3.018
0.467925	1.81	3.073
0.476923	1.83	3.120
0.484375	1.85	3.157
0.494024	1.88	3.204
0.506122	1.90	3.269
0.516667	1.93	3.325
0.527660	1.96	3.380
0.536797	1.98	3.436
0.548673	2.02	3.492
0.563636	2.05	3.557
0.576744	2.09	3.621
0.587678	2.12	3.678

```
0.601942    2.17    3.752
0.620000    2.21    3.845
0.635897    2.25    3.910
0.652632    2.31    3.994
0.670270    2.34    4.078
0.685083    2.40    4.133
0.708571    2.48    4.226
0.729412    2.54    4.301
0.746988    2.58    4.366
0.775000    2.67    4.505
0.800000    2.76    4.580
0.826667    2.83    4.663
0.855172    2.91    4.756
0.905109    3.04    4.896
```

FeO [1]

```
nk
irox  3000. 5.7 0.358 35.9
    0.2000    1.383000    1.162000
    0.2500    1.773000    1.159000
    0.3000    2.002000    1.047670
    0.3500    2.132850    0.947074
    0.4000    2.224000    0.868200
    0.4500    2.291330    0.799979
    0.5000    2.342000    0.742200
    0.6000    2.417670    0.637204
    0.7000    2.436000    0.554388
    0.8000    2.439000    0.513200
    0.9000    2.444000    0.495201
    1.0000    2.454000    0.490100
    1.2000    2.478990    0.507925
    1.4000    2.520990    0.528256
    1.6000    2.583490    0.534901
    1.8000    2.650260    0.510665
    2.0000    2.701000    0.460300
    2.5000    2.745000    0.343000
    3.0000    2.749000    0.270403
    3.5000    2.742860    0.224230
    4.0000    2.733000    0.192600
```

4.5000	2.721110	0.169779
5.0000	2.708000	0.152700
6.0000	2.677670	0.129337
7.0000	2.640730	0.115432
8.0000	2.597020	0.107902
9.0000	2.546040	0.105544
10.000	2.484000	0.108100
11.000	2.411740	0.116004
12.000	2.326140	0.130371
13.000	2.224320	0.153201
14.000	2.102160	0.187772
15.000	1.941790	0.241690
16.000	1.786860	0.358396
17.000	1.625470	0.424422
18.000	1.287330	0.595948
19.000	1.057240	1.024610
20.000	0.990049	1.455430
21.000	1.006623	1.879279
22.000	1.084007	2.286750
23.000	1.201510	2.688320
24.000	1.362126	3.110572
25.000	1.608089	3.558363
26.000	1.953133	4.001366
27.000	2.418045	4.420942
28.000	3.054750	4.785148
29.000	3.858260	5.008535
30.000	4.818734	4.918499
31.000	5.688979	4.427482
32.000	6.184770	3.643767
33.000	6.315354	2.876461
34.000	6.220329	2.352550
35.000	6.083755	1.962861
36.000	5.897287	1.678671
38.000	5.656481	1.325639
40.000	5.408080	1.126978
42.000	5.220735	0.992212
44.000	5.096131	0.920967
46.000	4.973061	0.876379
48.000	4.906060	0.853336
50.000	4.830129	0.819635

```
60.000    4.617743    0.830186
70.000    4.543011    0.874726
80.000    4.511551    0.934345
90.000    4.523560    0.992835
100.00    4.493102    1.059231
120.00    4.537204    1.243707
140.00    4.644652    1.378652
160.00    4.720002    1.464057
180.00    4.790472    1.539287
200.00    4.846388    1.616290
250.00    4.928175    1.806522
300.00    5.022462    2.032790
350.00    5.048345    2.183976
400.00    5.061842    2.475915
450.00    5.102378    2.658451
500.00    5.149173    2.815657
```

Fe_3O_4 [2]

Only the first 20 lines are shown, as there are over 600 (see source for remainder).

```
nk
irox2  3000. 5.18 0.298 33.1
    0.210    2.256    0.085
    0.220    2.305    0.109
    0.230    2.337    0.118
    0.240    2.364    0.120
    0.250    2.387    0.114
    0.260    2.400    0.102
    0.270    2.404    0.092
    0.280    2.401    0.085
    0.290    2.397    0.088
    0.300    2.398    0.091
    0.310    2.398    0.096
    0.320    2.403    0.103
    0.330    2.409    0.105
    0.340    2.415    0.108
    0.350    2.422    0.111
    0.360    2.434    0.112
    0.370    2.447    0.108
```

```
0.380    2.459    0.096

0.390    2.464    0.080

0.400    2.462    0.062

...
```

Al_2O_3 [2]

Only the first 20 lines are shown, as there are over 600 (see source for remainder).

```
nk

alox   2750. 3.97 0.445 20.4

     0.21000      1.831      -0.052

     0.22000      1.817      -0.039

     0.23000      1.805      -0.026

     0.24000      1.793      -0.019

     0.25000      1.789      -0.016

     0.26000      1.779      -0.010

     0.27000      1.776      -0.004

     0.28000      1.772      -0.001

     0.29000      1.767      0.0010

     0.30000      1.762      0.0070

     0.31000      1.762      0.0100

     0.32000      1.762      0.0120

     0.33000      1.761      0.0130

     0.34000      1.760      0.0140

     0.35000      1.758      0.0150

     0.36000      1.757      0.0170

     0.37000      1.757      0.0180

     0.38000      1.757      0.0180

     0.39000      1.757      0.0190

     0.40000      1.756      0.0190

     ...
```

G. Dominic Harlem Data

Original Data Set

The data that was found for the 1 MT case was from the Dominic Harlem test in 1962 [6]. Spectral data was taken in several different aircraft, from 0.05-20 seconds after the explosion, in the 0.3-1.6 micron range. It would have been preferable to find a spectrum that went further into the infrared, but no such data was found. The data that was used was not the actual collected values - these were not reported. They were first adjusted in a few ways. A caveat to the data was quoted as:

> NASL reviewed, corrected, smoothed and combined the various raw measurements into a final set of mean, average spectral powers at a standard set of wavelengths. This process included correcting obvious mistakes, eliminating data based upon inadequate signals (i.e. those with low signal-to-noise ratios) and combining the magnetic tape recorder data with the galvanometer oscillograph data. [6]

They also "corrected" the data based on transmission in the atmosphere, the aircraft window, and the filter, and for the alignment of the aircraft. If the attempt was being made to use MOCASSIN to its fullest extent, and match the exact energy and shape of the MOCASSIN output to the data, these corrections would need to be accounted for. However, the goal of this project is simply to try and see if the output is at all similar to the data, and it is therefore not important.

The full data set can be found in Brode's Thermal Radiation Metaguide. An example of one of the pages is shown in Figure 25.

Only the data from one aircraft (P1) was used, because it had far more data than any of the others (more wavelengths recorded). The data can be seen in Table 24. The empty spots did not contain data (or the data existed but was not readable),

Time								
0.050SEC								
0.100SEC								
0.150SEC								
0.200SEC	5.64E 11	2.64E 11			6.18E 11			
0.250SEC	2.26E 12	1.35E 11			6.18E 11	1.01E 12		
0.300SEC	6.20E 12	4.17E 12			2.23E 13	1.01E 13		
0.350SEC	1.14E 13	1.16E 13		7.19E 12	1.42E 13	3.04E 13		
0.400SEC	3.44E 13	3.24E 13		2.00E 13	4.20E 13	7.18E 13		
0.450SEC	8.01E 13	7.35E 13		4.80E 13	8.16E 13	1.42E 14		
0.500SEC	1.31E 14	1.20E 14		7.99E 13	1.37E 14	2.13E 14		
0.550SEC	1.70E 14	1.60E 14		1.16E 14	1.42E 14	2.73E 14		
0.600SEC	1.70E 14	1.90E 14	1.65E 14	1.44E 14	2.30E 14	3.15E 14	3.04E 14	
0.650SEC	2.32E 14	2.14E 14	2.13E 14	1.66E 14	2.54E 14	3.47E 14	3.04E 14	
0.700SEC	2.50E 14	2.28E 14	2.28E 14	1.81E 14	2.79E 14	3.79E 14	4.05E 14	
0.750SEC	2.66E 14	2.54E 14	2.43E 14	1.96E 14	3.03E 14	4.05E 14	4.04E 14	
0.800SEC	2.80E 14	2.60E 14	2.59E 14	2.12E 14	3.19E 14	4.25E 14	4.05E 14	
0.850SEC	2.94E 14		2.74E 14	2.24E 14	3.31E 14	4.40E 14	4.43E 14	
0.900SEC	2.99E 14		2.74E 14	2.31E 14	3.38E 14	4.50E 14	4.45E 14	1.55E 14
0.950SEC	2.94E 14		2.74E 14	2.32E 14	3.40E 14	4.55E 14	4.05E 14	
1.000SEC	2.94E 14		2.74E 14	2.32E 14	3.35E 14	4.45E 14	4.45E 14	
1.100SEC	2.69E 14	2.46E 14	2.46E 14	2.16E 14	3.10E 14	4.05E 14	4.05E 14	
1.200SEC	2.23E 14	2.02E 14	2.13E 14	1.80E 14	2.57E 14	3.24E 14	4.05E 14	
1.300SEC	1.72E 14	1.64E 14	1.66E 14	1.44E 14	2.02E 14	2.53E 14	2.02E 14	
1.400SEC	1.44E 14	1.36E 14	1.36E 14	1.20E 14	1.61E 14	2.12E 14	2.02E 14	
1.500SEC	1.22E 14	1.17E 14	1.20E 14	1.04E 14	1.43E 14	1.87E 14	2.02E 14	
1.600SEC	1.11E 14	1.04E 14	1.05E 14	9.51E 13	1.25E 14	1.62E 14	2.02E 14	
1.700SEC	9.76E 13	9.16E 13	9.24E 13	8.34E 13	1.11E 14	1.42E 14	1.62E 14	
1.800SEC	1.02E 14	8.08E 13	8.93E 13	7.19E 13	9.65E 13	1.26E 14	1.01E 14	
1.900SEC	7.50E 13	7.14E 13	7.39E 13	6.19E 13	8.66E 13	1.11E 14	1.01E 14	
2.000SEC	6.60E 13	6.34E 13	5.85E 13	6.39E 13	7.54E 13	1.11E 14	1.01E 14	
2.500SEC	3.78E 13	3.54E 13	4.31E 13	3.76E 13	4.33E 13	4.05E 13		
3.000SEC	1.81E 13	2.06E 13	2.46E 13	2.32E 13	2.41E 13	3.04E 13		
3.500SEC	1.30E 13	1.36E 13	1.23E 13	1.60E 13	1.55E 13	2.02E 13		
4.000SEC	7.33E 12	9.56E 12	3.08E 12	7.99E 12	1.11E 13	1.52E 13		
4.500SEC	6.20E 12	8.08E 12	3.08E 12	7.99E 12	6.16E 12	1.01E 13		
5.000SEC	6.20E 12	6.19E 12	1.23E 13	7.19E 12	6.04E 12	1.01E 13		
6.000SEC	4.51E 12	6.19E 12	4.31E 13	4.00E 12	6.18E 12	5.06E 12		
7.000SEC	4.51E 12	4.17E 12	1.23E 13	4.00E 12	6.16E 12	5.06E 12		
8.000SEC	2.82E 12	3.15E 12	6.16E 12	2.40E 12	5.57E 12	5.06E 12		
9.000SEC	1.13E 12	2.63E 12	3.08E 12	4.00E 12	1.71E 12	1.01E 12		
10.000SEC	1.13E 12	2.03E 12		4.00E 12	1.86E 12	1.01E 12		
15.000SEC	1.13E 12	2.42E 12			1.24E 12	5.06E 12		
20.000SEC	1.13E 12	1.48E 12		7.99E 11				

Figure 25. **Spectral output data from the Dominic Harlem test. Reproduced with permission from [6].**

and in order to be able to use these numbers it was necessary to fill in the data using extrapolated and interpolated values.

Filled Data Set

The data set was filled using two different methods. Both were based on a semi-log plot of power as a function of time, for various wavelengths (the wavelength lines were all evaluated individually). The first method found extrapolated data points in areas where there was data on only one side of the missing section (an example from Table 24 is 0.363 μm, where the first 0.30 seconds did not have any data). The second found interpolated data points in areas in the middle of the data set (an example is in 0.3685 μm, where there was no data from 0.45-3.00 seconds, but data both before and after).

For the first method, the decision was made to extrapolate the points using a line

111

Table 24. Table of original Dominic Harlem Data from aircraft P1, with wavelength in um, time in seconds, and data points in cal/s/um

	0.363	0.3685	0.403	0.455	0.455	0.555	0.596	0.755	1.039	1.282	1.605
0.05		2.65E+09				6.13E+11					
0.10		2.65E+09						7.62E+11	4.80E+12	1.35E+12	
0.15		1.33E+10				8.76E+11		1.85E+12	1.52E+13	2.88E+12	
0.20		2.65E+10	4.27E+11			6.13E+12	1.21E+14	6.44E+12	1.44E+13	4.88E+12	
0.25		6.10E+10	4.27E+11			1.59E+13	1.21E+14	1.14E+13	1.81E+13	6.52E+12	4.88E+12
0.30		1.72E+11	6.39E+11	4.17E+13		3.11E+13	1.82E+14	1.95E+13	2.23E+13	8.16E+12	
0.35	3.26E+11	5.12E+12	2.77E+12	1.16E+13		6.04E+13	3.64E+14	2.84E+13	2.37E+13	8.70E+12	
0.40	1.66E+12	1.82E+12	7.03E+12	3.34E+13		1.17E+14	3.64E+14	3.71E+13	2.59E+13	9.40E+12	
0.45	4.96E+12		1.51E+13				4.25E+14	3.98E+13	2.72E+13	9.83E+12	
0.50	8.06E+12		2.24E+13	1.20E+14			4.87E+14	4.89E+13	2.72E+13	1.17E+13	8.70E+12
0.55	1.07E+13		3.07E+13	1.80E+14			4.87E+14	4.92E+13	3.13E+13	1.23E+13	
0.60	1.28E+13		3.52E+13	1.90E+14	1.85E+14		4.87E+14	4.99E+13	3.23E+13	1.30E+13	
0.65				2.14E+14	2.13E+14			5.19E+13		1.26E+13	
0.70	1.91E+13		4.57E+13	2.28E+14	2.28E+14		7.26E+14	5.80E+13		1.32E+13	
0.75			4.76E+13	2.54E+14	2.43E+14		7.26E+14	5.19E+13			
0.80	2.17E+13		5.13E+13	2.60E+14	2.59E+14		7.26E+14				
0.85	2.17E+13		5.22E+13		2.74E+14		6.68E+14				
0.90	2.17E+13		5.37E+13		2.74E+14		6.68E+14		3.29E+13		
0.95	2.38E+13		5.17E+13		2.74E+14		6.68E+14		3.29E+13		
1.00	2.34E+13		4.98E+13		2.74E+14		5.45E+14	4.52E+13	3.53E+13	1.30E+13	8.62E+12
1.10	1.79E+13		4.12E+13	2.46E+14	2.46E+14		4.25E+14	4.52E+13	3.04E+13		
1.20	1.16E+13		3.05E+13	2.02E+14	2.13E+14		4.25E+14	3.33E+13	2.88E+13	1.30E+13	
1.30	1.22E+13		2.58E+13	1.6E+14	1.66E+14		3.03E+14	2.67E+13	2.88E+13	1.21E+13	
1.40	1.22E+13		2.20E+13	1.38E+14	1.36E+14		2.43E+14	2.67E+13	2.72E+13	1.11E+13	
1.50	1.24E+13		2.13E+13	1.17E+14	1.20E+14		1.82E+14	1.81E+13	2.64E+13	1.09E+13	4.88E+12
1.60	1.14E+13		1.94E+13	1.04E+14	1.05E+14		1.82E+14	1.65E+13	2.42E+13	1.05E+13	4.31E+12
1.70	1.03E+13		1.75E+13	9.16E+13	9.24E+13	1.31E+14	1.21E+14	1.51E+13	2.34E+13	1.00E+13	3.61E+12
1.80	9.75E+12		1.58E+13	8.08E+13	8.93E+13	1.16E+14	1.21E+14	1.27E+13	2.23E+13	9.21E+12	3.48E+12
1.90	9.10E+12		1.43E+13	7.14E+13	7.39E+13	1.03E+14	1.21E+14	1.13E+13	2.18E+13	8.78E+12	3.07E+12
2.00	8.26E+12		1.30E+13	6.34E+13	5.85E+13	9.11E+13	6.06E+13	1.11E+13	2.14E+13	8.57E+12	2.77E+12
2.50	5.77E+12		8.54E+12	3.58E+13	4.31E+13	5.60E+13		9.68E+12	1.75E+13	5.85E+12	1.67E+12
3.00	3.73E+12		5.46E+12	2.06E+13	2.46E+13	3.50E+13		8.63E+12	1.38E+13	4.39E+12	9.73E+11
3.50	3.10E+12	3.53E+12	4.48E+12	1.36E+13	1.23E+13	2.36E+13		7.89E+12	1.13E+13	3.10E+12	6.95E+11
4.00	2.28E+12	2.55E+12	3.20E+12	9.56E+12	3.08E+12	1.71E+13		6.91E+12	9.32E+12	2.64E+12	6.95E+11
4.50	1.85E+12	1.93E+12	2.77E+12	8.08E+12	3.08E+12	1.33E+13		4.32E+12	7.97E+12	2.11E+12	6.95E+11
5.00	1.66E+12	1.54E+12	2.13E+12	6.19E+12	1.23E+13	1.09E+13		3.21E+12	6.74E+12	1.76E+12	4.88E+11
6.00	1.03E+12	1.13E+12	1.71E+12	6.19E+12	4.31E+13	8.06E+12		1.77E+12	4.80E+12	1.26E+12	
7.00	1.45E+12	9.31E+11	1.71E+12	4.17E+12	1.23E+13	6.57E+12		1.44E+12	3.72E+12	1.00E+12	
8.00	1.03E+12	8.09E+11	1.49E+12	3.10E+12	6.16E+12	5.67E+12		1.19E+12	3.29E+12	6.38E+11	4.15E+11
9.00	6.22E+11	7.40E+11	1.07E+12	2.83E+12	3.08E+12	5.26E+12		1.19E+12	2.88E+12	7.11E+11	3.48E+11
10.00	6.22E+11	7.11E+11	1.07E+12	2.83E+12		4.47E+12		9.03E+11	2.55E+12	6.28E+11	3.48E+11
15.00	2.07E+11	6.23E+11	1.49E+12	2.42E+12		2.98E+12		9.03E+11	1.88E+12	3.77E+11	2.77E+11
20.00		3.66E+11	1.07E+12	1.48E+12		2.19E+12			1.45E+12	2.30E+11	

that would be linear on a semi-log plot (this was due to the semi-log nature of the data - logarithmic in power, linear in time). So, by creating a line between the two points nearest to the missing data, previous data points for the missing times could be extrapolated to be on this line. This was done for missing sections both at early time values and at late time values.

The second method used the MATLAB function `interp1`, which interpolates data points using several possible methods. The specific parameter `pchip`, which fills data using cubic interpolation, was used for most of the sections. In cases where this didn't work for some reason, `spline` would be used, or `linear` as a last resort. All of the data points were then multiplied by 4.184 to convert from cal/s/μm to W/μm. The result of this was Table 25, which is plotted in Figure 20 in section 4.4.

Table 25. Table of filled Dominic Harlem Data, with wavelength in um, time in seconds, and data points in cal/s/um

	0.363	0.3685	0.403	0.455	0.555	0.596	0.755	1.039	1.282	1.605
0.05	1.87E+07	2.65E+09	1.27E+11	3.93E+13	6.13E+11	3.56E+13	3.14E+11	1.52E+12	6.33E+11	3.07E+12
0.10	9.52E+07	2.65E+09	1.91E+11	4.52E+13	6.73E+11	5.35E+13	7.62E+11	4.80E+12	1.35E+12	3.45E+12
0.15	4.85E+08	1.33E+10	2.85E+11	5.20E+13	8.76E+11	8.04E+13	1.85E+12	1.52E+13	2.88E+12	3.87E+12
0.20	2.47E+09	2.65E+10	4.27E+11	5.99E+13	6.13E+12	1.21E+14	6.44E+12	1.44E+13	4.88E+12	4.35E+12
0.25	1.26E+10	6.10E+10	4.27E+11	6.90E+13	1.59E+13	1.21E+14	1.14E+13	1.81E+13	6.52E+12	4.88E+12
0.30	6.40E+10	1.72E+11	6.39E+11	7.94E+13	3.11E+13	1.82E+14	1.95E+13	2.23E+13	8.16E+12	5.48E+12
0.35	3.26E+11	5.12E+12	2.77E+12	9.14E+13	6.04E+13	3.64E+14	2.84E+13	2.37E+13	8.70E+12	6.15E+12
0.40	1.66E+12	1.11E+13	7.03E+12	1.05E+14	1.17E+14	3.64E+14	3.71E+13	2.59E+13	9.40E+12	6.90E+12
0.45	4.96E+12	1.66E+13	1.51E+13	1.21E+14	1.73E+14	4.25E+14	3.98E+13	2.72E+13	9.83E+12	7.75E+12
0.50	8.06E+12	2.19E+13	2.24E+13	1.40E+14	2.22E+14	4.87E+14	4.89E+13	2.72E+13	1.17E+13	8.70E+12
0.55	1.07E+13	2.67E+13	3.07E+13	1.61E+14	2.63E+14	4.87E+14	4.92E+13	3.13E+13	1.23E+13	9.46E+12
0.60	1.28E+13	3.13E+13	3.52E+13	1.85E+14	2.96E+14	4.87E+14	4.99E+13	3.23E+13	1.30E+13	9.98E+12
0.65	1.61E+13	3.55E+13	4.10E+13	2.13E+14	3.23E+14	6.07E+14	5.19E+13	3.24E+13	1.26E+13	1.03E+13
0.70	1.91E+13	3.94E+13	4.57E+13	2.28E+14	3.44E+14	7.26E+14	5.80E+13	3.27E+13	1.32E+13	1.04E+13
0.75	2.09E+13	4.29E+13	4.76E+13	2.43E+14	3.59E+14	7.26E+14	5.19E+13	3.31E+13	1.38E+13	1.03E+13
0.80	2.17E+13	4.62E+13	5.13E+13	2.59E+14	3.69E+14	7.26E+14	4.55E+13	3.34E+13	1.39E+13	1.01E+13
0.85	2.17E+13	4.92E+13	5.22E+13	2.74E+14	3.73E+14	6.68E+14	4.26E+13	3.33E+13	1.38E+13	9.85E+12
0.90	2.17E+13	5.18E+13	5.37E+13	2.74E+14	3.73E+14	6.68E+14	4.22E+13	3.29E+13	1.35E+13	9.48E+12
0.95	2.38E+13	5.42E+13	5.17E+13	2.74E+14	3.70E+14	6.68E+14	4.34E+13	3.29E+13	1.32E+13	9.06E+12
1.00	2.34E+13	5.64E+13	4.98E+13	2.74E+14	3.62E+14	5.45E+14	4.52E+13	3.53E+13	1.30E+13	8.62E+12
1.10	1.79E+13	5.98E+13	4.12E+13	2.46E+14	3.38E+14	4.25E+14	4.52E+13	3.04E+13	1.31E+13	7.75E+12
1.20	1.16E+13	6.23E+13	3.05E+13	2.02E+14	3.06E+14	4.25E+14	3.33E+13	2.88E+13	1.30E+13	6.92E+12
1.30	1.22E+13	6.39E+13	2.58E+13	1.60E+14	2.68E+14	3.03E+14	2.67E+13	2.88E+13	1.21E+13	6.15E+12
1.40	1.22E+13	6.46E+13	2.20E+13	1.38E+14	2.27E+14	2.43E+14	2.67E+13	2.72E+13	1.11E+13	5.46E+12
1.50	1.24E+13	6.45E+13	2.13E+13	1.17E+14	1.89E+14	1.82E+14	1.81E+13	2.64E+13	1.09E+13	4.88E+12
1.60	1.14E+13	6.37E+13	1.94E+13	1.04E+14	1.56E+14	1.82E+14	1.65E+13	2.42E+13	1.05E+13	4.31E+12
1.70	1.03E+13	6.23E+13	1.75E+13	9.16E+13	1.31E+14	1.21E+14	1.51E+13	2.34E+13	1.00E+13	3.61E+12
1.80	9.75E+12	6.03E+13	1.58E+13	8.08E+13	1.16E+14	1.21E+14	1.27E+13	2.23E+13	9.21E+12	3.48E+12
1.90	9.10E+12	5.78E+13	1.43E+13	7.14E+13	1.03E+14	1.21E+14	1.13E+13	2.18E+13	8.78E+12	3.07E+12
2.00	8.26E+12	5.48E+13	1.30E+13	6.34E+13	9.11E+13	6.06E+13	1.11E+13	2.14E+13	8.57E+12	2.77E+12
2.50	5.77E+12	3.58E+13	8.54E+12	3.58E+13	5.60E+13	5.04E+13	9.68E+12	1.75E+13	5.85E+12	1.67E+12
3.00	3.73E+12	1.59E+13	5.46E+12	2.06E+13	3.50E+13	4.15E+13	8.63E+12	1.38E+13	4.39E+12	9.73E+11
3.50	3.10E+12	3.53E+12	4.48E+12	1.36E+13	2.36E+13	3.37E+13	7.89E+12	1.13E+13	3.10E+12	6.95E+11
4.00	2.28E+12	2.55E+12	3.20E+12	9.56E+12	1.71E+13	2.70E+13	6.91E+12	9.32E+12	2.64E+12	6.95E+11
4.50	1.85E+12	1.93E+12	2.77E+12	8.08E+12	1.33E+13	2.12E+13	4.32E+12	7.97E+12	2.11E+12	6.95E+11
5.00	1.66E+12	1.54E+12	2.13E+12	6.19E+12	1.09E+13	1.64E+13	3.21E+12	6.74E+12	1.76E+12	4.88E+11
6.00	1.03E+12	1.13E+12	1.71E+12	6.19E+12	8.06E+12	9.16E+12	1.77E+12	4.80E+12	1.26E+12	2.59E+11
7.00	1.45E+12	9.31E+11	1.71E+12	4.17E+12	6.57E+12	4.61E+12	1.44E+12	3.72E+12	1.00E+12	3.10E+11
8.00	1.03E+12	8.09E+11	1.49E+12	3.10E+12	5.67E+12	2.13E+12	1.19E+12	3.29E+12	6.38E+11	4.15E+11
9.00	6.22E+11	7.40E+11	1.07E+12	2.83E+12	5.26E+12	1.11E+12	1.19E+12	2.88E+12	7.11E+11	3.48E+11
10.00	6.22E+11	7.11E+11	1.07E+12	2.83E+12	4.47E+12	9.03E+11	2.55E+12	6.28E+11	3.48E+11	3.48E+11
15.00	2.07E+11	6.23E+11	1.49E+12	2.42E+12	2.98E+12	9.03E+11	1.88E+12	3.77E+11	2.77E+11	2.77E+11
20.00	2.07E+11	3.66E+11	1.07E+12	1.48E+12	2.19E+12	9.03E+11	1.45E+12	2.3E+11	2.88E+11	1.11E+11

H. SED Plots

This section contains the method and code used for plotting the spectral energy distribution output files. Like the main input file, the only things that really needed to be done were unit conversions, since the units were meant for astrophysical applications.

The SED output files had three columns - the frequency, wavelength, and energy. The wavelength was in μm, as desired. The frequency values, however, were in units of Rydberg energy, which needed to be converted to Hz. This was accomplished using the method from Appendix A for the minimum and maximum frequency. The energy values also needed to be converted, as they started in units of Jy*(pc)^2, where 'Jy' is a Jansky and 'pc' is a parsec. The definition of a Jansky is $1 \text{ Jy} = 1 \times 10^{26} \text{ W/m}^2/\text{Hz}$, so the values were in power per area per unit frequency. This was multiplied by (1 pc)$^2 = (3.0857 \times 10^{16} \text{ m})^2$ to get rid of the area dependence. This leaves units of W/Hz, or power per unit frequency. Since the data is in terms of power per unit wavelength, this needs to be converted further. To convert a quantity from frequency (Hz) to wavelength (μm) dependence, the power must be multiplied by $10^6 \times c/\lambda^2$ [55].

The MATLAB code that was used to convert and then plot the spectra is shown in the next section.

MATLAB Code

```
1  test='test20';
2
3  loc=strcat('C:\Users\anita\Desktop\Thesis\Files\Output Files\',test);
4  name=strcat('C:\Users\anita\Desktop\Thesis\LaTeX with bib\Figures\',test,'.png');
5
```

```matlab
6   Array=dlmread(strcat(loc,'\SED.out'),'',[4 0 603 2]);    % eliminates ...
        header/footer
7
8   X=Array(:,1);            % [Ryd]
9   Y=Array(:,2);            % [um]
10  Z=Array(:,3);            %[Jy*(pc)^2]
11
12  % Define Constants
13  Ryd_E=2.180E-18;         % Rydberg Energy, Joules
14  h=6.626E-34;             % J-sec
15  pc=3.0857E16;            % parsec, meters
16  c=3*10^8;                % m/s, speed of light
17
18  % First column: Frequency
19  X1=X.*Ryd_E;             % convert to Joules
20  Freq=X1./h;              % convert to Hz
21
22  % Second Column: Wavelength
23  Wavelength=Y;            % in um
24  Wav2 = Y/10^6;           % in m
25
26  % Third Column: SED
27  SED1=Z.*pi;                              % total over all directions, W/m^2/Hz ...
        * (pc)^2
28  SED2=SED1*10^6*c./(Wav2.^2)*10^(-26);    % J/s/m^2/um * (pc)^2
```

Bibliography

1. T. Henning, B. Begemann, H. Mutschke, and J. Dorschner, "Optical properties of oxide dust grains.," *Astronomy and Astrophysics Supplement Series*, vol. 112, p. 143, 1995.

2. M. R. Querry, "Optical constants," tech. rep., MISSOURI UNIV-KANSAS CITY, 1985.

3. R. Wesson, M. J. Barlow, M. Matsuura, and B. Ercolano, "The timing and location of dust formation in the remnant of SN 1987A," *Monthly Notices of the Royal Astronomical Society*, vol. 446, no. 2, pp. 2089–2101, 2015.

4. C. J. Bridgman, *Introduction to the Physics of Nuclear Weapons Effects*. Defense Threat Reduction Agency, 2001.

5. H. L. Brode, "Fireball Phenomenolgy," 1964.

6. H. L. Brode, "Thermal Radiation Metaguide," Tech. Rep. October, 2000.

7. C. Sublette, "Nuclear Weapons Frequently Asked Questions," 2007.

8. A. Sluder, M. Milosavljevic, and M. H. Montgomery, "Molecular nucleation theory of dust formation in core-collapse supernovae applied to SN 1987A," *Monthly Notices of the Royal Astronomical Society*, vol. 000, no. December, 2016.

9. B. Mookerji, M. Stratman, M. Wall, and W. Siekhaus, "The optical constants of plutonium metal between . 7 and 4 . 3 eV measured by spectroscopic ellipsometry using a double-windowed experimental chamber .," 2006.

10. W. J. Broad, "Threat to U.S. Air Power: The Dust Factor.," *Science (New York, N.Y.)*, vol. 213, pp. 1475–7, sep 1981.

11. J. P. Auxier, J. D. Auxier, and H. L. Hall, "Review of current nuclear fallout codes," *Journal of Environmental Radioactivity*, vol. 171, pp. 246–252, 2017.

12. C. E. Adams, N. H. Farlow, and W. R. Schell, "The compositions, structures and origins of radioactive fall-out particles," *Geochimica et Cosmochimica Acta*, vol. 18, no. 1-2, pp. 42IN351IN553IN755—-50IN452IN65456, 1960.

13. M. W. Nathans, R. Thews, and I. J. Russell, "The Particle Size Distribution of Nuclear Cloud Samples," ACS Publications, 1970.

14. G. Crocker, J. O'Connor, and E. Freiling, "Physical and Radiochemical Properties of Fallout Particles," tech. rep., U.S. Naval Radiological Defense Laboratory, 1965.

15. R. P. Patrick, G. D. Arnett, and W. A. Yingling, "Aircraft Penetration of Clouds Generated by Nuclear Bursts," tech. rep., AIR FORCE WEAPONS LAB KIRTLAND AFB NM, 1974.

16. J. Zinn, C. D. Sutherland, and C. K. Mitchell, "Chemistry and Spectroscopy of a Fireball," p. 59, 1982.

17. D. Arnett, *Supernovae and nucleosynthesis: an investigation of the history of matter, from the big bang to the present.* Princeton University Press, 1996.

18. A. Sarangi and I. Cherchneff, "The chemically controlled synthesis of dust in type II-P supernovae," *Astrophysical Journal*, vol. 776, no. 2, 2013.

19. B. Ercolano, M. J. Barlow, P. J. Storey, and X. W. Liu, "MOCASSIN: A fully three-dimensional Monte Carlo photoionization code," *Monthly Notices of the Royal Astronomical Society*, vol. 340, no. 4, pp. 1136–1152, 2003.

20. "3d mocassin - publications." https://mocassin.nebulousresearch.org/publications.

21. B. Ercolano, M. J. Barlow, and P. J. Storey, "The dusty MOCASSIN: Fully self-consistent 3D photoionization and dust radiative transfer models," *Monthly Notices of the Royal Astronomical Society*, vol. 362, no. 3, pp. 1038–1046, 2005.

22. S. Glasstone and P. J. Dolan, "Effects of nuclear weapons," tech. rep., Department of Defense, Washington, DC (USA); Department of Energy, Washington, DC (USA), 1977.

23. "U.S. Standard Atmosphere." https://www.engineeringtoolbox.com/standard-atmosphere-d_604.html.

24. "Duralumin." https://www.revolvy.com/main/index.php?s=Duralumin&item_type=topic.

25. "ASTM A36 Mild/Low Carbon Steel," 2012.

26. "Natural Uranium." https://www.euronuclear.org/info/encyclopedia/n/naturaluranium.htm.

27. T. R. Gibbs, A. Popolato, and J. F. Baytos, *LASL explosive property data.* University of California Press, 1980.

28. U.S Army, "Engineering design handbook, Explosives series properties of explosives of military interest (No. 706-177)," no. January, 1971.

29. G. Baysinger, "CRC handbook of chemistry and physics," *National Institute of Standards and Technology*, 2015.

30. "Nuclear Tests." http://nucleartests.org/dominic.

31. "Operation Dominic." http://nuclearweaponarchive.org/Usa/Tests/Dominic.html.

32. "Nuclear Weapons in the Strategic Air Command Arsenal." http://www.strategic-air-command.com/weapons/nuclear_bomb_chart.htm.

33. D. D. Eilers, D. R. Westervelt, and C. G. Davis, "Fireball Yields - Absolute Energy Scale," vol. 31, 1999.

34. "Air Composition." https://www.engineeringtoolbox.com/air-composition-d_212.html.

35. D. L. Book, "The Sedov self-similar point blast solutions in nonuniform media," *Shock Waves*, vol. 4, no. 1, pp. 1–10, 1994.

36. R. Nave, "Adiabatic Processes." http://hyperphysics.phy-astr.gsu.edu/hbase/thermo/adiab.html.

37. C. L. Gerardy, R. A. Fesen, P. Holflich, and J. C. Wheeler, "Detection of CO and Dust Emission in Near-Infrared Spectra of SN 1998S," *The Astronomical Journal*, vol. 119, pp. 2968–2981, 2000.

38. F. F. Grinstein, *Coarse Grained Simulation and Turbulent Mixing*. Cambridge University Press, 2016.

39. "Aluminium oxide — Al2O3 - PubChem." https://pubchem.ncbi.nlm.nih.gov/compound/aluminum_oxide#.

40. G. S. Parkinson, "Iron oxide surfaces," vol. 71, no. 111, pp. 272–365, 2016.

41. "Plutonium dioxide." https://www.webelements.com/compounds/plutonium/plutonium_dioxide.html.

42. "Uranium dioxide." https://www.webelements.com/compounds/uranium/uranium_dioxide.html.

43. M. E. Thomas, "Temperature dependence of the complex index of refraction," in *Handbook of Optical Constants of Solids*, pp. 177–201, Elsevier, 1997.

44. M. E. Thomas, S. K. Andersson, R. M. Sova, and R. I. Joseph, "Frequency and temperature dependence of the refractive index of sapphire," *Infrared Physics & Technology*, vol. 39, no. 4, pp. 235–249, 1998.

45. J. A. Baldwin, G. J. Ferland, P. G. Martin, M. R. Corbin, S. A. Cota, B. M. Peterson, and A. Slettebak, "Physical Conditions in the Orion Nebula and an Assessment of its Helium Abundance," *The Astrophysical Journal*, vol. 374, pp. 580–609, 1991.

46. V. E. Henrich and P. A. Cox, *The surface science of metal oxides*. Cambridge University Press, 1994.

47. J. Antula, "Work function aluminum-aluminum oxide," *Solid-State Electronics*, vol. 9, pp. 825–826, aug 1966.

48. "Work Functions." https://www.fh-muenster.de/ciw/downloads/personal/juestel-/juestel/Work_function.pdf.

49. L. Blaney, "Magnetite (Fe3O4): Properties, Synthesis, and Applications," *Lehigh Review*, vol. 15, 2007.

50. Z. Viskadourakis, M. L. Paramê, O. Conde, M. Zervos, and J. Giapintzakis, "Very high thermoelectric power factor in a Fe 3 O 4 /SiO 2 /p-type Si(100) heterostructure,"

51. W. McLean and H. Chen, "The thermionic emission and work function of U and UO2," *Journal of Applied Physics*, vol. 58, pp. 4679–4684, dec 1985.

52. B. Sun, H. Liu, H. Song, G.-C. Zhang, H. Zheng, X.-G. Zhao, and P. Zhang, "First-principles study of surface properties of PuO 2 : Effects of thickness and O-vacancy on surface stability and chemical activity," 2012.

53. "3d mocassin - manual." https://mocassin.nebulousresearch.org/manual/.

54. B. Tummers, "DataThief III," 2006.

55. "The Planck Blackbody Formula in Units of Wavelength." http://www.spectralcalc.com/blackbody/units_of_wavelength.html.

REPORT DOCUMENTATION PAGE

Form Approved
OMB No. 0704-0188

1. REPORT DATE (DD-MM-YYYY)	2. REPORT TYPE	3. DATES COVERED (From - To)
22-03-2018	Master's Thesis	Sep 2016 - Mar 2018

4. TITLE AND SUBTITLE	5a. CONTRACT NUMBER
Using an Astrophysical Model to Characterize Nuclear Dust	
	5b. GRANT NUMBER
	5c. PROGRAM ELEMENT NUMBER

6. AUTHOR(S)	5d. PROJECT NUMBER
Dunsmore, Anita N, 2Lt, USAF	18P420
	5e. TASK NUMBER
	5f. WORK UNIT NUMBER

7. PERFORMING ORGANIZATION NAME(S) AND ADDRESS(ES)	8. PERFORMING ORGANIZATION REPORT NUMBER
Air Force Institute of Technology Graduate School of Engineering and Management (AFIT/EN) 2950 Hobson Way Wright-Patterson AFB OH 45433-7765	AFIT-ENP-MS-18-M-079

9. SPONSORING/MONITORING AGENCY NAME(S) AND ADDRESS(ES)	10. SPONSOR/MONITOR'S ACRONYM(S)
Defense Threat Reduction Agency - NTS Lieutenant Colonel Brian J. Fry 8725 John J. Kingman Rd. Ft. Belvoir, VA 22060 brian.j.fry.mil@mail.mil	DTRA
	11. SPONSOR/MONITOR'S REPORT NUMBER(S)

12. DISTRIBUTION/AVAILABILITY STATEMENT

Distribution Statement A. Approved for Public Release;Distribution Unlimited.

13. SUPPLEMENTARY NOTES

This work is declared a work of the U.S. Government and is not subject to copyright protection in the United States.

14. ABSTRACT

Dust clouds resulting from nuclear explosions are complex phenomena, and knowledge on how they form is lacking. Noting the similarities between supernovae and nuclear explosions led to the concept of modeling a nuclear dust cloud using a supernova simulation. MOCASSIN uses a Monte Carlo approach to model photons traveling through a dust cloud, allowing the cloud's characteristics to be discovered by comparing an observed spectrum to a calculated one and then changing input values to make the spectra match. Data files describing two nuclear fireballs of varying yields were created and analyzed using MOCASSIN, but yielded zero energy spectra. After varying the parameters of the tests, analyzing the resulting spectra, and comparing them to data, it was found that the differences between the nuclear explosion and supernova were too significant for MOCASSIN to accurately model both. Insufficient input data for nuclear materials, and low ionization levels and high densities in the fireball were insurmountable issues. Ultimately, it was concluded that MOCASSIN is not a viable method for analyzing nuclear explosions.

15. SUBJECT TERMS

nuclear dust cloud, supernova model, MOCASSIN, nuclear fireball model

16. SECURITY CLASSIFICATION OF:			17. LIMITATION OF ABSTRACT	18. NUMBER OF PAGES	19a. NAME OF RESPONSIBLE PERSON
a. REPORT	b. ABSTRACT	c. THIS PAGE			Dr. John W. McClory, AFIT/ENP
U	U	U	UU	136	19b. TELEPHONE NUMBER (Include area code) (937) 255-3636 x7308, John.McClory@afit.edu

Standard Form 298 (Rev. 8/98)
Prescribed by ANSI Std. Z39.18